December 2020

Coordination and Privacy Preservation in Multi-Agent Systems

Huan Gao
Clemson University, huangaonpu@hotmail.com

COORDINATION AND PRIVACY PRESERVATION IN MULTI-AGENT SYSTEMS

A Dissertation
Presented to
the Graduate School of
Clemson University

In Partial Fulfillment
of the Requirements for the Degree
Doctor of Philosophy
Electrical Engineering

---

by
Huan Gao
December 2020

Accepted by:
Dr. Yongqiang Wang, Committee Chair
Dr. Richard E. Groff
Dr. Yingjie Lao
Dr. Shitao Liu

Abstract

This dissertation considers two key problems in multi-agent systems: coordination (including both synchronization and desynchronization) and privacy preservation.

For coordination in multi-agent systems, we focus on synchronization/desynchronization of distributed pulse-coupled oscillator (PCO) networks and their applications in collective motion coordination. Pulse-coupled oscillators were originally proposed to model synchronization in biological systems such as flashing fireflies and firing neurons. In recent years, with proven scalability, simplicity, accuracy, and robustness, the PCO based synchronization strategy has become a powerful clock synchronization primitive for wireless sensor networks. Driven by these increased applications in biological networks and wireless sensor networks, synchronization of pulse-coupled oscillators has gained increased popularity. However, most existing results address the local synchronization of PCOs with initial phases constrained in a half cycle, and results on global synchronization from any initial condition are very sparse. In our work, we address global PCO synchronization from an arbitrary phase distribution under chain or directed tree graphs. More importantly, different from existing global synchronization studies on decentralized PCO networks, our work allows heterogeneous coupling functions and perturbations on PCOs' natural frequencies, and our results hold under any coupling strength between zero and one, which is crucial because a large coupling strength has been shown to be detrimental to the robustness of PCO synchronization to disturbances.

Compared with synchronization, desynchronization of PCOs is less explored. Desynchronization spreads the phase variables of all PCOs uniformly apart (with equal difference between neighboring phases). It has also been found in many biological phenomena, such as neuron spiking and fish signaling. Recently, phase desynchronization has been employed to achieve round-robin scheduling, which is crucial in applications as diverse as media access control of communication networks, realization of analog-to-digital converters, and scheduling of traffic flows in intersections. In our work, we systematically characterize pulse-coupled oscillators based decentralized phase desynchronization and propose an interaction function that is more gen-

eral than existing results. Numerical simulations show that the proposed pulse based interaction function also has better robustness to pulse losses, time delays, and frequency errors than existing results.

Collective motion coordination is fundamental in systems as diverse as mobile sensor networks, swarm robotics, autonomous vehicles, and animal groups. Inspired by the close relationship between phase synchronization/desynchronization of PCOs and the heading dynamics of connected vehicles/robots, we propose a pulse-based integrated communication and control approach for collective motion coordination. Our approach only employs simple and identical pulses, which significantly reduces processing latency and communication delay compared with conventional packet based communications. Not only can heading control be achieved in the proposed approach to coordinate the headings (orientations) of motions in a network, but also spacing control for circular motion is achievable to design the spacing between neighboring nodes (e.g., vehicles or robots).

The second part of this dissertation is privacy preservation in multi-agent systems. More specifically, we focus on privacy-preserving average consensus as it is key for multi-agent systems, with applications ranging from time synchronization, information fusion, load balancing, to decentralized control. Existing average consensus algorithms require individual nodes (agents) to exchange explicit state values with their neighbors, which leads to the undesirable disclosure of sensitive information in the state. In our work, we propose a novel average consensus algorithm for time-varying directed graphs which can protect the privacy of participating nodes' initial states. Leveraging algorithm-level obfuscation, the algorithm does not need the assistance of any trusted third party or data aggregator. By leveraging the inherent robustness of consensus dynamics against random variations in interaction, our proposed algorithm can guarantee privacy of participating nodes without compromising the accuracy of consensus. The algorithm is distinctly different from differential-privacy based average consensus approaches which enable privacy through compromising accuracy in obtained consensus value. The approach is able to protect the privacy of participating nodes even in the presence of multiple honest-but-curious nodes which can collude with each other.

Acknowledgments

I would like to express my sincere gratitude to my advisor Dr. Yongqiang Wang, who has mentored me and encouraged my academic development. Without your continued support, instruction, and encouragement, all that I have accomplished during my Ph.D. study would not have been possible. I would also like to acknowledge my committee, Dr. Richard E. Groff, Dr. Yingjie Lao, and Dr. Shitao Liu, for their critical review and insightful comments to my work. In addition, I would like to thank my past and present lab mates, Dr. Zhenqian Wang, Dr. Chunlei Zhang, Timothy Anglea, Muaz Ahmad, Dr. Francesco Ferrante, and Dr. Hafiz Ahmad. It was a great pleasure working with you all. Lastly, I would like to extend my special thanks to my father Xiangdong Gao, my mother Jianmei Zhao, my wife Li Yin, and my son Timothy Gao, for their moral support and encouragement.

Table of Contents

List of Tables

List of Figures

Chapter 1

Introduction

Our work focuses on coordination (including both synchronization and desynchronization) and privacy preservation in multi-agent systems. In the following two sections, we will introduce these two parts in more details, respectively.

1.1 Coordination in Multi-Agent Systems

It is well known that coordination is a key characteristic of multi-agent systems. In our work, we consider coordination (including both synchronization and desynchronization) in pulse-coupled oscillator (PCO) networks. Pulse-coupled oscillators (PCOs) are limit cycle oscillators coupled through exchanging pulses at discrete time instants. They were originally proposed to model the synchronization phenomena in biological systems, such as contracting cardiac cells, flashing fireflies, and firing neurons [31, 47, 95, 122]. Due to their amazing scalability, simplicity, and robustness, recently they have found applications in wireless sensor networks [60, 61, 114, 143, 143, 151, 158, 159, 161], image processing [131], and motion coordination [42].

1.1.1 PCO Synchronization

Early results on PCO synchronization were motivated by biological applications, and normally assume a fixed interaction or coupling mechanism [95, 122]. In engineering applications, such restrictions do not exist any more. In fact, the interaction mechanism becomes a design variable that provides opportunities to achieve desired performance. For example, [92] and [106] designed the interaction to improve the robust-

ness to communication delays. The work in [157] optimized the interaction, i.e., phase response function (PRF), to improve the speed of synchronization. However, most of these results are for local synchronization assuming that the initial phases are restricted within a half cycle [1, 2, 14, 26, 31, 32, 47, 54, 66, 70, 79, 93, 106, 127, 128, 147, 148, 153, 157, 158, 160].

Assuming restricted initial phase distribution severely hinders the application of PCO based synchronization, since in distributed networks it is hard to control the initial phase distribution. Recently, efforts have emerged to address global PCO synchronization from an arbitrary initial phase distribution. However, these results focus on special graphs, such as all-to-all graph [15, 74, 78, 110], cycle graph [109], strongly-rooted graph [110], or master/slave graph [111]. Moreover, they rely on sufficiently large coupling strengths, which may not be desirable as large coupling strengths are detrimental to robustness to disturbances [60].

In our work, we address the global synchronization of PCOs under arbitrary initial conditions and heterogeneous coupling functions (PRFs). Our main focus is on the global synchronization of PCOs under undirected chain graphs, but the results are easily extendable to PCO synchronization under directed chain/tree graphs. Note that the chain or directed tree graphs are basic elements for constructing more complicated graphs and are desirable in engineering applications where reducing the number of connections is important to save energy consumption and cost in deployment/maintenance. Furthermore, the chain graph has been regarded as the worst-case scenario for synchronization due to its minimum number of connections [73]. We also consider oscillators with perturbations on their natural frequencies.

Compared with existing results on PCO synchronization (cf. Table 1.1), our work has the following contributions:

1. Different from most existing results which focus on local PCO synchronization and assume that the initial phases of oscillators are restricted within a half cycle, our work addresses global synchronization from an arbitrary initial phase distribution;

2. Different from existing global synchronization studies on decentralized PCO networks, our work allows heterogeneous phase response functions, and we analyze the behavior of oscillators with perturbations on their natural frequencies. These scenarios, to our knowledge, have not been considered in any existing global synchronization results on decentralized PCO networks;

3. In contrast to existing global PCO synchronization results requiring a strong enough coupling strength, our results guarantee global synchronization under any coupling strength between zero and one, which is more desirable since a very strong coupling strength, although can bring fast convergence, has been

Table 1.1: Comparison of our work with other existing results on PCO synchronization

		Homogeneous coupling		Heterogeneous coupling	
		PCO network having (at least) a global node[1]	Decentralized PCO networks	PCO network having (at least) a global node	Decentralized PCO networks
Non-global synchronization	Local synchronization	[31, 32, 54, 153] [2, 47, 70, 78] [1, 14, 110]	[47, 79, 106, 148] [66, 93, 127, 147] [110, 157, 158, 160] [109]	[111]	[26, 128]
	Almost global synchronization or synchronization with probability one	[18, 91, 95]	[75, 76, 86]	\	\
Global synchronization	Discrete state synchronization	[6]	[86]	\	\
	(Continuous) phase synchronization	[15, 74, 78, 110]	[87, 109, 110][2]	[111]	Our work

[1] A node is called as a global node if it is directly connected to all the other nodes.
[2] Note that when the maximum degree of an undirected tree graph is not over 3, [87] obtained global synchronization results for the conventional phase-only PCO model, though results were also obtained under general undirected tree graphs for a more complicated PCO model with multiple additional state variables.

shown to be detrimental to the robustness of synchronization to disturbances [60].

1.1.2 PCO Desynchronization

Compared with synchronization, desynchronization of PCOs is less explored. Desynchronization spreads the phase variables of all PCOs uniformly apart (with equal difference between neighboring phases). It has also been found in many biological phenomena, such as neuron spiking [144] and fish signaling [9]. What's more, desynchronization is also very important for Deep Brain Stimulation (DBS) which has been proven an effective treatment for Parkinson's disease [100]. Recently, phase desynchronization has also been employed to perform time-division multiple access (TDMA), a medium access control (MAC) protocol for communications [8, 22, 146].

In the literature, a number of papers have emerged on PCO based desynchronization. Based on the PCO model in [95], the authors in [120] proposed a desynchronization algorithm (INVERSE-MS) for an all-to-all network. The convergence properties of INVERSE-MS were further explored in [113, 123, 124], using an algebraic framework and a hybrid systems framework, respectively. However, these results are about the achievement of uniform firing time interval (equal time interval between two consecutive firings), which is

referred to as weak desynchronization [113, 120]. Weak desynchronization relies on persistent phase jumps to maintain equal firing intervals, and hence cannot guarantee a uniform spread of phases. Furthermore, it is sensitive to disturbances such as pulse loss and time delay because a lost or delayed pulse will directly lead to errors in the spread of firing time instants.

Recently, algorithms also emerged for phase desynchronization which is also referred to as strict desynchronization. Existing phase desynchronization algorithms can be divided into two categories based on the employed interaction mechanism. In the first mechanism, an oscillator adjusts its phase according to the firing information of its two immediate firing neighbors (the one fires before it and the one after). Typical examples include [12, 13, 23, 24, 82, 120, 142]. Generally speaking, performance of these desynchronization algorithms are difficult to rigorously analyze since an oscillator can never know the exact current phases of its two immediate neighbors (the one fires before it and the one after). Furthermore, because each oscillator only updates once during its cycle, such desynchronization algorithms tend to have very slow convergence rates, as confirmed by our numerical results in Section 3.4.

The second mechanism is using phase response function (PRF) based interaction. In this mechanism, each oscillator will make phase adjustments every time it receives a pulse, and the adjustment is determined by the phase response function which describes the phase shift induced by a pulse. As in an all-to-all network with N PCOs, every oscillator will receive $N-1$ pulses when its phase evolves one cycle, and will make $N-1$ adjustments during its phase cycle, which significantly improves the convergence speed. Existing results [12, 13, 35, 36, 113] fall within this category.

In our work, we rigorously analyze the category of phase response function (PRF) based phase desynchronization algorithms. Our contributions can be summarized as follows:

1. We rigorously characterize the decentralized phase desynchronization process and propose a general phase-desynchronizing phase response function (PRF) that includes previous results as special cases;

2. The proposed PRF provides high robustness to pulse losses, time delays, and frequency errors which will significantly degrade the performance of all existing phase desynchronization approaches, as illustrated in numerical simulations in Chapter 3;

3. The proposed PRF can significantly improve convergence speed compared with existing results, according to our numerical simulations.

1.1.3 Pulse-Based Collective Motion Coordination

Inspired by the pulse-based synchronization/desynchronization of PCOs and the close relationship between the phase dynamics of PCOs and the heading dynamics of vehicles, we aim to propose a pulse-based approach for collective motion coordination. Recently, the collective motion (coordination of movement) of multiple vehicle systems has received great attention because of its broad range of engineering applications. Typical applications include the formation control of unmanned aerial vehicles [28, 34, 65, 129], cooperative robotics [19, 94], the coordination of autonomous underwater vehicles [3], and the deployment of mobile sensor networks [20, 59, 158].

In the past decade, numerous results have been published on collective motion coordination of multi-agent systems. In order to simplify the mathematical treatment, early results used an integrator to model the dynamics of vehicles, which restricts their practical applications. Moreover, most existing results on collective motion coordination were based on special communication structures such as all-to-all structure [140], cyclic structure [90, 116], and circulant structure [118]. The authors in [25] and [97] showed that collective motion can be achieved under a general communication structure in the synchronized-state collective motion (aligning vehicles to the same heading). Furthermore, the authors in [141] showed that circular collective motion can be achieved under a general communication structure if additional information about the relative estimates of averaged quantities can be exchanged among vehicles.

However, in the above results, all the cooperative motion controllers are designed in the continuous-time domain assuming that neighbor's information is continuously available, which contradicts the fact that information can only be exchanged at discrete-time instants among vehicles in practical applications. In order to simplify the design and analysis, the controller is usually designed in the continuous-time domain, and then discretized in implementation to conform to the discrete-time nature of communication. But this commonly used approach cannot work in many cases, because a very small discretization period is required to guarantee the original design performance which significantly increases the communication frequency and causes heavy communication burden [49]. To make things worse, discretization can harm or even destabilize the closed-loop system.

Motivated by pulse-based synchronization/desynchronization of PCOs, which only relies on exchanging simple identical pulse at discrete-time instants, we propose a pulse-based integrated communication and control approach for collective motion coordination. Based on the close relationship between the phase dynamics of PCOs and the heading dynamics of vehicles, the communication design is solved natu-

rally in the proposed approach, which circumvents the problem of discretization and guarantees the original design performance in implementation. Both heading control and spacing control are achieved in the unified approach.

1.2 Privacy Preservation in Multi-Agent Systems

Our work focuses on privacy preservation for average consensus as achieving average consensus is an important problem in multi-agent systems. For a multi-agent system of N nodes (agents) interacting on a connected graph, average consensus can enable all nodes converge to the average of their initial values through iterations based on local interaction between neighboring nodes.

In recent years, average consensus is finding increased applications in load balancing [11, 21], network synchronization [85], distributed information fusion [136, 162], and decentralized control [112, 130]. To ensure all nodes converge to the average value of their initial values, conventional average consensus approaches require individual nodes to exchange explicit state values with their neighbors. This results in the disclosure of sensitive state information, which is sometimes undesirable in terms of privacy. In fact, in many applications such as the smart grid, health-care or banking networks, privacy is crucial for promoting participation in collaboration since individual nodes tend not to trade privacy for performance [58, 84, 88]. For instance, a group of people using average consensus to reach a common opinion may want to keep their individual opinions secret [150]. Another typical example is power systems in which multiple generators have to reach agreement on cost while maintaining their individual generation information private [165]. Moreover, exchanging information in the plaintext form (without encryption) is vulnerable to adversaries which try to steal sensitive information through hacking into communication links. As the number of reported attack-events increases and the awareness of security grows, keeping data encrypted in communications becomes necessary in many applications, particularly in a lot of real-time sensing and control systems like wireless sensor networks and power systems.

To enable privacy preservation in average consensus, recently results have started to emerge. A commonly used privacy-preserving mechanism is differential privacy from the database literature [45, 62, 63, 67, 107, 108, 163] (and its variants [68, 154]) which injects independent (and hence uncorrelated) noises directly to nodes' states in order to enable privacy preservation in average consensus. However, the use of independent noises on the states in these approaches prevents converging to the exact average value [156]. To improve consensus accuracy, which is crucial in cyber-physical systems and sensor networks, [17, 50, 55–57,

89, 96, 125] inject carefully calculated correlated additive noises to nodes' states, instead of independent (and hence uncorrelated) noises used in differential-privacy based approaches. (A similar approach was proposed in [27] to achieve maximum consensus.) However, these prior works only consider average consensus under balanced and static network topologies. Different from injecting noises to nodes' states in the aforementioned approaches, [5] employed carefully designed mask maps to protect the actual states. Observability based approaches have also been reported to protect the privacy of multi-agent consensus [4, 121, 132]. Its idea is to design the topology of interactions such that the observability from a compromised node is minimized, which amounts to minimizing the ability of the compromised node to infer the initial states of other nodes. Recently, encryption based approaches have been proposed to protect the privacy by encrypting exchanged messages with the assistance of additive homomorphic encryption [33,52,71,135], with the price of increasing computation and communication overhead. Another privacy-preserving approach was proposed in [155] where each node's privacy is protected by decomposing its state into two sub-states. However, [155] relies on undirected interactions and is inapplicable to time-varying directed graphs considered in our work.

In our work, we address privacy preservation of average consensus under time-varying directed graphs that are not necessarily balanced. Building on the conventional push-sum based average consensus algorithm, we enable privacy by judiciously adding uncertainties in interaction dynamics and leverage the inherent robustness of the push-sum algorithm to ensure consensus to the exact average value. More specifically, in the first several steps, each node sends completely independent random numbers to its out-neighbors and updates its own state under a sum-invariant (column-stochastic) constraint to completely obfuscate its initial value without affecting the final convergence result. This is in distinct difference from differential-privacy based average consensus approaches which enable privacy through sacrificing accuracy in obtained consensus value. The proposed approach is able to preserve privacy even when multiple honest-but-curious nodes collude with each other. Numerical simulations are provided to verify the effectiveness and efficiency of the proposed approach.

1.3 Outline of this Dissertation

The outline of this dissertation is as follows. Chapters 2 and 3 focus on PCO synchronization and desynchronization, respectively. In Chapter 4, we study the applications of PCO in collective motion coordination. Chapter 5 addresses privacy preservation for average consensus in multi-agent systems. Finally, we conclude the dissertation in Chapter 6.

It is worth noting that the dissertation is comprised of six papers from my research work [39–44]. More specifically, [43], [40], [39, 42], and [41, 44] are included in Chapters 2, 3, 4, and 5, respectively.

Chapter 2

Synchronization of Pulse-Coupled Oscillators

2.1 Introduction

In this chapter, we consider synchronization of pulse-coupled oscillators (PCOs). Pulse-coupled oscillators are limit cycle oscillators coupled through exchanging pulses at discrete time instants. They were originally proposed to model the synchronization phenomena in biological systems, such as contracting cardiac cells, flashing fireflies, and firing neurons [31, 95, 122]. Due to their amazing scalability, simplicity, and robustness, the PCO based synchronization strategy has become a powerful clock synchronization primitive for wireless sensor networks [143, 151, 158, 159, 161].

Driven by increased applications in biological networks and wireless sensor networks, synchronization of pulse-coupled oscillators has gained increased popularity. However, most existing results are for local synchronization assuming that the initial phases are restricted within a half cycle [1, 2, 14, 26, 31, 32, 47, 54, 66, 70, 79, 93, 106, 127, 128, 147, 148, 153, 157, 158, 160].

Assuming restricted initial phase distribution severely hinders the application of PCO based synchronization, since in distributed networks it is hard to control the initial phase distribution. Recently, efforts have emerged to address global PCO synchronization from an arbitrary initial phase distribution. However, these results focus on special graphs, such as all-to-all graph [15, 74, 78, 110], cycle graph [109], strongly-rooted graph [110], or master/slave graph [111]. Moreover, they rely on sufficiently large coupling strengths,

which may not be desirable as large coupling strengths are detrimental to robustness to disturbances [60].

In our work, we address the global synchronization of PCOs under arbitrary initial conditions and heterogeneous phase response functions (PRFs). Due to the hybrid nature of PCO dynamics, we present a hybrid model for PCO networks by using the hybrid systems framework in [46]. Our main focus is on the global synchronization of PCOs under undirected chain graphs, but the results are easily extendable to PCO synchronization under directed chain/tree graphs. We also analyze the behavior of oscillators with perturbations on their natural frequencies.

The remainder of this chapter is organized as follows. In Section 2.2, we introduce some preliminary concepts, such as basic notations, hybrid systems, and communication graphs. A hybrid model for PCO networks and its dynamical properties are presented in Section 2.3. In Section 2.4, we analyze global synchronization on both chain and directed tree graphs and provide robustness analysis under frequency perturbations. Numerical experiments are given in Section 2.5. Finally, we conclude this chapter in Section 2.6.

2.2 Preliminaries

2.2.1 Basic Notations

$\mathbb{R}$, $\mathbb{R}_{\geq 0}$, and $\mathbb{Z}_{\geq 0}$ denote real numbers, nonnegative real numbers, and nonnegative integers, respectively. $\mathbb{R}^n$ denotes the Euclidean space of dimension n, and $\mathbb{R}^{n\times n}$ denotes the set of $n \times n$ square matrices with real coefficients. $\mathbb{B}$ denotes the closed unit ball in the Euclidean norm. A set-valued map $M : A \rightrightarrows B$ associates an element $\alpha \in A$ with a set $M(\alpha) \subseteq B$; the graph of M is defined as $\operatorname{graph}(M) := \{(\alpha, \beta) \in A \times B : \beta \in M(\alpha)\}$. M is outer-semicontinuous if and only if its graph is closed [134]. The range of a function $f : \mathbb{R}^n \to \mathbb{R}^m$ is denoted as $\operatorname{rge} f$. The closure of set $\mathcal{A}$ is denoted as $\overline{\mathcal{A}}$. The distance of a vector $x \in \mathbb{R}^n$ to a closed set $\mathcal{A} \subset \mathbb{R}^n$ is denoted as $|x|_{\mathcal{A}} = \inf_{y\in\mathcal{A}} |x - y|$. The μ-level set of function $V : \operatorname{dom} V \to \mathbb{R}$ is denoted as $V^{-1}(\mu) = \{x \in \operatorname{dom} V : V(x) = \mu\}$ [46].

2.2.2 Hybrid Systems

We use hybrid systems framework with state $x \in \mathbb{R}^n$ [46]

$$\mathcal{H} : \begin{cases} \dot{x} = f(x), & x \in \mathcal{C} \\ x^+ \in G(x), & x \in \mathcal{D} \end{cases} \tag{2.1}$$

where f, $\mathcal{C}$, G, and $\mathcal{D}$ are the flow map, flow set, jump map, and jump set, respectively. The hybrid system can be represented by $\mathcal{H} = (\mathcal{C}, f, \mathcal{D}, G)$. In hybrid system, a hybrid time point $(t,\, j) \in E$ is parameterized by both t, the amount of time passed since initiation, and j, the number of jumps that have occurred. A subset $E \subset \mathbb{R}_{\geq 0} \times \mathbb{Z}_{\geq 0}$ is a hybrid time domain if it is the union of a finite or infinite sequence of interval $[t_k, t_{k+1}] \times \{k\}$. A solution to $\mathcal{H}$ is a function $\phi : E \to \mathbb{R}^n$ where ϕ satisfies the dynamics of $\mathcal{H}$, E is a hybrid time domain, and for each $j \in \mathbb{N}$, the function $t \mapsto \phi(t, j)$ is locally absolutely continuous on $I_j = \{t : (t, j) \in E\}$. $\phi(t, j)$ is called a hybrid arc. A hybrid arc ϕ is nontrivial if its domain contains at least two points, is maximal if it is not the truncation of another solution, and is complete if its domain is unbounded. Moreover, a hybrid arc ϕ is Zeno if it is complete and $\sup_t \operatorname{dom} \phi < \infty$, is continuous if it is nontrivial and $\operatorname{dom} \phi \subset \mathbb{R}_{\geq 0} \times \{0\}$, is eventually continuous if $J = \sup_j \operatorname{dom} \phi < \infty$ and $\operatorname{dom} \phi \cap (\mathbb{R}_{\geq 0} \times \{\mathrm{J}\})$ contains at least two points, is discrete if it is nontrivial and $\operatorname{dom} \phi \subset \{0\} \times \mathbb{Z}_{\geq 0}$, and is eventually discrete if $T = \sup_t \operatorname{dom} \phi < \infty$ and $\operatorname{dom} \phi \cap (\{\mathrm{T}\} \times \mathbb{Z}_{\geq 0})$ contains at least two points. Given a set $\mathcal{M}$, we denote $\mathcal{S}_{\mathcal{H}}(\mathcal{M})$ the set of all maximal solutions ϕ to $\mathcal{H}$ with $\phi(0, 0) \in \mathcal{M}$.

Some notions and results for the hybrid system $\mathcal{H}$ from [46] which will be used in this chapter are given as follows.

Definition 2.1. *$\mathcal{H} = (\mathcal{C}, f, \mathcal{D}, G)$ satisfies the hybrid basic conditions if: 1) $\mathcal{C}$ and $\mathcal{D}$ are closed in $\mathbb{R}^n$; 2) $f : \mathbb{R}^n \to \mathbb{R}^n$ is continuous and locally bounded on $\mathcal{C} \subset \operatorname{dom} f$; and 3) $G : \mathbb{R}^n \rightrightarrows \mathbb{R}^n$ is outer-semicontinuous and locally bounded on $\mathcal{D} \subset \operatorname{dom} G$.*

Definition 2.2. *A set $S \subset \mathbb{R}^n$ is said to be strongly forward invariant if for every $\phi \in \mathcal{S}_{\mathcal{H}}(S)$, $\operatorname{rge} \phi \subset \mathrm{S}$.*

Definition 2.3. *Given a set $S \subset \mathbb{R}^n$, a hybrid system $\mathcal{H}$ on $\mathbb{R}^n$ is pre-forward complete from S if every $\phi \in \mathcal{S}_{\mathcal{H}}(S)$ is either bounded or complete.*

Definition 2.4. *A compact set $\mathcal{A} \subset \mathbb{R}^n$ is said to be uniformly attractive from a set $S \subset \mathbb{R}^n$ if every $\phi \in \mathcal{S}_{\mathcal{H}}(S)$ is bounded and for every $\varepsilon > 0$ there exists $\tau > 0$ such that $|\phi(t,\, j)|_{\mathcal{A}} \leq \varepsilon$ for every $\phi \in \mathcal{S}_{\mathcal{H}}(S)$ and $(t,\, j) \in \operatorname{dom} \phi$ with $t + j \geq \tau$.*

Definition 2.5. *A compact set $\mathcal{A} \subset \mathbb{R}^n$ is said to be*

- *stable for $\mathcal{H}$ if for every $\varepsilon > 0$ there exists $\delta > 0$ such that every solution ϕ to $\mathcal{H}$ with $|\phi(0,0)|_{\mathcal{A}} \leq \delta$ satisfies $|\phi(t,j)|_{\mathcal{A}} \leq \varepsilon$ for all $(t,j) \in \operatorname{dom} \phi$;*
- *locally attractive for $\mathcal{H}$ if every maximal solution to $\mathcal{H}$ is bounded and complete, and there exists $\mu > 0$ such that every solution ϕ to $\mathcal{H}$ with $|\phi(0,0)|_{\mathcal{A}} \leq \mu$ converges to $\mathcal{A}$, i.e., $\lim_{t+j\to\infty} |\phi(t,j)|_{\mathcal{A}} = 0$ holds;*
- *locally asymptotically stable for $\mathcal{H}$ if it is both stable and locally attractive for $\mathcal{H}$.*

Definition 2.6. *Let $\mathcal{A} \subset \mathbb{R}^n$ be locally asymptotically stable for $\mathcal{H}$. Then the basin of attraction of $\mathcal{A}$, denoted by $\mathcal{B}_{\mathcal{A}}$, is the set of points such that every $\phi \in \mathcal{S}_{\mathcal{H}}(\mathcal{B}_{\mathcal{A}})$ is bounded, complete, and $\lim_{t+j\to\infty} |\phi(t,j)|_{\mathcal{A}} = 0$.*

Definition 2.7. *Given $\tau, \varepsilon > 0$, two hybrid arcs ϕ_1 and ϕ_2 are (τ,ε)-close if*

- *$\forall\, (t,j) \in \operatorname{dom} \phi_1$ with $t + j \leq \tau$ there exists s such that $(s,j) \in \operatorname{dom} \phi_2$, $|t - s| < \varepsilon$ and $|\phi_1(t,j) - \phi_2(s,j)| < \varepsilon$;*
- *$\forall\, (t,j) \in \operatorname{dom} \phi_2$ with $t + j \leq \tau$ there exists s such that $(s,j) \in \operatorname{dom} \phi_1$, $|t - s| < \varepsilon$ and $|\phi_2(t,j) - \phi_1(s,j)| < \varepsilon$.*

Lemma 2.1. *(Theorem 8.2 in [46]) Consider a continuous function $V : \mathbb{R}^n \to \mathbb{R}$, any functions $u_C, u_D : \mathbb{R}^n \to [-\infty, \infty]$, and a set $U \subset \mathbb{R}^n$ such that $u_C(z) \leq 0$, $u_D(z) \leq 0$ for every $z \in U$ and such that the growth of V along solutions to $\mathcal{H}$ is bounded by u_C, u_D on U. Let a precompact solution $\phi^* \in \mathcal{S}_{\mathcal{H}}$ be such that $\overline{\operatorname{rge} \phi^*} \subset U$. Then, for some $r \in V(U)$, ϕ^* approaches the nonempty set that is the largest weakly invariant subset of $V^{-1}(r) \cap U \cap \big[\overline{u_C^{-1}(0)} \cup \big(u_D^{-1}(0) \cap G(u_D^{-1}(0))\big)\big]$.*

Lemma 2.2. *(Proposition 7.5 in [46]) Let $\mathcal{H}$ be nominally well-posed. Suppose that a compact set $\mathcal{A} \subset \mathbb{R}^n$ has the following properties: 1) it is strongly forward invariant, and 2) it is uniformly attractive from a neighborhood of itself, i.e., there exists $\mu > 0$ such that $\mathcal{A}$ is uniformly attractive from $\mathcal{A} + \mu\mathbb{B}$. Then the compact set $\mathcal{A}$ is locally asymptotically stable.*

Lemma 2.3. *(Proposition 6.34 in [46]) Let $\mathcal{H}$ be well-posed. Suppose that $\mathcal{H}$ is pre-forward complete from a compact set $K \subset \mathbb{R}^n$ and $\rho : \mathbb{R}^n \to \mathbb{R}_{\geq 0}$. Then for every $\varepsilon > 0$ and $\tau \geq 0$, there exists $\delta > 0$ with the following property: for every solution ϕ_δ to $\mathcal{H}_{\delta\rho}$ with $\phi_\delta(0,\,0) \in K + \delta\mathbb{B}$, there exists a solution ϕ to $\mathcal{H}$ with $\phi(0,\,0) \in K$ such that ϕ_δ and ϕ are (τ,ε)-close.*

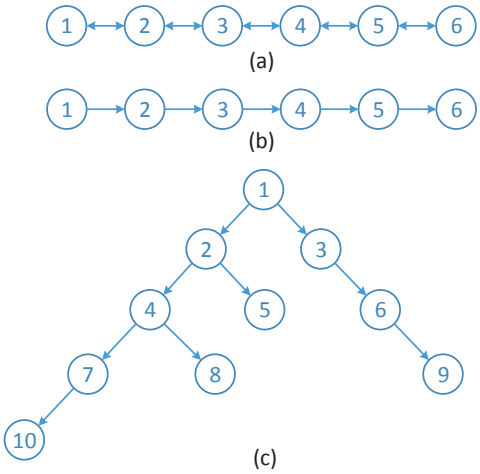

Figure 2.1: Illustration of graphs: (a) undirected chain graph with six nodes; (b) directed chain graph with six nodes; (c) directed tree graph with ten nodes.

2.2.3 Communication Graphs

We use a graph $\mathcal{G} = (\mathcal{V}, \mathcal{E}, \mathcal{W})$ to represent the interaction pattern of PCOs, where the node set $\mathcal{V} = \{1, 2, \ldots, N\}$ denotes all oscillators. $\mathcal{E} \subseteq \mathcal{V} \times \mathcal{V}$ is the edge set, whose elements are such that $(i, j) \in \mathcal{E}$ holds if and only if node j can receive messages from node i. We assume that no self edge exists, i.e., $(i, i) \notin \mathcal{E}$. $\mathcal{W} = [w_{ij}] \in \mathbb{R}^{N \times N}$ is the weighted adjacency matrix of $\mathcal{G}$ with $w_{ij} \geq 0$, where $w_{ij} > 0$ if and only if $(i, j) \in \mathcal{E}$ holds. The out-neighbor set of node i, which represents the set of nodes that can receive messages from node i, is denoted as $\mathcal{N}_i^{out} := \{j \in \mathcal{V} : (i, j) \in \mathcal{E}\}$.

We focus on chain graphs (both undirected and directed) and directed tree graphs which are defined as follows:

Definition 2.8. *An undirected chain graph $\mathcal{G}$ is a graph whose nodes can be indexed such that there exist two edges $(i, i+1)$ and $(i+1, i)$ between nodes i and $i+1$ for $i = 1, 2, \ldots, N-1$.*

Definition 2.9. *A directed chain graph $\mathcal{G}$ is a graph whose nodes can be indexed such that there is only one edge between nodes i and $i+1$ for $i = 1, 2, \ldots, N-1$ and all edges are directed in the same direction. Without loss of generality, we suppose that the edge between nodes i and $i+1$ is $(i, i+1)$.*

Definition 2.10. *A directed tree graph $\mathcal{G}$ is a cycle-free graph with a designated node as a root such that the root has exactly one directed chain to every other node.*

Examples of undirected chain graph, directed chain graph, and directed tree graph are given in Fig.

2.1.

2.3 Problem Statement

2.3.1 PCO Model

We consider a network of N PCOs interacting on a graph $\mathcal{G} = (\mathcal{V}, \mathcal{E}, \mathcal{W})$. Each oscillator has a phase variable $x_i \in \mathbb{S}^1$ for each $i \in \mathcal{V}$ where $\mathbb{S}^1$ denotes the one-dimensional torus. Each phase variable x_i evolves continuously towards 2π according to integrate-and-fire dynamics, i.e., $\dot{x_i} = \omega$, where $\omega \in \mathbb{R}_{>0}$ is the natural frequency of the oscillators. When x_i reaches 2π, oscillator i fires (emits a pulse) and resets x_i to 0, after which the cycle repeats. When a neighboring oscillator j receives the pulse from oscillator i, it shifts its phase according to its coupling strength $l_j \in (0,\ 1)$ (a scalar value) and its phase response function (PRF) F_j, which is defined below [1, 14, 26, 31, 54, 64].

Definition 2.11. *Phase response function (PRF) F_j of PCO j is defined as the phase shift (or jump) induced by a pulse as a function of phase at which the pulse is received.*

Therefore, the interaction mechanism of PCOs can be described as follows.

1. Each PCO has a phase variable $x_i \in [0,\ 2\pi]$ for each $i \in \mathcal{V}$. Each phase variable x_i evolves continuously towards 2π with its natural frequency ω;

2. When the phase variable x_i of PCO i reaches 2π, this PCO fires, i.e., emits a pulse, and simultaneously resets x_i to 0. Then the same process repeats;

3. When PCO j receives a pulse from neighboring PCO i, it updates its phase variable x_j according its coupling strength l_j and its PRF F_j:

$$x_j^+ = x_j + l_j F_j(x_j) \tag{2.2}$$

where x_j^+ denotes the phase of PCO j right after phase shift.

2.3.2 Hybrid Model and Dynamical Properties of PCO Networks

Due to the hybrid behavior of PCOs similar to [36, 109, 110], we model them as a hybrid system $\mathcal{H}$ with state $x = [x_1, \ldots, x_N]^T$. To this end, we define the flow set $\mathcal{C}$ and the flow map $f(x)$ as follows

$$\mathcal{C} = [0,\, 2\pi]^N, \quad f(x) = \omega \mathbf{1}_N \quad \forall\, x \in \mathcal{C} \tag{2.3}$$

According to [109, 110], the jump set $\mathcal{D}$ and the jump map $G(x)$ can be defined as the union of the individual jump sets $\mathcal{D}_i$ and individual jump maps $G_i(x)$, respectively

$$\mathcal{D} := \bigcup_{i \in \mathcal{V}} \mathcal{D}_i, \quad G(x) := \bigcup_{i \in \mathcal{V}: x \in \mathcal{D}_i} G_i(x) \tag{2.4}$$

where $\mathcal{D}_i$ is defined as $\mathcal{D}_i = \{x \in \mathcal{C} : x_i = 2\pi\}$ and $\forall\, x \in \mathcal{D}_i$, $G_i(x)$ is given by

$$G_i(x) = \{x^+ : x_i^+ = 0,\, x_j^+ \in x_j + w_{ij} F_j(x_j)\, \forall\, j \neq i\} \tag{2.5}$$

Note $w_{ij} = l_j \in (0,\, 1)$ if $j \in \mathcal{N}_i^{out}$; otherwise, $w_{ij} = 0$.

To make $\mathcal{H}$ an accurate description of PCOs, we make the following assumptions on the PRF F_j.

Assumption 2.1. *The graph of F_j for $j \in \mathcal{V}$ is such that* $\mathrm{graph}(F_j) \subseteq \{(x_j,\, y_j) : x_j \in [0,\, 2\pi], -x_j \leq y_j \leq 2\pi - x_j\}$.

This assumption ensures that $G(\mathcal{D}) \subset \mathcal{C} \cup \mathcal{D} = \mathcal{C}$ since $l_j \in (0,\, 1)$ holds, which avoids the existence of solutions ending in finite time due to jumping outside $\mathcal{C}$.

Assumption 2.2. *The PRF F_j for $j \in \mathcal{V}$ is an outer-semicontinuous set-valued map with $F_j(0) = F_j(2\pi) =$ 0.*

The constraint $F_j(0) = F_j(2\pi) = 0$ rules out discrete and eventually discrete solutions, meaning that PCOs will not fire continuously without rest [110, 111]. In fact, there are at most N consecutive jumps with no flow in between because an incoming pulse cannot trigger an oscillator who just fired to fire again under the constraint $F_j(0) = F_j(2\pi) = 0$.

The dynamical properties of $\mathcal{H}$ are characterized as follows.

Lemma 2.4. *Under Assumptions 2.1 and 2.2, we have*

1. *$\mathcal{H}$ satisfies the hybrid basic conditions in Definition 2.1;*

2. *For every initial condition $\xi \in \mathcal{C} \cup \mathcal{D} = \mathcal{C}$, there exists at least one nontrivial solution to $\mathcal{H}$. In particular, every solution $\phi \in \mathcal{S}_{\mathcal{H}}(\mathcal{C})$ is maximal, complete, and non-Zeno;*

3. *For every solution $\phi \in \mathcal{S}_{\mathcal{H}}(\mathcal{C})$, $\sup_j \operatorname{dom}\phi = \infty$ holds, which rules out the existence of continuous and eventually continuous solutions.*

Proof. First we prove statement 1. According to the hybrid model in (2.3)–(2.5), $\mathcal{C}$ and $\mathcal{D}$ are closed, and f is continuous and locally bounded on $\mathcal{C}$. Also G is locally bounded since the PRF F_j satisfies Assumption 2.1. To prove G is outer-semicontinuous on $\mathcal{D}$, it suffices to show that $\operatorname{graph}(G) = \bigcup_{i\in\mathcal{V}}\{(x,\, x^+) : x \in \mathcal{D}_i,\, x^+ \in G_i(x)\}$ is closed. According to [109–111], the outer-semicontinuity of F_j in Assumption 2.2 ensures that $\{(x,\, x^+) : x \in \mathcal{D}_i,\, x^+ \in G_i(x)\}$ is closed for $i \in \mathcal{V}$, and hence G is outer-semicontinuous on $\mathcal{D}$. Therefore, $\mathcal{H}$ satisfies the hybrid basic conditions in Definition 2.1.

Next we prove statement 2. Since $\mathcal{H}$ satisfies the hybrid basic conditions, according to Proposition 6.10 in [46], there exists at least one nontrivial solution to $\mathcal{H}$ for every initial condition $\xi \in \mathcal{C} \cup \mathcal{D} = \mathcal{C}$, and every solution $\phi \in \mathcal{S}_{\mathcal{H}}(\mathcal{C})$ is complete due to the facts that $G(\mathcal{D}) \subset \mathcal{C} \cup \mathcal{D} = \mathcal{C}$ holds and $\mathcal{C}$ is compact, which also implies that ϕ is maximal. Since $G(\mathcal{D}) \subset \mathcal{C}$ holds, we have $\operatorname{rge}\phi \subset \mathcal{C}$ for every $\phi \in \mathcal{S}_{\mathcal{H}}(\mathcal{C})$. So, according to Definition 2.2, $\mathcal{C}$ is strongly forward invariant. Since the constraint $F_j(0) = F_j(2\pi) = 0$ in Assumption 2.2 rules out complete discrete solutions, from Proposition 6.35 in [46] we have that $\mathcal{S}_{\mathcal{H}}(\mathcal{C})$ is uniformly non-Zeno, which means that every $\phi \in \mathcal{S}_{\mathcal{H}}(\mathcal{C})$ is non-Zeno.

Finally we prove statement 3. Since every $\phi \in \mathcal{S}_{\mathcal{H}}(\mathcal{C})$ is complete and the length of each flow interval is at most $\frac{2\pi}{\omega}$, we have $\sup_j \operatorname{dom}\phi = \infty$. So the existence of continuous and eventually continuous solutions is ruled out. ■

Remark 2.1. *As indicated in [109], such hybrid model $\mathcal{H}$ is able to handle multiple simultaneous pulses, i.e., if an oscillator receives multiple pulses simultaneously, it will respond to these pulses sequentially (in whatever order), but the oscillation behavior is the same as if the components of x jumped simultaneously.*

2.3.3 General Delay-Advance PRF

In this chapter, we consider general delay-advance PRFs.

Assumption 2.3. *A delay-advance PRF F_j is such that*

$$F_j(x_j) = \begin{cases} F_j^{(1)}(x_j), & \text{if } x_j \in [0,\, \pi) \\ \{F_j^{(1)}(\pi),\, F_j^{(2)}(\pi)\}, & \text{if } x_j = \pi \\ F_j^{(2)}(x_j), & \text{if } x_j \in (\pi,\, 2\pi] \end{cases} \tag{2.6}$$

where $F_j^{(1)}(x_j)$ and $F_j^{(2)}(x_j)$ are continuous functions on $[0,\, \pi]$ and $[\pi,\, 2\pi]$, respectively, and satisfy

$$\begin{cases} F_j^{(1)}(0) = 0,\ \ F_j^{(1)}(x_j) \in [-x_j,\, 0) \ \text{ if } \ x_j \in (0,\, \pi] \\ F_j^{(2)}(2\pi) = 0,\ F_j^{(2)}(x_j) \in (0,\, 2\pi - x_j] \ \text{ if } \ x_j \in [\pi,\, 2\pi) \end{cases} \tag{2.7}$$

Similar to [109–111], F_j is an outer-semicontinuous set-valued map. Note that oscillators with phases in $(0, \pi)$ will be delayed after receiving a pulse, meaning that their phases will be pushed closer to zero by each pulse received, whereas oscillators with phases in $(\pi, 2\pi)$ will be advanced, meaning that their phases will be pushed toward 2π by each pulse. If an oscillator has phase 0 (or 2π) upon receiving a pulse, its phase is unchanged by the pulse.

Since Assumption 2.3 implies Assumptions 2.1 and 2.2, the properties of $\mathcal{H}$ in Lemma 2.4 still hold. Several examples of delay-advance PRF are illustrated in Fig. 2.2.

Remark 2.2. *It is worth noting that our PRF can be heterogeneous and is also very general. In fact, it includes the PRFs used in [66, 109, 110, 157, 158, 160, 164] as special cases. Therefore, our work has broad potential applications in engineered systems [159] as well as biological systems [64].*

2.4 Global Synchronization of PCOs

In this section, we analyze global PCO synchronization on both chain and directed tree graphs, and provide robustness analysis in the presence of frequency perturbations.

To this end, we first define the synchronization set $\mathcal{A}$:

$$\mathcal{A} = \{x \in \mathcal{C} : |x_i - x_j| = 0 \,\text{or}\, |x_i - x_j| = 2\pi,\, \forall\, i,\, j \in \mathcal{V}\} \tag{2.8}$$

The PCO network synchronizes if the state x converges to the synchronization set $\mathcal{A}$. Note that $\mathcal{A}$ is compact since it is closed and bounded (included in $\mathcal{C}$ that is bounded).

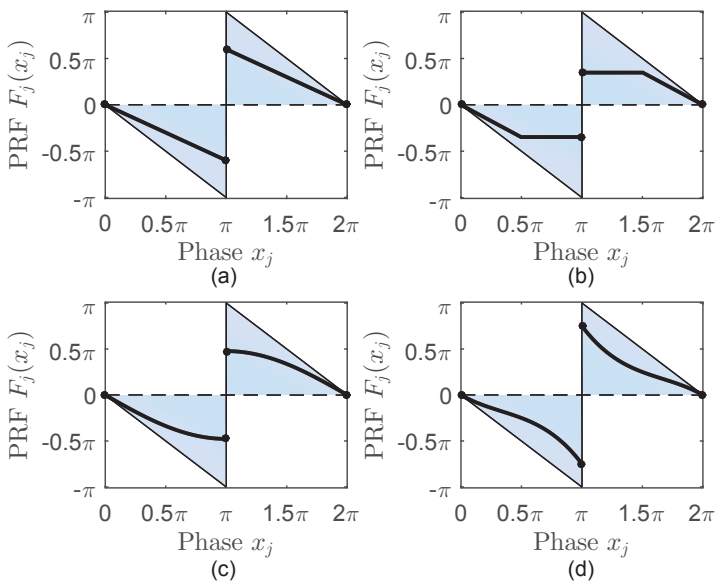

Figure 2.2: Examples of the general delay-advance PRF $F_j(x_j)$.

In the following, we refer to an arc as a connected subset of $[0,\ 2\pi]$ where 0 and 2π are associated with each other. So phase difference Δ_i that measures the length of the shorter arc between x_i and x_{i+1} on the unit cycle is given by

$$\Delta_i = \min\{|x_i - x_{i+1}|,\ 2\pi - |x_i - x_{i+1}|\} \tag{2.9}$$

where x_{N+1} is mapped to x_1 in Δ_N. It is straightforward to show that Δ_i satisfies $0 \leq \Delta_i \leq \pi$.

To measure the degree of synchronization, we define L as

$$L = \sum_{i=1}^{N} \Delta_i \tag{2.10}$$

Since $0 \leq \Delta_i \leq \pi$ holds, we have $0 \leq L \leq N\pi$. Note that both Δ_i for $i \in \mathcal{V}$ and L are dependent on x, and L is positive definite with respect to $\mathcal{A}$ on $\mathcal{C} \cup \mathcal{D} = \mathcal{C}$ because $L = 0$ holds if and only if $\Delta_1 = \Delta_2 = \cdots = \Delta_N = 0$ holds. Therefore, in order to prove synchronization, we only need to show that L will converge to 0. It is worth noting that L is continuous in $x \in \mathcal{C}$ but not differentiable with respect to it.

2.4.1 Global Synchronization on Undirected Chain Graphs

Lemma 2.5. *For N PCOs interacting on an undirected chain, if the PRF $F_j(x_j)$ satisfies Assumption 2.3 and $l_j \in (0,\, 1)$ holds for all $j \in \mathcal{V}$, then L in (2.10) is non-increasing along any solution $\phi \in \mathcal{S}_{\mathcal{H}}(\mathcal{C})$.*

Proof. Since there is no interaction among oscillators during flows and all oscillators have the same natural frequency, we have that L is constant during flows and its dynamics only depends on jumps. Without loss of generality, we assume that at time (t_i^*, k_i^*), we have $x(t_i^*, k_i^*) \in \mathcal{D}_i$, i.e., $x_i(t_i^*, k_i^*) = 2\pi$. (In the following, we omit time index (t_i^*, k_i^*) to simplify the notation.) When oscillator i fires and resets its phase to $x_i^+ = 0$, an oscillator $j \in \mathcal{N}_i^{out}$ has $x_j^+ \in x_j + l_j F_j(x_j)$ but an oscillator $j \notin \mathcal{N}_i^{out}$ still has $x_j^+ = x_j$.

For the undirected chain graph, we call oscillator $i-1$ as the left-neighbor of oscillator i for $i = 2, 3, \ldots, N$, and call oscillator $i+1$ as the right-neighbor of oscillator i for $i = 1, 2, \ldots, N-1$. Upon the firing of oscillator i, if the left-neighbor oscillator $i-1$ exists, it will update its phase and affect Δ_{i-2} and Δ_{i-1}. Note that for $i = 2$, Δ_{i-2} is mapped to Δ_N. Similarly, if the right-neighbor oscillator $i+1$ exists, Δ_i and Δ_{i+1} will be affected. No other Δ_ks will be affected by this pulse, i.e., $\Delta_k^+ = \Delta_k$ holds for $k \notin \{i-2, i-1, i, i+1\}$ where Δ_k^+ denotes the phase difference between oscillators k and $k+1$ after the jump. Therefore, we only need to consider two situations when oscillator i fires, i.e., how Δ_{i-2} and Δ_{i-1} change if the left-neighbor oscillator $i-1$ exists and how Δ_i and Δ_{i+1} change if the right-neighbor oscillator $i+1$ exists.

Situation I: If the left-neighbor oscillator $i-1$ exists, from (2.5) and (2.6) we have

$$x_{i-1}^+ = \begin{cases} x_{i-1} + l_{i-1} F_{i-1}^{(1)}(x_{i-1}), & \text{if } x_{i-1} \in [0,\, \pi] \\ x_{i-1} + l_{i-1} F_{i-1}^{(2)}(x_{i-1}), & \text{if } x_{i-1} \in [\pi,\, 2\pi] \end{cases} \tag{2.11}$$

To facilitate the proof, we use an nonnegative variable δ_{i-1} to denote the jump magnitude of oscillator $i-1$. According to (2.7) and $l_{i-1} \in (0,\, 1)$, δ_{i-1} is determined by

$$\delta_{i-1} = \begin{cases} -\, l_{i-1} F_{i-1}^{(1)}(x_{i-1}), & \text{if } x_{i-1} \in [0,\, \pi] \\ l_{i-1} F_{i-1}^{(2)}(x_{i-1}), & \text{if } x_{i-1} \in [\pi,\, 2\pi] \end{cases} \tag{2.12}$$

Since $x_i = 2\pi$ and $x_i^+ = 0$ hold, from (2.11) and (2.12) we know that oscillator $i-1$ jumps δ_{i-1} towards oscillator i, as illustrated in Fig. 2.3. So we have $\Delta_{i-1}^+ = \Delta_{i-1} - \delta_{i-1}$.

Now we analyze how Δ_{i-2} changes upon oscillator i's firing. Note that $x_{i-2}^+ = x_{i-2}$ holds as

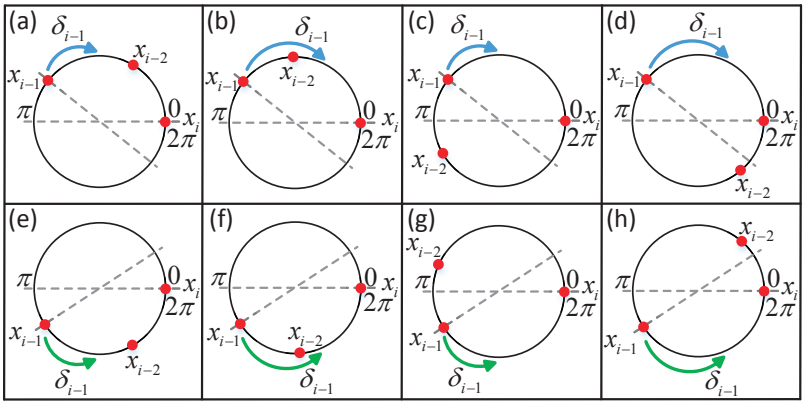

Figure 2.3: Illustration of Situation I.

$i-2 \notin \mathcal{N}_i^{out}$. According to the direction of oscillator $i-1$'s jump and the relationship between δ_{i-1} and Δ_{i-2}, we have four following cases:

Case 1: If oscillator $i-1$ jumps δ_{i-1} towards oscillator $i-2$ and $\delta_{i-1} \leq \Delta_{i-2}$ holds (cf. Fig. 2.3 (a) and (e)), we have $\Delta_{i-2}^+ = \Delta_{i-2} - \delta_{i-1}$, which leads to

$$\Delta_{i-1}^+ + \Delta_{i-2}^+ = \Delta_{i-1} + \Delta_{i-2} - 2\delta_{i-1} \leq \Delta_{i-1} + \Delta_{i-2} \tag{2.13}$$

Note that the equality holds if and only if $\delta_{i-1} = 0$ exists, i.e., $\Delta_{i-1}^+ + \Delta_{i-2}^+ = \Delta_{i-1} + \Delta_{i-2}$ holds if and only if $\Delta_{i-2}^+ = \Delta_{i-2} - \delta_{i-1} = \Delta_{i-2} + \delta_{i-1}$ holds.

Case 2: If oscillator $i-1$ jumps δ_{i-1} towards oscillator $i-2$ and $\delta_{i-1} > \Delta_{i-2}$ holds (cf. Fig. 2.3 (b) and (f)), we have $\Delta_{i-2}^+ = \delta_{i-1} - \Delta_{i-2}$. So it follows

$$\Delta_{i-1}^+ + \Delta_{i-2}^+ = \Delta_{i-1} - \Delta_{i-2} \leq \Delta_{i-1} + \Delta_{i-2} \tag{2.14}$$

where the equality occurs when $\Delta_{i-2} = 0$, i.e., $\Delta_{i-1}^+ + \Delta_{i-2}^+ = \Delta_{i-1} + \Delta_{i-2}$ holds if and only if $\Delta_{i-2}^+ = \delta_{i-1} - \Delta_{i-2} = \Delta_{i-2} + \delta_{i-1}$ holds.

Case 3: If oscillator $i-1$ jumps δ_{i-1} away from oscillator $i-2$ and $\Delta_{i-2} + \delta_{i-1} \leq \pi$ holds (cf. Fig. 2.3 (c) and (g)), we have $\Delta_{i-2}^+ = \Delta_{i-2} + \delta_{i-1}$, which leads to

$$\Delta_{i-1}^+ + \Delta_{i-2}^+ = \Delta_{i-1} + \Delta_{i-2} \tag{2.15}$$

Case 4: If oscillator $i-1$ jumps δ_{i-1} away from oscillator $i-2$ and $\Delta_{i-2} + \delta_{i-1} > \pi$ holds (cf.

Fig. 2.3 (d) and (h)), we have $\Delta_{i-2}^{+} = 2\pi - \Delta_{i-2} - \delta_{i-1} < \pi < \Delta_{i-2} + \delta_{i-1}$ and

$$\Delta_{i-1}^{+} + \Delta_{i-2}^{+} < (\Delta_{i-1} - \delta_{i-1}) + (\Delta_{i-2} + \delta_{i-1}) = \Delta_{i-1} + \Delta_{i-2} \tag{2.16}$$

Summarizing the above four cases, we have

$$\Delta_{i-1}^{+} + \Delta_{i-2}^{+} \leq \Delta_{i-1} + \Delta_{i-2} \tag{2.17}$$

where the equality occurs when $\Delta_{i-2}^{+} = \Delta_{i-2} + \delta_{i-1}$.

Situation II: If the right-neighbor oscillator $i+1$ exists, it will update its phase according to (2.5) and (2.6) as follows

$$x_{i+1}^{+} = \begin{cases} x_{i+1} + l_{i+1} F_{i+1}^{(1)}(x_{i+1}), & \text{if } x_{i+1} \in [0,\, \pi] \\ x_{i+1} + l_{i+1} F_{i+1}^{(2)}(x_{i+1}), & \text{if } x_{i+1} \in [\pi,\, 2\pi] \end{cases} \tag{2.18}$$

Also the nonnegative magnitude of oscillator $i+1$'s phase jump (denoted by δ_{i+1}) is given as

$$\delta_{i+1} = \begin{cases} -\, l_{i+1} F_{i+1}^{(1)}(x_{i+1}), & \text{if } x_{i+1} \in [0,\, \pi] \\ l_{i+1} F_{i+1}^{(2)}(x_{i+1}), & \text{if } x_{i+1} \in [\pi,\, 2\pi] \end{cases} \tag{2.19}$$

Since $x_i = 2\pi$ and $x_i^{+} = 0$ hold, and oscillator $i+1$ jumps δ_{i+1} towards oscillator i, we have $\Delta_i^{+} = \Delta_i - \delta_{i+1}$.

According to the relationship between δ_{i+1} and Δ_{i+1}, there are also four cases on the change of Δ_{i+1}. Similar to Situation I, we can obtain the following result

$$\Delta_i^{+} + \Delta_{i+1}^{+} \leq \Delta_i + \Delta_{i+1} \tag{2.20}$$

where the equality occurs when $\Delta_{i+1}^{+} = \Delta_{i+1} + \delta_{i+1}$.

Summarizing Situation I and Situation II, we can see that L will not increase during jumps. Therefore, L is non-increasing along any solution $\phi \in \mathcal{S}_{\mathcal{H}}(\mathcal{C})$. ■

Now we are in position to introduce our results for global synchronization on undirected chain graphs.

Theorem 2.1. *For N PCOs interacting on an undirected chain, if the PRF $F_j(x_j)$ satisfies Assumption 2.3*

and $l_j \in (0,\, 1)$ holds for all $j \in \mathcal{V}$, then the synchronization set $\mathcal{A}$ in (2.8) is globally asymptotically stable, i.e., global synchronization can be achieved from an arbitrary initial condition.

Proof. According to the derivation in Lemma 2.5, the continuous function L in (2.10) is constant during flows and will not increase during jumps, which implies that $L(g) - L(x) \leq 0$ holds for all $x \in \mathcal{D}$ and $g \in G(x)$. Defining $u_C(x) = 0$ for each $x \in \mathcal{C}$ and $u_C(x) = -\infty$ otherwise; $u_D(x) = \max_{g \in G(x)}\{L(g) - L(x)\} \leq 0$ for each $x \in \mathcal{D}$ and $u_D(x) = -\infty$ otherwise, we can bound the growth of L along solutions by u_C and u_D on $\mathcal{C}$ [46]. According to Lemma 2.4, every solution $\phi \in \mathcal{S}_{\mathcal{H}}(\mathcal{C})$ is precompact, i.e., complete and bounded, and satisfies $\overline{\operatorname{rge}\phi} \subset \mathcal{C} \cup \mathcal{D} = \mathcal{C}$. From Lemma 2.1, for some $r \in L(\mathcal{C}) = [0,\, N\pi]$, ϕ approaches the nonempty set that is the largest weakly invariant subset of $L^{-1}(r) \cap \mathcal{C} \cap \left[\overline{u_C^{-1}(0)} \cup \left(u_D^{-1}(0) \cap G(u_D^{-1}(0))\right)\right]$ where $L^{-1}(r)$ denotes the r-level set of L defined in Section 2.2.1 (note that Lemma 2.1 does not need L to be continuously differentiable in $x \in \mathcal{C}$ [46]). Since $\overline{u_C^{-1}(0)} = \mathcal{C}$ and $u_D^{-1}(0) \cap G(u_D^{-1}(0)) \subset \mathcal{D}$ hold, we have $L^{-1}(r) \cap \mathcal{C} \cap \left[\overline{u_C^{-1}(0)} \cup \left(u_D^{-1}(0) \cap G(u_D^{-1}(0))\right)\right] = L^{-1}(r) \cap \mathcal{C}$.

According to Lemma A.1 in Appendix A, L cannot be retained at any nonzero value along a complete solution ϕ. So the largest weakly invariant subset of $L^{-1}(r) \cap \mathcal{C}$ is empty for every $r \in (0,\, N\pi]$, which implies that every solution $\phi \in \mathcal{S}_{\mathcal{H}}(\mathcal{C})$ approaches $L^{-1}(0) \cap \mathcal{C} = \mathcal{A}$.

Next we show that $\mathcal{A}$ is locally asymptotically stable. Since every solution $\phi \in \mathcal{S}_{\mathcal{H}}(\mathcal{C})$ approaches $\mathcal{A}$, from Definition 2.4, $\mathcal{A}$ is uniformly attractive from $\mathcal{C}$. As Assumption 2.2 guarantees that $\operatorname{rge}\phi \subset \mathcal{A}$ for every $\phi \in \mathcal{S}_{\mathcal{H}}(\mathcal{A})$, $\mathcal{A}$ is strongly forward invariant according to Definition 2.2. Therefore, from Lemma 2.2, $\mathcal{A}$ is locally asymptotically stable.

To show $\mathcal{A}$ is globally asymptotically stable, it suffices to show that $\mathcal{A}$'s basin of attraction $\mathcal{B}_{\mathcal{A}}$ contains $\mathcal{C} \cup \mathcal{D} = \mathcal{C}$. Since we have shown that the largest weakly invariant subset of $L^{-1}(r) \cap \mathcal{C}$ is empty for every $r \in (0,\, N\pi]$ and every solution $\phi \in \mathcal{S}_{\mathcal{H}}(\mathcal{C})$ approaches $\mathcal{A}$, according to Definition 2.6, $\mathcal{A}$'s basin of attraction $\mathcal{B}_{\mathcal{A}}$ contains $\mathcal{C}$. Therefore, $\mathcal{A}$ is globally asymptotically stable.

In summary, $\mathcal{A}$ is globally asymptotically stable, meaning that global synchronization can be achieved from an arbitrary initial condition. ■

Remark 2.3. *Because using four phase differences (Δ_{i-2}, Δ_{i-1}, Δ_i, and Δ_{i+1}, which requires $N \geq 4$) is essential to describe and characterize the dynamics of a general number of N oscillators in a uniform manner, we assumed $N \geq 4$ in the proof. However, the results are also applicable to $N = 2$ and $N = 3$. In fact, following the analysis in Lemma 2.5, we can obtain that L is non-increasing when $N = 2$ or 3. Then using the Invariance Principle based derivation in Theorem 2.1 gives the convergence of L to 0 and thus the*

achievement of global synchronization for $N = 2$ and 3.

Remark 2.4. *Compared with existing results in [47] which show that local synchronization on chain graphs can be obtained as long as the coupling is not too strong, our results can guarantee global synchronization under any coupling strength between zero and one.*

Remark 2.5. *It is worth noting that different from local PCO synchronization analysis [47, 60] and global PCO synchronization analysis under all-to-all topology [15, 110] where the firing order is time-invariant, the coupling strength $l \in (0, 1)$ cannot guarantee invariant firing order in our considered scenarios, as confirmed by numerical simulations in Fig. 2.5.*

2.4.2 Global Synchronization on Directed Chain and Tree Graphs

In this subsection, we extend the global synchronization results to directed chain and tree graphs.

Theorem 2.2. *For N PCOs interacting on a directed chain, if the PRF $F_j(x_j)$ satisfies Assumption 2.3 and $l_j \in (0, 1)$ holds for all $j \in \mathcal{V}$, then the synchronization set $\mathcal{A}$ in (2.8) is globally asymptotically stable, i.e., global synchronization can be achieved from an arbitrary initial condition.*

Proof. The proof is similar to Theorem 2.1 and omitted. ■

Remark 2.6. *Different from the cycle graph in [109] where a strong enough coupling strength is required, global synchronization can be achieved here under any coupling strength between zero and one. This is because in the chain case, the absence of interaction between oscillators 1 and N allows Δ_N to increase freely until it triggers L to decrease; in other words, the absence of interaction between oscillators 1 and N breaks the symmetry of the chain graph [48], which is key to remove undesired equilibria where L keeps unchanged. In comparison, the symmetry of the cycle graph can make L stay at some undesired equilibria under a weak coupling strength. So a strong enough coupling strength is required in the cycle graph case to achieve global synchronization.*

Theorem 2.3. *For N PCOs interacting on a directed tree, if the PRF $F_j(x_j)$ satisfies Assumption 2.3 and $l_j \in (0, 1)$ holds for all $j \in \mathcal{V}$, then global synchronization can be achieved from an arbitrary initial condition.*

Proof. Suppose in a directed tree graph there are m nodes without any out-neighbors which are represented as $v_1, v_2, \ldots, v_m$. Take the graph in Fig. 2.1 (c) as an example, nodes 5, 8, 9, and 10 do not have any out-neighbors. According to Definition 2.10, for every node v_i ($i = 1, 2, \ldots, m$) there is a unique directed chain

from the root v_r to node v_i. So the directed tree graph is composed of m directed chains. Note that for every directed chain from the root v_r to node v_i, it is not affected by oscillators outside the chain. So the m directed chains are decoupled from each other. According to Theorem 2.2, global synchronization can be achieved on the directed chain from an arbitrary initial condition if $F_j(x_j)$ satisfies Assumption 2.3 and if $l_j \in (0,\, 1)$ holds. Adding the fact that the root oscillator v_r belongs to all m directed chains implies synchronization of all PCOs. ■

Remark 2.7. *Different from the arguments in the proofs of Theorems 2.2 and 2.3, an alternative approach to proving global synchronization on direct chain (and tree) graphs is using inductive reasoning based on the following two facts: first, a parent node can affect its child node but a child node never affects its parent node; secondly, under the given piecewise continuous delay-advance PRF (with values being nonzero in* $(0,\, 2\pi)$*), the phases of all oscillators on a directed chain will be reduced to within a half cycle, which always leads to synchronization (cf. Theorem 2 in [128]).*

Remark 2.8. *Different from the "probability-one synchronization" in [75, 76, 86] where oscillators synchronize with probability one under a stochastic phase-responding mechanism and the "almost global synchronization" in [18, 91, 95] where synchronization is guaranteed for all initial conditions except a set of Lebesgue-measure zero, our studied global synchronization is achieved in a deterministic manner from any initial condition, which is not only important theoretically but also mandatory in many safety-critical applications. A typical application justifying the necessity of deterministic global synchronization is synchronization based motion coordination of AUV (autonomous underwater vehicles) [119] and UAV (unmanned aerial vehicles) [152]. In such an application, even one single failure in synchronization might be too costly in money, time, energy, or even lives (cf. the multi-UAV based target engagement problem in [38]).*

2.4.3 Robustness Analysis for Frequency Perturbations

In this subsection, we analyze the robustness property of PCOs under small frequency perturbations on the natural frequency ω. It is worth noting that robustness is important since frequency perturbations are unavoidable and under an inappropriate synchronization mechanism, even a small difference in natural frequency may accumulate and lead to large phase differences. The hybrid systems model with frequency

perturbations is given as follows:

$$\mathcal{H}_p : \begin{cases} \dot{x} = \omega \mathbf{1}_N + p, & x \in \mathcal{C} \\ x^+ \in G(x), & x \in \mathcal{D} \end{cases} \tag{2.21}$$

where $p = [p_1, \ldots, p_N]^T$ represents the frequency perturbations. Using the notion of (τ, ε)-closeness given in Definition 2.7 in Section 2.2.2, we have the following result:

Theorem 2.4. *Consider N PCOs with frequency perturbations as described by $\mathcal{H}_p$ in (2.21). For every $\varepsilon > 0$, $\tau \geq 0$, and $\rho : \mathbb{R}^N \to \mathbb{R}_{\geq 0}$, there exists a scalar $\sigma > 0$ such that under any $p \in \sigma\rho(x)\mathbb{B}$ every solution ϕ_p to $\mathcal{H}_p$ from $\mathcal{C}$ is (τ, ε)-close to a solution ϕ to the perturbation-free dynamics $\mathcal{H}$.*

Proof. According to Lemma 2.4 in Section 2.3.2, $\mathcal{H}$ satisfies the hybrid basic conditions, and is pre-forward complete from the compact set $\mathcal{C}$ since every $\phi \in \mathcal{S}_{\mathcal{H}}(\mathcal{C})$ is complete (see Definition 2.3). So from Lemma 2.3, for every $\varepsilon > 0$, $\tau \geq 0$, and $\rho : \mathbb{R}^N \to \mathbb{R}_{\geq 0}$, there exists a scalar $\sigma > 0$ with the following property: for every solution ϕ_σ to $\mathcal{H}_{\sigma\rho}$ from $\mathcal{C}$, there exists a solution ϕ to $\mathcal{H}$ from $\mathcal{C}$ such that ϕ_σ and ϕ are (τ, ε)-close, where $\mathcal{H}_{\sigma\rho} = (\mathcal{C}, f_{\sigma\rho}, \mathcal{D}, G)$ is the $\sigma\rho$-perturbation of $\mathcal{H}$ and $f_{\sigma\rho}(x) = f(x) + \sigma\rho(x)\mathbb{B} = \omega \mathbf{1}_N + \sigma\rho(x)\mathbb{B}$ for every $x \in \mathcal{C}$. Note that if $p \in \sigma\rho(x)\mathbb{B}$, every solution ϕ_p to $\mathcal{H}_p$ from $\mathcal{C}$ is in fact the solution to $\mathcal{H}_{\sigma\rho}$, which implies that ϕ_p and ϕ are (τ, ε)-close. ■

According to Theorem 2.4, the behavior of perturbed PCOs is close to the perturbation-free case, i.e., the solutions to the perturbed PCOs converge to the neighborhood of the synchronization set $\mathcal{A}$. Therefore, the phases of oscillators will remain close to each other under small frequency perturbations.

2.5 Numerical Experiments

2.5.1 Unperturbed Case

We first considered the unperturbed case, i.e., all oscillators had an identical frequency $\omega = 2\pi$.

First we considered $N = 6$ PCOs on an undirected chain graph. Oscillators $1, \ldots, 6$ adopted the PRFs (a), (b), (c), (d), (a), and (b) in Fig. 2.2, respectively. The respective analytical expressions of these

PRFs are given below.

$$(a): F_j(x_j) = \begin{cases} -0.6x_j, & \text{if } x_j \in [0,\, \pi) \\ \{-0.6\pi,\, 0.6\pi\}, & \text{if } x_j = \pi \\ 0.6(2\pi - x_j), & \text{if } x_j \in (\pi,\, 2\pi] \end{cases} \tag{2.22}$$

$$(b): F_j(x_j) = \begin{cases} -0.7x_j, & \text{if } x_j \in [0,\, \frac{\pi}{2}) \\ -0.35\pi, & \text{if } x_j \in [\frac{\pi}{2},\, \pi) \\ \{-0.35\pi,\, 0.35\pi\}, & \text{if } x_j = \pi \\ 0.35\pi, & \text{if } x_j \in (\pi,\, \frac{3\pi}{2}] \\ 0.7(2\pi - x_j), & \text{if } x_j \in (\frac{3\pi}{2},\, 2\pi] \end{cases} \tag{2.23}$$

$$(c): F_j(x_j) = \begin{cases} -1.5\sin(0.5x_j), & \text{if } x_j \in [0,\, \pi) \\ \{-1.5,\, 1.5\}, & \text{if } x_j = \pi \\ 1.5\sin(0.5x_j), & \text{if } x_j \in (\pi,\, 2\pi] \end{cases} \tag{2.24}$$

$$(d): F_j(x_j) = \begin{cases} -x_j^3/\pi^2 + x_j^2/\pi - 0.75x_j, & \text{if } x_j \in [0,\, \pi) \\ \{-0.75\pi,\, 0.75\pi\}, & \text{if } x_j = \pi \\ -x_j^3/\pi^2 + 5x_j^2/\pi - 8.75x_j + 5.5\pi, & \text{if } x_j \in (\pi,\, 2\pi] \end{cases} \tag{2.25}$$

The coupling strength $l_1, \ldots, l_6$ were set to 0.4, 0.5, 0.6, 0.6, 0.5, and 0.4, respectively. The initial phase $x(0, 0)$ was randomly chosen from $\mathcal{C} \cup \mathcal{D}$. Fig. 2.4 shows the evolutions of phases and L. It can be seen that L converged to 0, which confirmed Theorem 2.1.

From the lower plot of Fig. 2.4, we can also see that the length of the shortest containing arc V_c, which is widely used as a Lyapunov function in local synchronization analysis [66, 110, 111, 128], is not appropriate for global PCO synchronization as it may not decrease monotonically. Along the same line, the firing order which is invariant in [15, 47, 60], and [110], is not constant in the considered dynamics as exemplified in Fig. 2.5. These unique properties of chain and directed tree PCOs corroborate the novelty and importance of our results.

Then we considered $N = 10$ PCOs on a directed tree graph, as illustrated in Fig. 2.1 (c). There are 4 directed chains in this graph, namely, oscillators $1 \to 2 \to 5$, oscillators $1 \to 2 \to 4 \to 8$, oscillators

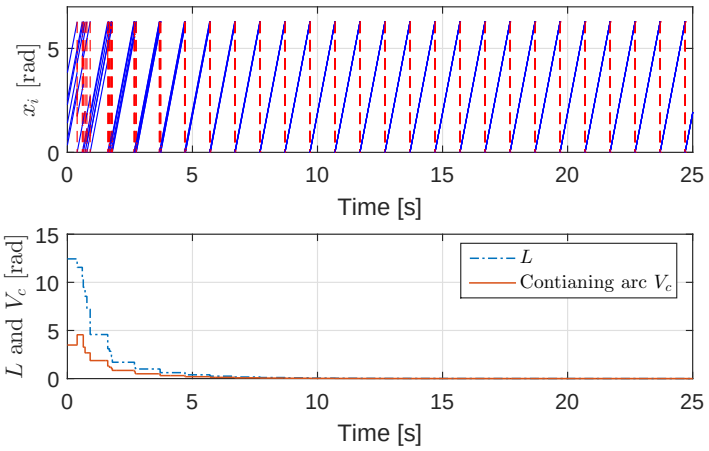

Figure 2.4: Evolutions of phases and L for PCOs on an undirected chain graph.

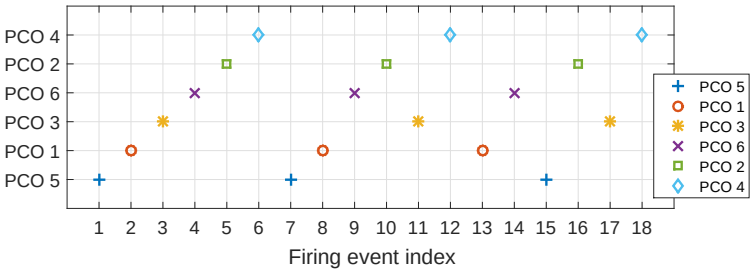

Figure 2.5: Firing order of PCOs on the undirected chain graph.

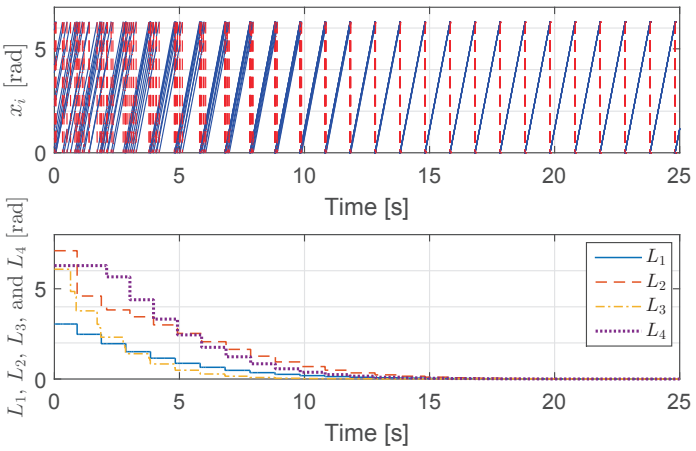

Figure 2.6: Evolutions of phases, L_1, L_2, L_3, and L_4 for PCOs on a directed tree graph. PCOs synchronized as L_1, L_2, L_3, and L_4 converged to 0.

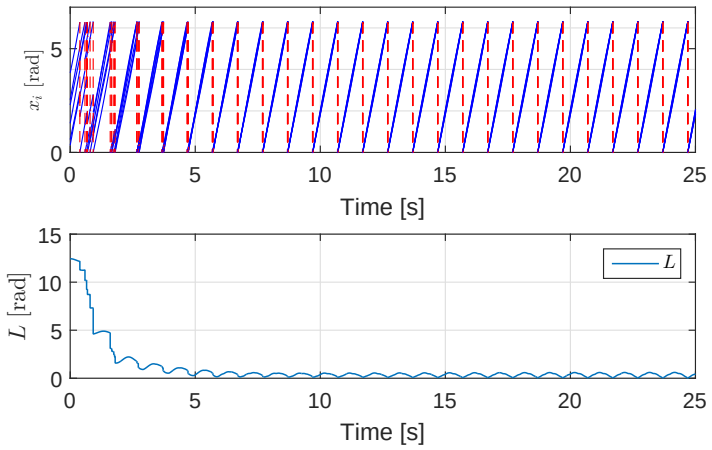

Figure 2.7: Evolutions of phases and L for PCOs on an undirected chain graph under frequency perturbations.

$1 \to 3 \to 6 \to 9$, and oscillators $1 \to 2 \to 4 \to 7 \to 10$. The same as (2.10), L_1, L_2, L_3, and L_4 were defined to measure the degree of synchronization corresponding to the 4 directed chains, respectively. Oscillators $1, \ldots, 10$ adopted the PRFs (a), (b), (c), (d), (a), (b), (c), (d), (a), and (b) in Fig. 2.2, respectively. The coupling strength $l_1, \ldots, l_{10}$ were set to 0.6, 0.5, 0.4, 0.6, 0.5, 0.4, 0.6, 0.5, 0.4, and 0.6, respectively. The initial phase $x(0, 0)$ was randomly chosen from $\mathcal{C} \cup \mathcal{D}$. The convergence of L_i $(i = 1, \ldots, 4)$ to zero in Fig. 2.6 implies the synchronization of the ith directed chain, which confirmed Theorem 2.2. The simultaneous synchronization of all four directed chains also means synchronization of the entire directed tree graph, which confirmed Theorem 2.3.

2.5.2 Perturbed Case

We considered $N = 6$ PCOs on an undirected chain graph with frequency perturbations on oscillator k set to $p_k = 0.5 \sin(2\pi t + 2\pi k/N)$. The other settings were the same as the undirected chain case. The evolutions of phases and L were shown in Fig. 2.7. It can be seen that the perturbed behaviors did not differ too much from the unperturbed case in Fig. 2.4, and the solution converged to a neighborhood of the synchronization set $\mathcal{A}$ as L approached a ball containing zero, which confirmed Theorem 2.4.

2.6 Summaries

In this chapter, we addressed global synchronization of PCOs interacting on chain and directed tree graphs. It was proven that PCOs can be synchronized from an arbitrary initial phase distribution under heterogeneous phase response functions (PRFs) and coupling strengths. The results are also applicable when oscillators are heterogeneous and subject to time-varying perturbations on their natural frequencies. Note that different from existing global synchronization results, the coupling strengths in our results can be freely chosen between zero and one, which is desirable since a very strong coupling strength, although can bring fast convergence, has been shown to be detrimental to the robustness of synchronization to disturbances. Given that a very weak coupling may not be desirable either due to low convergence speed which may allow disturbances to accumulate, the results give flexibility in meeting versatile requirements in practical PCO applications.

Chapter 3

Desynchronization of Pulse-Coupled Oscillators

3.1 Introduction

In this chapter, we consider desynchronization of pulse-coupled oscillators (PCOs), which spreads the phase variables of all PCOs uniformly apart (with equal difference between neighboring phases).

In the literature, based on the PCO model in [95], the authors in [113, 120, 123, 124] explored the performance of desynchronization algorithm (INVERSE-MS) using different frameworks. However, these results are about the achievement of uniform firing time interval (equal time interval between two consecutive firings), which is referred to as weak desynchronization [113, 120]. Weak desynchronization relies on persistent phase jumps to maintain equal firing intervals, and hence cannot guarantee a uniform spread of phases. Furthermore, it is sensitive to disturbances such as pulse loss and time delay because a lost or delayed pulse will directly lead to errors in the spread of firing time instants.

Recently, algorithms also emerged for phase desynchronization which is also referred to as strict desynchronization. Existing phase desynchronization algorithms can be divided into two categories based on the employed interaction mechanism. In the first mechanism, an oscillator adjusts its phase according to the firing information of its two immediate firing neighbors (the one fires before it and the one after). Typical examples include [12, 13, 23, 24, 82, 120, 142]. Since each oscillator only updates once during its cycle, such desynchronization algorithms tend to have very slow convergence rates, as confirmed by our numerical results

in Section 3.4.

The second mechanism is using phase response function (PRF) based interaction. In this mechanism, each oscillator will make phase adjustments every time it receives a pulse, and the adjustment is determined by the phase response function which describes the phase shift induced by a pulse. As in an all-to-all network with N PCOs, every oscillator will receive $N-1$ pulses when its phase evolves one cycle, and will make $N-1$ adjustments during its phase cycle, which significantly improves the convergence speed. Existing results [12, 13, 35, 36, 113] fall within this category.

In our work, we rigorously analyze the category of phase response function (PRF) based phase desynchronization algorithms. More specifically, we rigorously characterize the decentralized phase desynchronization process and propose a general phase-desynchronizing PRF that includes previous results as special cases. More interestingly, the proposed phase response function provides high robustness to pulse losses, time delays, and frequency errors which will significantly degrade the performance of all existing phase desynchronization approaches, as illustrated in the numerical simulation in Section 3.4. Furthermore, numerical simulations also show that the proposed PRF can significantly improve convergence speed compared with existing results.

The remainder of this chapter is organized as follows. In Section 3.2, we first review the PCO model, then we propose a general phase response function for phase desynchronization. Rigorous analysis of the convergence to desynchronization is provided in Section 3.3. In Section 3.4, the effectiveness and robustness properties of the proposed phase desynchronization algorithm are verified through numerical simulation results. Finally, we conclude this chapter in Section 3.5.

3.2 PCO Based Phase Desynchronization

In this section, we will first review the PCO model, and then we will propose a new phase response function for phase desynchronization.

3.2.1 PCO Model

We consider a network of N PCOs with an all-to-all communication pattern. Each oscillator has a phase variable $\phi_k \in \mathbb{S}^1$ ($k = 1, 2, \ldots, N$) where $\mathbb{S}^1$ denotes the one-dimensional torus. The interaction mechanism of PCOs can be described as follows:

1. Each PCO has a phase variable $\phi_k \in \mathbb{S}^1$ with initial value set to $\phi_k(0)$. ϕ_k evolves continuously from 0 to 2π with a constant speed (natural frequency) ω;

2. When the phase variable ϕ_k of PCO k reaches 2π, this PCO fires, i.e., emits a pulse, and simultaneously resets ϕ_k to 0. Then the same process repeats;

3. When a PCO receives a pulse from a neighboring PCO, it updates its phase variable according to the phase response function (PRF) $F(\phi_k)$:

$$\phi_k^+ = \phi_k + F(\phi_k) \tag{3.1}$$

where ϕ_k^+ and ϕ_k denote the phases of the kth oscillator after and before receiving the pulse, respectively.

3.2.2 Phase Response Function

It is already well-known that if the phase response function is chosen appropriately, pulse-coupled oscillators can achieve synchronization. For example, [157, 158] showed that using a delay-advance phase response function in which the value of phase shift is negative in the interval $(0, \pi]$, positive in the interval $(\pi, 2\pi)$, and zero at 0 and 2π, oscillator phases can achieve synchronization.

First, phase desynchronization is defined as follows:

Definition 3.1. *For a network of N oscillators, phase desynchronization denotes the state on which all phases are distributed evenly on the unit circle with identical differences $\frac{2\pi}{N}$ between two neighboring phases.*

As discussed earlier, in PCO networks, phase desynchronization is more stringent than weak desynchronization [113, 120] which uniformly spreads firing time instants of constituent oscillators. This is because weak desynchronization can be realized using persistent phase jumps (caused by pulse interactions), which are not permitted by phase desynchronization; whereas weak synchronization follows naturally if phase desynchronization is achieved.

We propose the following phase response function (PRF) $F(\phi_k)$:

$$F(\phi_k) = \begin{cases} -l_1(\phi_k - \dfrac{2\pi}{N}) & 0 < \phi_k < \dfrac{2\pi}{N} \\ 0 & \dfrac{2\pi}{N} \le \phi_k \le 2\pi - \dfrac{2\pi}{N} \\ -l_2(\phi_k - (2\pi - \dfrac{2\pi}{N})) & 2\pi - \dfrac{2\pi}{N} < \phi_k < 2\pi \end{cases} \tag{3.2}$$

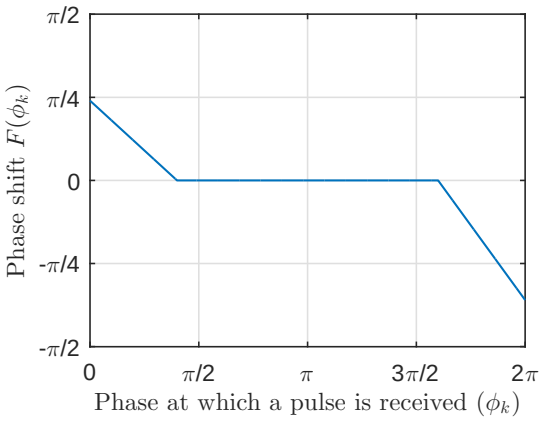

Figure 3.1: Proposed phase response function $F(\phi_k)$ in (3.2) for phase desynchronization ($N = 5$, $l_1 = 0.6$, and $l_2 = 0.9$).

where $0 \leq l_1 < 1$ and $0 \leq l_2 < 1$ denote the strengths of coupling (interaction). It is obvious that l_1 and l_2 can not be zero at the same time. According to this PRF, PCO k updates its phase variable ϕ_k (upon receiving a pulse) only when ϕ_k is within the interval $(0, \frac{2\pi}{N}) \cup (2\pi - \frac{2\pi}{N}, 2\pi)$ as illustrated in Fig. 3.1. Therefore, the phase update rule (3.1) for PCO k can be rewritten as:

$$\phi_k^+ = \begin{cases} (1-l_1)\phi_k + l_1\dfrac{2\pi}{N} & 0 < \phi_k < \dfrac{2\pi}{N} \\ \phi_k & \dfrac{2\pi}{N} \leq \phi_k \leq 2\pi - \dfrac{2\pi}{N} \\ (1-l_2)\phi_k + l_2(2\pi - \dfrac{2\pi}{N}) & 2\pi - \dfrac{2\pi}{N} < \phi_k < 2\pi \end{cases} \tag{3.3}$$

According to (3.3), $\phi_k^+ \in (0,\, 2\pi)$ is a monotonically increasing function of ϕ_k when ϕ_k resides in $(0,\, 2\pi)$, as shown in Fig. 3.2.

Remark 3.1. *Our proposed phase update rule (3.3) is more general than [113], which in fact is a special case of our phase update rule (3.3) by setting* $l_1 = 0$.

Remark 3.2. *The phase response function in (3.2) with* $l_1 > 0$ *allows non-zero interaction when oscillator phases are within the interval* $(0, \frac{2\pi}{N})$*, which is key to improve the robustness to time delays and contributes to a significant advantage over the results in [35, 36, 113, 120], as illustrated by numerical simulations in Fig.* 3.14.

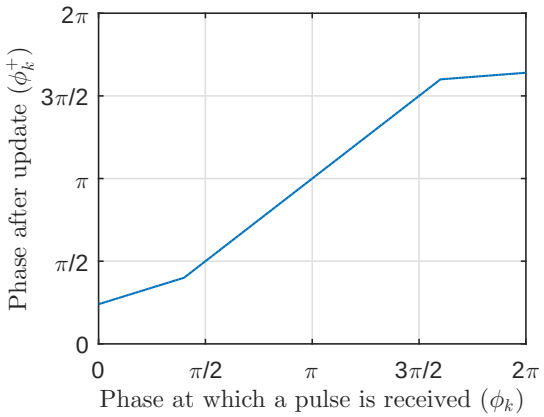

Figure 3.2: Proposed phase update rule in (3.3) for phase desynchronization ($N = 5$, $l_1 = 0.6$, and $l_2 = 0.9$).

3.3 Convergence Properties of the Proposed Phase Desynchronization Algorithm

In this section, we rigorously prove that the phase update rule (3.3) can guarantee phase desynchronization. To this end, we will first introduce Lemma 3.1 on the firing order of PCOs.

Lemma 3.1. *For a network of N PCOs with no two PCOs having equal initial phases, the firing order of PCOs is time-invariant under the phase update rule (3.3), i.e., if at any time instant t, we have $0 < \phi_{i_1} < \phi_{i_2} < \cdots < \phi_{i_N} \leq 2\pi$ for some sequence of nonrepeated elements $\{i_1, i_2, \ldots, i_N\}$ of $I = \{1, 2, \ldots, N\}$ (i.e., a reordering of the elements of I), then after N pulses, $0 < \phi_{i_1} < \phi_{i_2} < \cdots < \phi_{i_N} \leq 2\pi$ still holds.*

Proof. Assume that at any time instant t, the phases satisfy the following relationship $0 < \phi_{i_1} < \phi_{i_2} < \cdots < \phi_{i_N} \leq 2\pi$. Since ϕ_{i_N} is the largest, it will reach 2π first and send a pulse that will be received by all the other PCOs. After receiving this pulse, all the other PCOs update their phases according to the phase update rule (3.3). Since $\phi_k^+ \in (0,\, 2\pi)$ is a monotonically increasing function of ϕ_k when ϕ_k resides in $(0,\, 2\pi)$, we have $0 = \phi_{i_N} < \phi_{i_1} < \cdots < \phi_{i_{N-1}} < 2\pi$ after this update. Following the same line of reasoning, it follows that after N pulses, $0 < \phi_{i_1} < \phi_{i_2} < \cdots < \phi_{i_N} \leq 2\pi$ holds, which means that the firing order of PCOs is time-invariant. ■

In order to rigorously analyze the convergence process, we also need a measure to quantify the degree of achievement of desynchronization. Without loss of generality, we denote the initial time instant as $t = 0$ and assume at this time instant the phases of PCOs are arranged in a way such that $\phi_1(0) > \phi_2(0) > \ldots > \phi_N(0)$ holds, as illustrated in Fig. 3.3. (Note that here we assume that no two PCOs' initial phases are

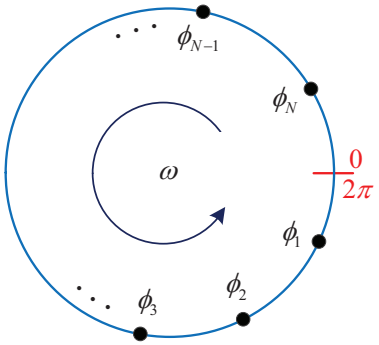

Figure 3.3: Initially (at $t = 0$), the phases of PCOs are arranged in a way such that $\phi_1(0) > \phi_2(0) > \ldots > \phi_N(0)$ holds.

equal.) From Lemma 3.1, we know that the firing order of PCOs will not be affected by the pulse-induced update. So if ϕ_k is the immediate follower (anti-clockwisely) of ϕ_{k-1} on the unit circle $\mathbb{S}^1$ at $t = 0$, it will always be the immediate follower (anti-clockwisely) of ϕ_{k-1} on $\mathbb{S}^1$. Therefore, the phase differences between neighboring PCOs (in terms of phase) can always be expressed as:

$$\begin{cases} \Delta_k = (\phi_k - \phi_{k+1}) \bmod 2\pi, \quad k = 1, 2, \ldots, N-1 \\ \Delta_N = (\phi_N - \phi_1) \bmod 2\pi \end{cases} \tag{3.4}$$

According to Definition 3.1, phase desynchronization implies that the phase differences between neighboring (in terms of phase) oscillators are equal to $\frac{2\pi}{N}$. Therefore, in order to quantify the degree of achievement of phase desynchronization, we introduce a measure P based on phase differences as follows:

$$P \triangleq \sum_{k=1}^{N} |\Delta_k - \frac{2\pi}{N}| \tag{3.5}$$

When phase desynchronization is achieved, the phase differences between neighboring PCOs are equal to $\frac{2\pi}{N}$, so P in (3.5) will reach its minimum 0. It can also be easily verified that P equals 0 only when phase desynchronization is achieved.

Therefore, from the relationship between phase desynchronization and P, to prove the achievement of phase desynchronization, we need to prove that P will converge to 0. Since P will not change between two consecutive pulses, we only need to concentrate on firing events.

To analyze the changes of P caused by firing events (or pulses), we define "active pulse" and "silent pulse" as follows:

Definition 3.2. *A pulse is called an "active pulse" if there exists at least one $k \in \{1, 2, \ldots, N\}$ such that $\phi_k \in (0,\ \frac{2\pi}{N}) \cup (2\pi - \frac{2\pi}{N},\ 2\pi)$ holds when the pulse is emitted.*

Definition 3.3. *A pulse is called a "silent pulse" if there does not exist any $k \in \{1, 2, \ldots, N\}$ such that $\phi_k \in (0,\ \frac{2\pi}{N}) \cup (2\pi - \frac{2\pi}{N},\ 2\pi)$ holds when the pulse is emitted.*

According to Definition 3.2 and Definition 3.3, a pulse is either a "silent pulse" or an "active pulse." Since no oscillator phases reside in $(0,\ \frac{2\pi}{N}) \cup (2\pi - \frac{2\pi}{N},\ 2\pi)$ when a "silent pulse" is emitted, no phase variables are affected according to (3.2). Therefore, a "silent pulse" will not affect phase differences and the measure P. Similarly, an "active pulse" may change the measure P since the phase variables residing in $(0,\ \frac{2\pi}{N}) \cup (2\pi - \frac{2\pi}{N},\ 2\pi)$ will be affected by the pulse-induced update.

Next we will introduce Lemma 3.2 on the lack of existence of N consecutive "silent pulses" before achieving phase desynchronization.

Lemma 3.2. *For a network of N PCOs with no two PCOs having equal initial phases, there cannot be N consecutive "silent pulses" unless phase desynchronization is achieved.*

Proof. We use proof of contradiction. Assume that N consecutive pulses are all "silent pulses" but phase desynchronization has not been achieved. From Lemma 3.1, the firing order of oscillators is time-invariant, so the N consecutive pulses must be from N different oscillators. For a pulse from oscillator i to be a "silent pulse," the phase variable of the oscillator who sends a pulse immediately before oscillator i must be no less than $\frac{2\pi}{N}$, and the phase variable of the oscillator who sends a pulse immediately after oscillator i must be no greater than $2\pi - \frac{2\pi}{N}$, which means that the phases of all the other oscillators are outside $(0,\ \frac{2\pi}{N}) \cup (2\pi - \frac{2\pi}{N},\ 2\pi)$. Therefore, for the N consecutive "silent pulses," the phase differences between any two neighboring phases are no less than $\frac{2\pi}{N}$. Given that the sum of all phase differences has to be 2π, we have all phase differences being equal to $\frac{2\pi}{N}$, meaning that phase desynchronization is achieved, which contradicts the initial assumption. Therefore, there cannot be N consecutive "silent pulses" unless phase desynchronization is achieved. ■

Using Lemma 3.2, the existence of "active pulses" before achieving phase desynchronization can be guaranteed. Further taking into account the fact that only "active pulses" may change P, we can infer that the evolution of P only depends on the changes caused by "active pulses."

Now, we introduce our main result.

Theorem 3.1. *For a network of N PCOs with no two PCOs having equal initial phases, the PCOs will achieve phase desynchronization if the phase response function $F(\phi_k)$ is given by (3.2) for $0 < l_1 < 1$ and $0 < l_2 < 1$.*

Proof. In order to prove the achievement of phase desynchronization, we need to prove that P will converge to 0. Further taking into account the fact that the evolution of P only depends on "active pulses," without loss of generality, we assume that oscillator k emits an "active pulse" at time instant $t = t_k$. According to Definition 3.2, there is at least one phase variable within $(0, \frac{2\pi}{N}) \cup (2\pi - \frac{2\pi}{N}, 2\pi)$ when the pulse is sent. Without loss of generality, we assume that there are M phase variables within $(0, \frac{2\pi}{N})$ and S phase variables within $(2\pi - \frac{2\pi}{N}, 2\pi)$, where M and S are positive integers satisfying $2 \leq M + S \leq N - 1$. The M and S phase variables are represented as $\phi_{\widehat{k-1}}, \ldots, \phi_{\widehat{k-M}}$ and $\phi_{\widehat{k+1}}, \ldots, \phi_{\widehat{k+S}}$, respectively, where the superscript "$\widehat{\ }$" represents modulo operation on N, i.e., $\widehat{\bullet} \triangleq (\bullet) \bmod N$, as illustrated in Fig. 3.4. According to the assumption, we have $\phi_{\widehat{k-M}} < \frac{2\pi}{N} \leq \phi_{\widehat{k-M-1}}$ and $\phi_{\widehat{k+S+1}} \leq 2\pi - \frac{2\pi}{N} < \phi_{\widehat{k+S}}$. Since $\phi_{\widehat{k-1}}, \ldots, \phi_{\widehat{k-M}}$ and $\phi_{\widehat{k+1}}, \ldots, \phi_{\widehat{k+S}}$ reside in $(0, \frac{2\pi}{N}) \cup (2\pi - \frac{2\pi}{N}, 2\pi)$, they will update their values after receiving the pulse from oscillator k according to the phase update rule in (3.3) as follows:

$$\begin{cases} \phi^+_{\widehat{k-i}} = (1 - l_1)\phi_{\widehat{k-i}} + l_1 \dfrac{2\pi}{N}, & i = 1, \ldots, M \\ \phi^+_{\widehat{k+j}} = (1 - l_2)\phi_{\widehat{k+j}} + l_2(2\pi - \dfrac{2\pi}{N}), & j = 1, \ldots, S \end{cases} \tag{3.6}$$

Note that we also have $\phi^+_k = 0$ and $\phi^+_{\widehat{k+q}} = \phi_{\widehat{k+q}}$ for $q = S + 1, \ldots, N - M - 1$ (because $\phi_{\widehat{k+q}}$ for $q = S + 1, \ldots, N - M - 1$ reside in $[\frac{2\pi}{N}, 2\pi - \frac{2\pi}{N}]$ and thus will not be changed according to the PRF in (3.2)).

According to (3.4) and (3.6), phase differences after the update caused by the "active pulse" from

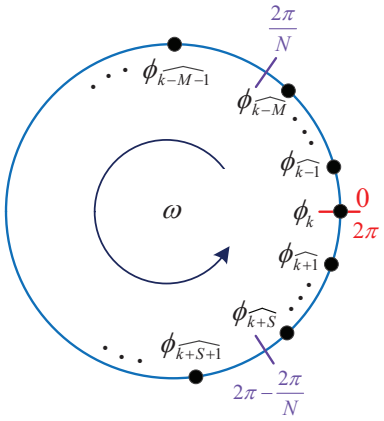

Figure 3.4: The phase variables $\phi_{\widehat{k-1}}, \ldots, \phi_{\widehat{k-M}}$ and $\phi_{\widehat{k+1}}, \ldots, \phi_{\widehat{k+S}}$ reside in $(0, \frac{2\pi}{N}) \cup (2\pi - \frac{2\pi}{N}, 2\pi)$ when oscillator k sends the first "active pulse" at $t = t_k$.

oscillator k are given by:

$$\begin{cases} \Delta^+_{\widehat{k-M-1}} = \phi^+_{\widehat{k-M-1}} - \phi^+_{\widehat{k-M}} = \phi_{\widehat{k-M-1}} - (1-l_1)\phi_{\widehat{k-M}} - l_1\dfrac{2\pi}{N} \\ \Delta^+_{\widehat{k-i}} = \phi^+_{\widehat{k-i}} - \phi^+_{\widehat{k-i+1}} = (1-l_1)(\phi_{\widehat{k-i}} - \phi_{\widehat{k-i+1}}),\ i = 2, \ldots, M \\ \Delta^+_{\widehat{k-1}} = \phi^+_{\widehat{k-1}} - \phi^+_k = (1-l_1)\phi_{\widehat{k-1}} + l_1\dfrac{2\pi}{N} \\ \Delta^+_k = \phi^+_k - \phi^+_{\widehat{k+1}} + 2\pi = 2\pi - (1-l_2)\phi_{\widehat{k+1}} - l_2(2\pi - \dfrac{2\pi}{N}) \\ \Delta^+_{\widehat{k+j}} = \phi^+_{\widehat{k+j}} - \phi^+_{\widehat{k+j+1}} = (1-l_2)(\phi_{\widehat{k+j}} - \phi_{\widehat{k+j+1}}),\ j = 1, \ldots, S-1 \\ \Delta^+_{\widehat{k+S}} = \phi^+_{\widehat{k+S}} - \phi^+_{\widehat{k+S+1}} = (1-l_2)\phi_{\widehat{k+S}} + l_2(2\pi - \dfrac{2\pi}{N}) - \phi_{\widehat{k+S+1}} \\ \Delta^+_{\widehat{k+q}} = \phi^+_{\widehat{k+q}} - \phi^+_{\widehat{k+q+1}} = \phi_{\widehat{k+q}} - \phi_{\widehat{k+q+1}},\ q = S+1, \ldots, N-M-2 \end{cases} \tag{3.7}$$

Then the new P (denote it as P^+) after the update is given by:

$$P^+ = \sum_{k=1}^{N} |\Delta^+_k - \frac{2\pi}{N}| \tag{3.8}$$

To show the change of measure P caused by the "active pulse" from oscillator k, we calculate the difference of P before and after the pulse-induced update:

$$P^+ - P = \sum_{k=1}^{N} |\Delta^+_k - \frac{2\pi}{N}| - \sum_{k=1}^{N} |\Delta_k - \frac{2\pi}{N}| \tag{3.9}$$

Therefore, $P^+ - P$ can be divided into 7 parts as follows:

$$\begin{aligned}
P^+ - P =& \sum_{k=1}^{N} |\Delta_k^+ - \frac{2\pi}{N}| - \sum_{k=1}^{N} |\Delta_k - \frac{2\pi}{N}| \\
=& \underbrace{|\Delta^+_{\widehat{k-M-1}} - \frac{2\pi}{N}| - |\Delta_{\widehat{k-M-1}} - \frac{2\pi}{N}|}_{\textbf{Part 1}} + \underbrace{\sum_{i=2}^{M} |\Delta^+_{\widehat{k-i}} - \frac{2\pi}{N}| - \sum_{i=2}^{M} |\Delta_{\widehat{k-i}} - \frac{2\pi}{N}|}_{\textbf{Part 2}} \\
&+ \underbrace{|\Delta^+_{\widehat{k-1}} - \frac{2\pi}{N}| - |\Delta_{\widehat{k-1}} - \frac{2\pi}{N}|}_{\textbf{Part 3}} + \underbrace{|\Delta_k^+ - \frac{2\pi}{N}| - |\Delta_k - \frac{2\pi}{N}|}_{\textbf{Part 4}} \\
&+ \underbrace{\sum_{j=1}^{S-1} |\Delta^+_{\widehat{k+j}} - \frac{2\pi}{N}| - \sum_{j=1}^{S-1} |\Delta_{\widehat{k+j}} - \frac{2\pi}{N}|}_{\textbf{Part 5}} + \underbrace{|\Delta^+_{\widehat{k+S}} - \frac{2\pi}{N}| - |\Delta_{\widehat{k+S}} - \frac{2\pi}{N}|}_{\textbf{Part 6}} \\
&+ \underbrace{\sum_{q=S+1}^{N-M-2} |\Delta^+_{\widehat{k+q}} - \frac{2\pi}{N}| - \sum_{q=S+1}^{N-M-2} |\Delta_{\widehat{k+q}} - \frac{2\pi}{N}|}_{\textbf{Part 7}}
\end{aligned} \tag{3.10}$$

Part 2, **Part 3**, **Part 4**, **Part 5**, and **Part 7** in (3.10) can be simplified as follows:

$$\begin{aligned}
\textbf{Part 2} =& \sum_{i=2}^{M} \big\{ |(1-l_1)(\phi_{\widehat{k-i}} - \phi_{\widehat{k-i+1}}) - \frac{2\pi}{N}| - |(\phi_{\widehat{k-i}} - \phi_{\widehat{k-i+1}}) - \frac{2\pi}{N}| \big\} \\
=& \sum_{i=2}^{M} \big\{ \frac{2\pi}{N} - (1-l_1)(\phi_{\widehat{k-i}} - \phi_{\widehat{k-i+1}}) - \frac{2\pi}{N} + (\phi_{\widehat{k-i}} - \phi_{\widehat{k-i+1}}) \big\} \\
=& l_1(\phi_{\widehat{k-M}} - \phi_{\widehat{k-1}})
\end{aligned} \tag{3.11}$$

where we used the relationships $\phi_{\widehat{k-i}} - \phi_{\widehat{k-i+1}} < \frac{2\pi}{N}$ and $(1-l_1)(\phi_{\widehat{k-i}} - \phi_{\widehat{k-i+1}}) < \frac{2\pi}{N}$ for $i = 2, \ldots, M$ as $0 < l_1 < 1$.

$$\begin{aligned}
\textbf{Part 3} =& |(1-l_1)\phi_{\widehat{k-1}} + l_1\frac{2\pi}{N} - \frac{2\pi}{N}| - |\phi_{\widehat{k-1}} - \frac{2\pi}{N}| \\
=& (1-l_1)(\frac{2\pi}{N} - \phi_{\widehat{k-1}}) - (\frac{2\pi}{N} - \phi_{\widehat{k-1}}) \\
=& -l_1(\frac{2\pi}{N} - \phi_{\widehat{k-1}})
\end{aligned} \tag{3.12}$$

In the above derivation we used $\phi_{\widehat{k-1}} < \frac{2\pi}{N}$.

$$\begin{aligned}\textbf{Part 4} =&|2\pi - (1-l_2)\phi_{\widehat{k+1}} - l_2(2\pi - \frac{2\pi}{N}) - \frac{2\pi}{N}| - |2\pi - \phi_{\widehat{k+1}} - \frac{2\pi}{N}| \\ =&\frac{2\pi}{N} - 2\pi + (1-l_2)\phi_{\widehat{k+1}} + l_2(2\pi - \frac{2\pi}{N}) - \frac{2\pi}{N} + 2\pi - \phi_{\widehat{k+1}} \\ =&l_2(2\pi - \frac{2\pi}{N} - \phi_{\widehat{k+1}})\end{aligned} \tag{3.13}$$

where we used the inequalities $2\pi - \phi_{\widehat{k+1}} < \frac{2\pi}{N}$ and $2\pi - (1-l_2)\phi_{\widehat{k+1}} - l_2(2\pi - \frac{2\pi}{N}) < \frac{2\pi}{N}$ due to $0 < l_2 < 1$.

$$\begin{aligned}\textbf{Part 5} =& \sum_{j=1}^{S-1} \big\{|(1-l_2)(\phi_{\widehat{k+j}} - \phi_{\widehat{k+j+1}}) - \frac{2\pi}{N}| - |(\phi_{\widehat{k+j}} - \phi_{\widehat{k+j+1}}) - \frac{2\pi}{N}|\big\} \\ =& \sum_{j=1}^{S-1} \big\{\frac{2\pi}{N} - (1-l_2)(\phi_{\widehat{k+j}} - \phi_{\widehat{k+j+1}}) - \frac{2\pi}{N} + (\phi_{\widehat{k+j}} - \phi_{\widehat{k+j+1}})\big\} \\ =& l_2(\phi_{\widehat{k+1}} - \phi_{\widehat{k+S}})\end{aligned} \tag{3.14}$$

where we used the relationships $\phi_{\widehat{k+j}} - \phi_{\widehat{k+j+1}} < \frac{2\pi}{N}$ and $(1-l_2)(\phi_{\widehat{k+j}} - \phi_{\widehat{k+j+1}}) < \frac{2\pi}{N}$ for $j = 1, \ldots, S-1$ because of $0 < l_2 < 1$.

$$\textbf{Part 7} = \sum_{q=S+1}^{N-M-2} \big\{|\phi_{\widehat{k+q}} - \phi_{\widehat{k+q+1}} - \frac{2\pi}{N}| - |\phi_{\widehat{k+q}} - \phi_{\widehat{k+q+1}} - \frac{2\pi}{N}|\big\} = 0 \tag{3.15}$$

Combining (3.9)-(3.15) leads to:

$$\begin{aligned}&P^+ - P \\ =& \underbrace{|\Delta^+_{\widehat{k-M-1}} - \frac{2\pi}{N}| - |\Delta_{\widehat{k-M-1}} - \frac{2\pi}{N}| + l_1(\phi_{\widehat{k-M}} - \frac{2\pi}{N})}_{\textbf{Part A}} \\ +& \underbrace{|\Delta^+_{\widehat{k+S}} - \frac{2\pi}{N}| - |\Delta_{\widehat{k+S}} - \frac{2\pi}{N}| + l_2(2\pi - \frac{2\pi}{N} - \phi_{\widehat{k+S}})}_{\textbf{Part B}}\end{aligned} \tag{3.16}$$

Next, we discuss the value of **Part A** in (3.16) under three different cases:

Case 1': If $\Delta_{\widehat{k-M-1}} > \frac{2\pi}{N}$ and $\Delta^{+}_{\widehat{k-M-1}} \geq \frac{2\pi}{N}$ hold, **Part A** in (3.16) can be rewritten as:

$$\begin{aligned}
\textbf{Part A} &= \Delta^{+}_{\widehat{k-M-1}} - \Delta_{\widehat{k-M-1}} + l_1(\phi_{\widehat{k-M}} - \frac{2\pi}{N}) \\
&= \phi_{\widehat{k-M-1}} - (1-l_1)\phi_{\widehat{k-M}} - l_1\frac{2\pi}{N} - \phi_{\widehat{k-M-1}} + \phi_{\widehat{k-M}} + l_1(\phi_{\widehat{k-M}} - \frac{2\pi}{N}) \\
&= 2l_1(\phi_{\widehat{k-M}} - \frac{2\pi}{N}) \\
&< 0
\end{aligned} \tag{3.17}$$

Case 2': If $\Delta_{\widehat{k-M-1}} > \frac{2\pi}{N}$ and $\Delta^{+}_{\widehat{k-M-1}} < \frac{2\pi}{N}$ hold, we have $\phi_{\widehat{k-M}} - \phi_{\widehat{k-M-1}} + \frac{2\pi}{N} < 0$. Then **Part A** in (3.16) can be rewritten as:

$$\begin{aligned}
\textbf{Part A} &= \frac{2\pi}{N} - \Delta^{+}_{\widehat{k-M-1}} - \Delta_{\widehat{k-M-1}} + \frac{2\pi}{N} + l_1(\phi_{\widehat{k-M}} - \frac{2\pi}{N}) \\
&= \frac{2\pi}{N} - \phi_{\widehat{k-M-1}} + (1-l_1)\phi_{\widehat{k-M}} + l_1\frac{2\pi}{N} - \phi_{\widehat{k-M-1}} + \phi_{\widehat{k-M}} + \frac{2\pi}{N} + l_1(\phi_{\widehat{k-M}} - \frac{2\pi}{N}) \\
&= 2(\phi_{\widehat{k-M}} - \phi_{\widehat{k-M-1}} + \frac{2\pi}{N}) \\
&< 0
\end{aligned} \tag{3.18}$$

Case 3': If $\Delta_{\widehat{k-M-1}} \leq \frac{2\pi}{N}$ and $\Delta^{+}_{\widehat{k-M-1}} < \frac{2\pi}{N}$ hold, **Part A** in (3.16) can be rewritten as:

$$\begin{aligned}
\textbf{Part A} &= -\Delta^{+}_{\widehat{k-M-1}} + \Delta_{\widehat{k-M-1}} + l_1(\phi_{\widehat{k-M}} - \frac{2\pi}{N}) \\
&= -\phi_{\widehat{k-M-1}} + (1-l_1)\phi_{\widehat{k-M}} + l_1\frac{2\pi}{N} + \phi_{\widehat{k-M-1}} - \phi_{\widehat{k-M}} + l_1(\phi_{\widehat{k-M}} - \frac{2\pi}{N}) \\
&= 0
\end{aligned} \tag{3.19}$$

According to (3.2), we cannot have a fourth case where $\Delta_{\widehat{k-M-1}} \leq \frac{2\pi}{N}$ and $\Delta^{+}_{\widehat{k-M-1}} \geq \frac{2\pi}{N}$ hold because of the following constraint:

$$\begin{aligned}
\Delta^{+}_{\widehat{k-M-1}} - \Delta_{\widehat{k-M-1}} =& \phi_{\widehat{k-M-1}} - (1-l_1)\phi_{\widehat{k-M}} - l_1\frac{2\pi}{N} - \phi_{\widehat{k-M-1}} + \phi_{\widehat{k-M}} \\
=& l_1(\phi_{\widehat{k-M}} - \frac{2\pi}{N}) \\
<& 0
\end{aligned} \tag{3.20}$$

It is worth noting that in (3.20) we used the initial assumption $\phi_{\widehat{k-M}} < \frac{2\pi}{N}$ and the inequality $0 < l_1 < 1$.

Similarly, we also discuss the value of **Part B** in (3.16) under three different cases:

Case 1": If $\Delta_{\widehat{k+S}} > \frac{2\pi}{N}$ and $\Delta^{+}_{\widehat{k+S}} \geq \frac{2\pi}{N}$ hold, **Part B** in (3.16) can be rewritten as:

$$\begin{aligned}\textbf{Part B} &= \Delta^{+}_{\widehat{k+S}} - \Delta_{\widehat{k+S}} + l_2(2\pi - \frac{2\pi}{N} - \phi_{\widehat{k+S}}) \\ &= (1-l_2)\phi_{\widehat{k+S}} + l_2(2\pi - \frac{2\pi}{N}) - \phi_{\widehat{k+S+1}} - \phi_{\widehat{k+S}} + \phi_{\widehat{k+S+1}} + l_2(2\pi - \frac{2\pi}{N} - \phi_{\widehat{k+S}}) \\ &= 2l_2(2\pi - \frac{2\pi}{N} - \phi_{\widehat{k+S}}) \\ &< 0\end{aligned} \tag{3.21}$$

Case 2": If $\Delta_{\widehat{k+S}} > \frac{2\pi}{N}$ and $\Delta^{+}_{\widehat{k+S}} < \frac{2\pi}{N}$ hold, we have $\phi_{\widehat{k+S+1}} - \phi_{\widehat{k+S}} + \frac{2\pi}{N} < 0$. Then **Part B** in (3.16) can be rewritten as:

$$\begin{aligned}\textbf{Part B} &= \frac{2\pi}{N} - \Delta^{+}_{\widehat{k+S}} - \Delta_{\widehat{k+S}} + \frac{2\pi}{N} + l_2(2\pi - \frac{2\pi}{N} - \phi_{\widehat{k+S}}) \\ &= \frac{2\pi}{N} - (1-l_2)\phi_{\widehat{k+S}} - l_2(2\pi - \frac{2\pi}{N}) + \phi_{\widehat{k+S+1}} - \phi_{\widehat{k+S}} + \phi_{\widehat{k+S+1}} + \frac{2\pi}{N} + l_2(2\pi - \frac{2\pi}{N} - \phi_{\widehat{k+S}}) \\ &= 2(\phi_{\widehat{k+S+1}} - \phi_{\widehat{k+S}} + \frac{2\pi}{N}) \\ &< 0\end{aligned} \tag{3.22}$$

Case 3": If $\Delta_{\widehat{k+S}} \leq \frac{2\pi}{N}$ and $\Delta^{+}_{\widehat{k+S}} < \frac{2\pi}{N}$ hold, **Part B** in (3.16) can be rewritten as:

$$\begin{aligned}\textbf{Part B} &= -\Delta^{+}_{\widehat{k+S}} + \Delta_{\widehat{k+S}} + l_2(2\pi - \frac{2\pi}{N} - \phi_{\widehat{k+S}}) \\ &= -(1-l_2)\phi_{\widehat{k+S}} - l_2(2\pi - \frac{2\pi}{N}) + \phi_{\widehat{k+S+1}} + \phi_{\widehat{k+S}} - \phi_{\widehat{k+S+1}} + l_2(2\pi - \frac{2\pi}{N} - \phi_{\widehat{k+S}}) \\ &= 0\end{aligned} \tag{3.23}$$

According to (3.2), we cannot have a fourth case where $\Delta_{\widehat{k+S}} \leq \frac{2\pi}{N}$ and $\Delta^{+}_{\widehat{k+S}} \geq \frac{2\pi}{N}$ hold due to the following constraint:

$$\begin{aligned}\Delta^{+}_{\widehat{k+S}} - \Delta_{\widehat{k+S}} =& (1-l_2)\phi_{\widehat{k+S}} + l_2(2\pi - \frac{2\pi}{N}) - \phi_{\widehat{k+S+1}} - \phi_{\widehat{k+S}} + \phi_{\widehat{k+S+1}} \\ =& l_2(2\pi - \frac{2\pi}{N} - \phi_{\widehat{k+S}}) \\ <& 0\end{aligned} \tag{3.24}$$

where we used the initial assumption $\phi_{\widehat{k+S}} > 2\pi - \frac{2\pi}{N}$ and the inequality $0 < l_2 < 1$.

To make the proof easy to follow, we use Table 3.1 to show the flow of the proof.

From the above analysis, we have $P^{+} - P \leq 0$, meaning that the value of P will be decreased

Table 3.1: Flow of the proof of Theorem 3.1

Part A[1]	**Case 1':** $\Delta_{\widehat{k-M-1}} > \frac{2\pi}{N}$, $\Delta^{+}_{\widehat{k-M-1}} \geq \frac{2\pi}{N}$	**Part A** < 0
	Case 2': $\Delta_{\widehat{k-M-1}} > \frac{2\pi}{N}$, $\Delta^{+}_{\widehat{k-M-1}} < \frac{2\pi}{N}$	**Part A** < 0
	Case 3': $\Delta_{\widehat{k-M-1}} \leq \frac{2\pi}{N}$, $\Delta^{+}_{\widehat{k-M-1}} < \frac{2\pi}{N}$	**Part A** $= 0$
Part B[2]	**Case 1":** $\Delta_{\widehat{k+S}} > \frac{2\pi}{N}$, $\Delta^{+}_{\widehat{k+S}} \geq \frac{2\pi}{N}$	**Part B** < 0
	Case 2": $\Delta_{\widehat{k+S}} > \frac{2\pi}{N}$, $\Delta^{+}_{\widehat{k+S}} < \frac{2\pi}{N}$	**Part B** < 0
	Case 3": $\Delta_{\widehat{k+S}} \leq \frac{2\pi}{N}$, $\Delta^{+}_{\widehat{k+S}} < \frac{2\pi}{N}$	**Part B** $= 0$

[1] There does not exist a fourth case for **Part A** where $\Delta_{\widehat{k-M-1}} \leq \frac{2\pi}{N}$ and $\Delta^{+}_{\widehat{k-M-1}} \geq \frac{2\pi}{N}$ hold due to the constraint in (3.20).

[2] There does not exist a fourth case for **Part B** where $\Delta_{\widehat{k+S}} \leq \frac{2\pi}{N}$ and $\Delta^{+}_{\widehat{k+S}} \geq \frac{2\pi}{N}$ hold due to the constraint in (3.24).

or unchanged by each "active pulse." According to Lemma B.1 in Appendix B.1, **Case 3'** and **Case 3"** above cannot always exist before phase desynchronization is achieved, i.e., $\Delta_{\widehat{k-M-1}} \leq \frac{2\pi}{N}$ and $\Delta_{\widehat{k+S}} \leq \frac{2\pi}{N}$ cannot always be true before the achievement of phase desynchronization. Consequently, P will not be retained at a non-zero value, and will keep decreasing until it reaches 0, i.e., until phase desynchronization is achieved. Therefore, the PCOs will achieve phase desynchronization under the PRF (3.2) for $0 < l_1 < 1$ and $0 < l_2 < 1$. ■

Remark 3.3. *In the above proof, in order to obtain the expression of $P^+ - P$ in (3.16), we only considered the situation where there is at least one phase variable within each of the intervals $(0, \frac{2\pi}{N})$, $[\frac{2\pi}{N}, 2\pi - \frac{2\pi}{N}]$, and $(2\pi - \frac{2\pi}{N}, 2\pi)$ when an oscillator fires. If one or two of the intervals do not contain any phase variables, the same conclusion can be drawn, as detailed below. Note that when one oscillator fires, if all the other $N-1$ phase variables are within $[\frac{2\pi}{N}, 2\pi - \frac{2\pi}{N}]$, then this pulse is a "silent pulse" which will not cause any change on P, and we have proved that there cannot be N consecutive "silent pulses" unless phase desynchronization is achieved. Therefore, there are five more situations that need to be taken into consideration. Using the same line of reasoning as above and assuming that the update of P is triggered by the pulse of oscillator k, we have the expression of $P^+ - P$ under the five situations as follows:*

Situation 1 *(there are M, $N-M-1$, and 0 phase variables within $(0, \frac{2\pi}{N})$, $[\frac{2\pi}{N}, 2\pi - \frac{2\pi}{N}]$, and*

$(2\pi - \frac{2\pi}{N}, 2\pi)$*, respectively): In this case, we have*

$$P^+ - P = |\Delta^+_{\widehat{k-M-1}} - \frac{2\pi}{N}| - |\Delta_{\widehat{k-M-1}} - \frac{2\pi}{N}| + l_1(\phi_{\widehat{k-M}} - \frac{2\pi}{N}) \tag{3.25}$$

which is the same as ***Part A*** *in (3.16).*

Situation 2 *(there are* 0*,* $N - S - 1$*, and* S *phase variables within* $(0, \frac{2\pi}{N})$*,* $[\frac{2\pi}{N}, 2\pi - \frac{2\pi}{N}]$*, and* $(2\pi - \frac{2\pi}{N}, 2\pi)$*, respectively): In this case, we have*

$$P^+ - P = |\Delta^+_{\widehat{k+S}} - \frac{2\pi}{N}| - |\Delta_{\widehat{k+S}} - \frac{2\pi}{N}| + l_2(2\pi - \frac{2\pi}{N} - \phi_{\widehat{k+S}}) \tag{3.26}$$

which is the same as ***Part B*** *in (3.16).*

Situation 3 *(there are* M*,* 0*, and* $N - M - 1$ *phase variables within* $(0, \frac{2\pi}{N})$*,* $[\frac{2\pi}{N}, 2\pi - \frac{2\pi}{N}]$*, and* $(2\pi - \frac{2\pi}{N}, 2\pi)$*, respectively): In this case, we have*

$$P^+ - P = 2l_1(\phi_{\widehat{k-M}} - \frac{2\pi}{N}) + 2l_2(2\pi - \frac{2\pi}{N} - \phi_{\widehat{k-M-1}}) < 0 \tag{3.27}$$

where we used $\phi_{\widehat{k-M}} < \frac{2\pi}{N}$ *and* $\phi_{\widehat{k-M-1}} > 2\pi - \frac{2\pi}{N}$*.*

Situation 4 *(there are* $N - 1$*,* 0*, and* 0 *phase variables within* $(0, \frac{2\pi}{N})$*,* $[\frac{2\pi}{N}, 2\pi - \frac{2\pi}{N}]$*, and* $(2\pi - \frac{2\pi}{N}, 2\pi)$*, respectively): In this case, we have*

$$P^+ - P = 2l_1(\phi_{\widehat{k+1}} - \frac{2\pi}{N}) < 0 \tag{3.28}$$

where we used $\phi_{\widehat{k+1}} < \frac{2\pi}{N}$*.*

Situation 5 *(there are* 0*,* 0*, and* $N - 1$ *phase variables within* $(0, \frac{2\pi}{N})$*,* $[\frac{2\pi}{N}, 2\pi - \frac{2\pi}{N}]$*, and* $(2\pi - \frac{2\pi}{N}, 2\pi)$*, respectively): In this case, we have*

$$P^+ - P = 2l_2(2\pi - \frac{2\pi}{N} - \phi_{\widehat{k-1}}) < 0 \tag{3.29}$$

where we used $\phi_{\widehat{k-1}} > 2\pi - \frac{2\pi}{N}$*.*

In summary, we have $P^+ - P < 0$ *under* ***Situations 3, 4, 5****, meaning that the value of* P *will decrease under these situations. Note that* $P^+ - P$ *will become the same as* ***Part A*** *and* ***Part B*** *in (3.16) under* ***Situations 1, 2****, respectively. According to the above proof of Theorem 3.1,* ***Part A*** *and* ***Part B*** *will be*

*negative unless **Case 3'** and **Case 3"** hold. From Lemma B.1 in Appendix B.1, **Case 3'** and **Case 3"** cannot always be true, it can be inferred that no matter which situation occurs, the value of P will keep decreasing until phase desynchronization is achieved.*

Next, we show that phase desynchronization can also be achieved under the PRF (3.2) with either l_1 or l_2 being zero. It is worth noting that when l_1 is zero, our PRF reduces to the one in [113].

Corollary 3.1. *For a network of N PCOs with no two PCOs having equal initial phases, the PCOs will achieve phase desynchronization if the phase response function $F(\phi_k)$ is given by (3.2) for $l_1 = 0$ and $0 < l_2 < 1$.*

Proof. The proof is given in Appendix B.2. ■

Corollary 3.2. *For a network of N PCOs with no two PCOs having equal initial phases, the PCOs will achieve phase desynchronization if the phase response function $F(\phi_k)$ is given by (3.2) for $0 < l_1 < 1$ and $l_2 = 0$.*

Proof. Following the same line of reasoning for Corollary 3.1, the proof of Corollary 3.2 can be easily obtained and hence omitted here. ■

Remark 3.4. *If there are two oscillators having equal initial phases, these two PCOs will always have equal phases. This is because they will always make updates simultaneously with identical phase shifts. Therefore, the existence of oscillators having identical phases makes phase desynchronization impossible. In fact, the situation with equal initial phases fails all existing algorithms on phase desynchronization to the best of our knowledge.*

3.4 Numerical Experiments

In this section, we use numerical simulation results to verify that the proposed phase desynchronization algorithm has better robustness than existing results.

We first verify the effectiveness of the proposed phase desynchronization algorithm under an ideal condition where all PCOs have identical nature frequency and there is no pulse loss or time delay in Section 3.4.1. Then under this ideal condition, we compared our algorithm with existing results in terms of convergence speed in Section 3.4.2.

Given that pulse loss is prevalent in wireless communications due to interferences, congestions, and intermittent faulty hardware, we also compared our results with existing results in the case where pulses are lost randomly in Section 3.4.3. Note that in this case, the virtual interaction pattern is not all-to-all any more as the firing of one oscillator will not affect oscillators that fail to receive the pulse corresponding to the firing. In fact, in this case the connection becomes multi-hop and time-varying.

Since time delay is not negligible when the order of processing/transmission delays is comparable to the length of the oscillating period, we also compared our results with existing results in the presence of random communication delays in Section 3.4.4.

Finally, given that there always exists heterogeneity in the natural frequency ω, we simulated and compared our results with existing results when different oscillators have different frequencies in Section 3.4.5.

In all simulations, we record the convergence time of the achievement of phase desynchronization when $|\Delta_k - \frac{2\pi}{N}| < 10^{-3}$ holds for $k = 1, \ldots, N$.

3.4.1 Effectiveness of the Proposed Phase Desynchronization Algorithm in the Ideal Case

Under ideal condition where the natural frequencies are identical and no pulse loss or time delay exists, we verified that the proposed PRF can indeed achieve phase desynchronization on all-to-all graph. The initial phases of a network of $N = 5$ PCOs were randomly chosen from the interval $[0, 2\pi)$, and the natural frequency ω was set to 2π. The coupling strengths (l_1, l_2) in the PRF (3.2) were set to $(0.6, 0.9)$, $(0, 0.9)$, and $(0.6, 0)$, respectively. The evolutions of PCO phases and P are given in Fig. 3.5, Fig. 3.6, and Fig. 3.7, respectively. It can be seen that the PCO phases were uniformly spread apart and the measure P converged to 0 in the three cases.

Besides the all-to-all graph, we also considered ring and circulant symmetric graphs (cf. Fig. 3.8) in the numerical experiments. The initial phases can be randomly chosen but subject to a constraint that the oscillators are indexed in the order of their initial phase magnitude. This constraint is imposed because otherwise two nonadjacent oscillators may converge to the same phase value and become non-separable, making phase desynchronization impossible. In the simulation, the initial phases were set to $\{0.05\pi, 0.26\pi, 0.72\pi, 1.03\pi, 1.24\pi, 1.69\pi\}$, and ω was set to 2π. The coupling strengths (l_1, l_2) in (3.2) were set to $(0.3, 0.45)$. The evolutions of phases and P are given in Fig. 3.9 and Fig. 3.10, respectively,

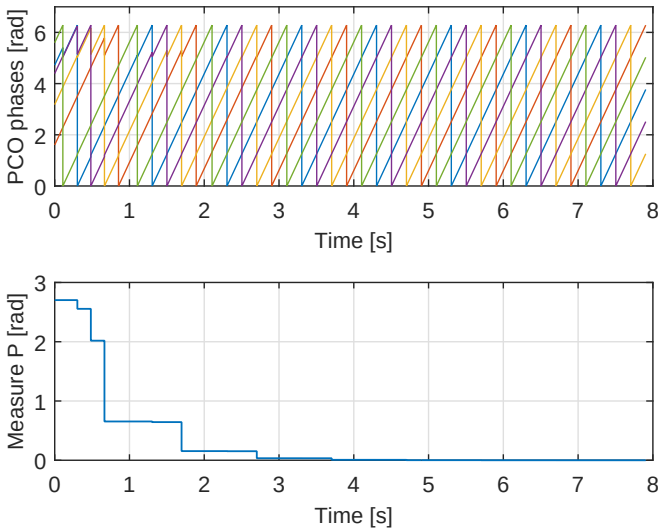

Figure 3.5: The evolutions of PCO phases $\phi_k (k = 1, \ldots, N)$ (upper panel) and measure P (lower panel) under the PRF (3.2) with (l_1, l_2) set to $(0.6, 0.9)$.

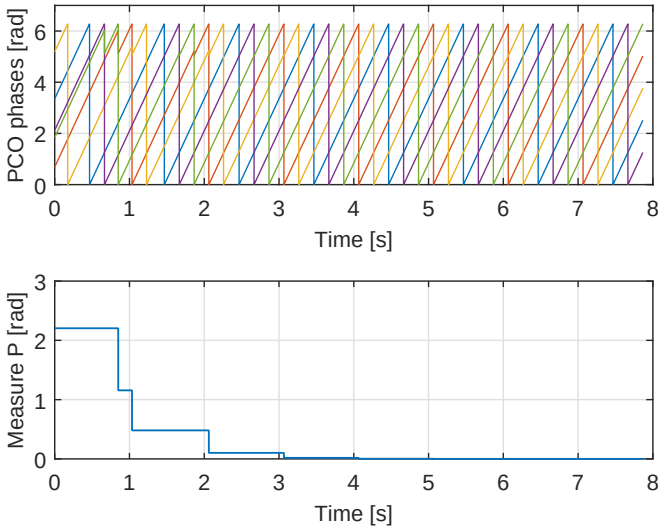

Figure 3.6: The evolutions of PCO phases $\phi_k (k = 1, \ldots, N)$ (upper panel) and measure P (lower panel) under the PRF (3.2) with (l_1, l_2) set to $(0, 0.9)$.

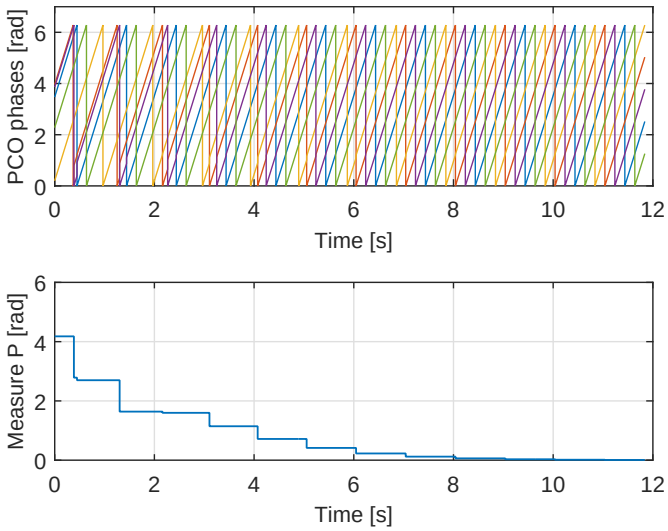

Figure 3.7: The evolutions of PCO phases $\phi_k (k = 1, \ldots, N)$ (upper panel) and measure P (lower panel) under the PRF (3.2) with (l_1, l_2) set to $(0.6, 0)$.

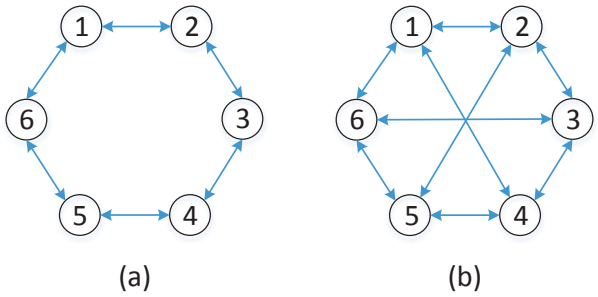

Figure 3.8: Ring and circulant symmetric graphs with six oscillators: (a) ring graph; (b) circulant symmetric graph.

which confirmed the effectiveness of the proposed desynchronization algorithm.

3.4.2 Comparison with Existing Results in the Ideal Case

In the ideal case, we compared our algorithm with the DESYNC-STALE algorithm in [120], the desynchronization algorithm in [113], and the FAST-DESYNC algorithm in [24]. For our algorithm, the coupling strengths (l_1, l_2) in (3.2) were set to $(0.6, 0.9)$. The jump size α in the DESYNC-STALE algorithm in [120], the coupling parameter α in the desynchronization algorithm in [113], and the jump-phase parameter α in the FAST-DESYNC algorithm in [24] were set to 0.95, 0.75, and 0.5, respectively, as used in their own respective papers. The initial phases were randomly chosen from $[0, 2\pi)$, and ω was set to 2π. The results on

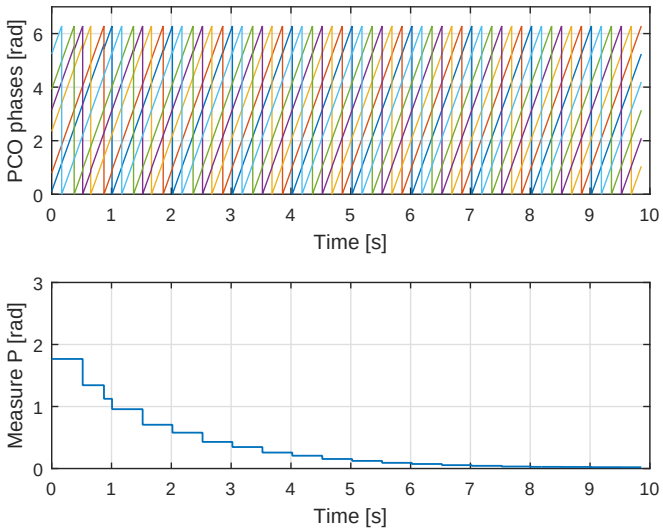

Figure 3.9: The evolutions of PCO phases $\phi_k (k = 1, \ldots, N)$ (upper panel) and measure P (lower panel) under the PRF (3.2) with (l_1, l_2) set to $(0.3, 0.45)$ on the ring graph.

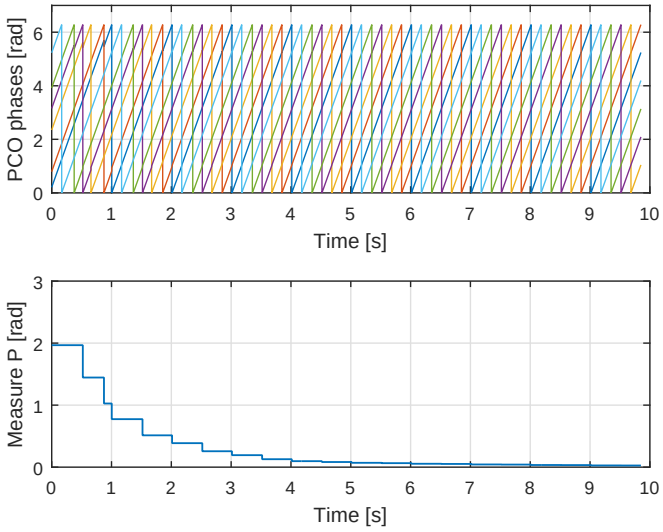

Figure 3.10: The evolutions of PCO phases $\phi_k (k = 1, \ldots, N)$ (upper panel) and measure P (lower panel) under the PRF (3.2) with (l_1, l_2) set to $(0.3, 0.45)$ on the circulant symmetric graph.

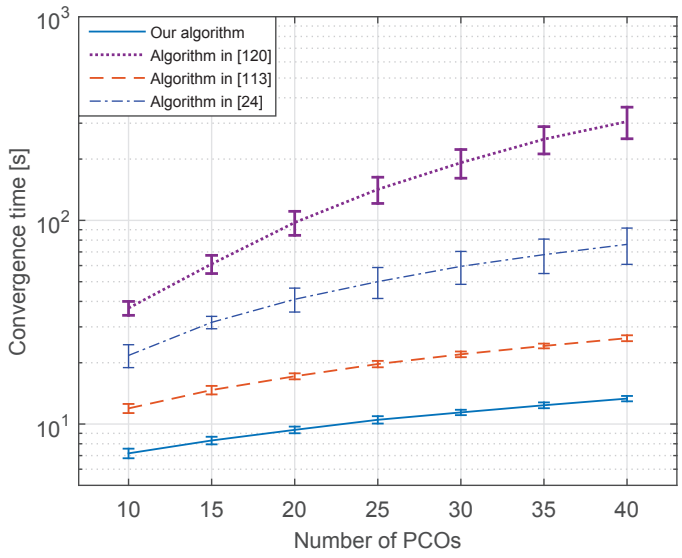

Figure 3.11: Comparison of the proposed algorithm with the DESYNC-STALE algorithm [120], the desynchronization algorithm [113], and the FAST-DESYNC algorithm [24] in the ideal case.

convergence time under different network sizes are given in Fig. 3.11 in which the error bars represent the standard variation of 1000 runs. From the simulation results we can see that our algorithm converges faster than the algorithms in [24, 113, 120].

3.4.3 Comparison with Existing Results under Pulse Losses

In this case, we compared our approach with the DESYNC-STALE algorithm in [120] and the desynchronization algorithm in [113] under pulse losses. The communication links are not reliable and every pulse is transmitted with a failure probability p ($0 \leq p < 1$). For any pulse, it has a probability $1 - p$ to successfully affect an oscillator, and with probability p it will fail to affect the oscillator. Moreover, we assume that the probability for one oscillator to successfully receive a pulse is independent of other oscillators.

For our algorithm, the coupling strengths (l_1, l_2) in (3.2) were set to $(0.6, 0.9)$. The jump size α in the DESYNC-STALE algorithm in [120] and the coupling parameter α in the desynchronization algorithm in [113] were set to 0.95 and 0.75, respectively, as given in their respective papers. The initial phases of a network of $N = 10$ PCOs were randomly chosen from the interval $[0, 2\pi)$, and ω was set to 2π. The probability p was set to 0.05. The evolutions of P are illustrated in Fig. 3.12. It can be seen that our algorithm and the one in [113], both of which are PRF based approaches, could still guarantee desynchronization, whereas the DESYNC-STALE algorithm in [120], which relies on the information of two firing neighbors,

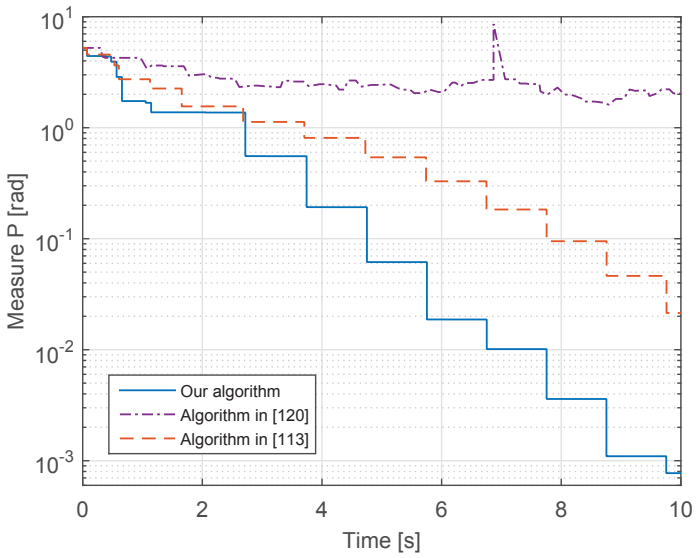

Figure 3.12: The evolutions of measure P for the proposed algorithm, the DESYNC-STALE algorithm in [120], and the desynchronization algorithm in [113] under pulse loss probability $p = 0.05$.

loses its effectiveness.

We also compared our convergence time with [113] under pulse losses. The probabilities of pulse losses p were set to 0.05 and 0.10, respectively. Other parameters were the same as above. The results on convergence time under different network sizes are given in Fig. 3.13 where the error bars represent the standard variation of 1000 runs. We can see that the proposed phase desynchronization algorithm converges faster than the algorithm in [113]. However, compared with the ideal communication case (cf. Fig. 3.11), it is obvious that pulse losses indeed increase the time to convergence for both algorithms.

3.4.4 Comparison with Existing Results under Random Time Delays

In this case, we assume that there is a random delay associated with each communication link, which is uniformly distributed in $[0,\ \tau]$ with τ denoting the maximal delay. Moreover, we assume that delays on different links are independent of each other.

We compared the proposed phase desynchronization algorithm with the DESYNC-STALE algorithm in [120] and the desynchronization algorithms in [35, 36, 113] on a network of $N = 10$ PCOs. The initial phases were randomly chosen from $[0, 2\pi)$ and ω was set to 2π. The maximal delay τ was set to 5% of the free-running firing period. The coupling strengths (l_1, l_2) in (3.2) were set to $(0.9, 0)$. The jump size α in the DESYNC-STALE algorithm in [120] and the coupling parameter α in the desynchronization algorithm in

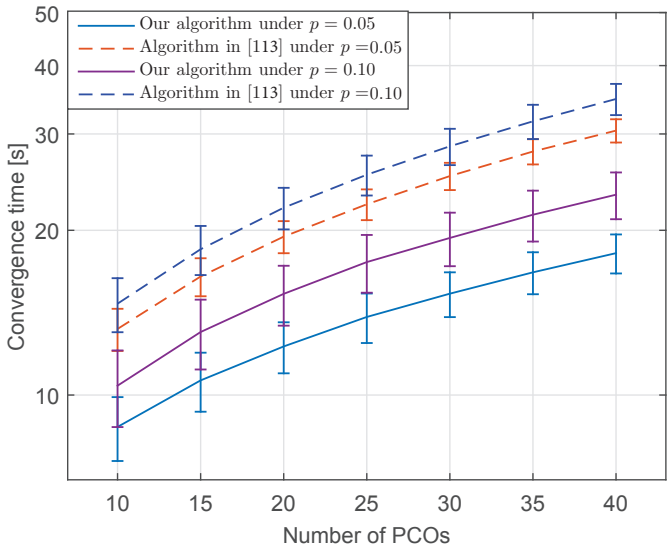

Figure 3.13: The convergence time of the proposed algorithm and the desynchronization algorithm in [113] under pulse losses.

[113] were set to 0.95 and 0.75, respectively, as used in their own respective papers. Both linear and nonlinear realizations of phase response functions in F. Ferrante's work [35, 36] were considered, which are given by

$$F(\phi_k) = \begin{cases} 0 & \phi_k \leq 2\pi - \dfrac{2\pi}{N} \\ -l(\phi_k - 2\pi + \dfrac{2\pi}{N}) & \phi_k > 2\pi - \dfrac{2\pi}{N} \end{cases} \tag{3.30}$$

and

$$F(\phi_k) = \begin{cases} 0 & \phi_k \leq 2\pi - \dfrac{2\pi}{N} \\ l\dfrac{N}{4\pi}\left[(\phi_k - 2\pi)^2 - (\dfrac{2\pi}{N})^2\right] & \phi_k > 2\pi - \dfrac{2\pi}{N} \end{cases} \tag{3.31}$$

The coupling strength l was set to 0.7, as used in [35, 36]. The evolutions of P are given in Fig. 3.14. It can be seen that our phase desynchronization algorithm can still achieve desynchronization under time delays, whereas none of the algorithms in [35, 113, 120], or [36] works anymore.

3.4.5 Comparison with Existing Results under Random Frequency Errors

Given that there always exist errors on the natural frequency ω, we compared the proposed phase desynchronization algorithm with the DESYNC-STALE algorithm in [120] and the desynchronization algorithm in [113] under constant and time-varying frequency errors.

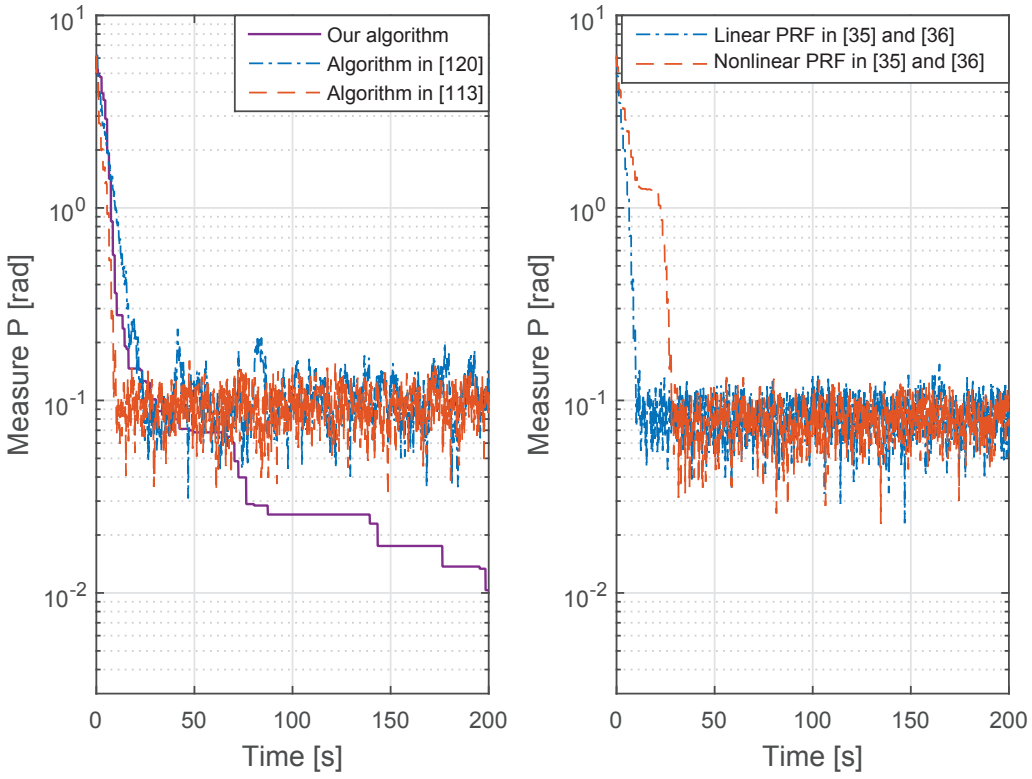

Figure 3.14: The evolutions of measure P for the proposed algorithm, the DESYNC-STALE algorithm in [120], and the desynchronization algorithm in [113] (left panel), and linear and nonlinear PRF based desynchronization algorithm in [35, 36] (right panel) under time delays uniformly distributed in $[0, 5\text{ms}]$.

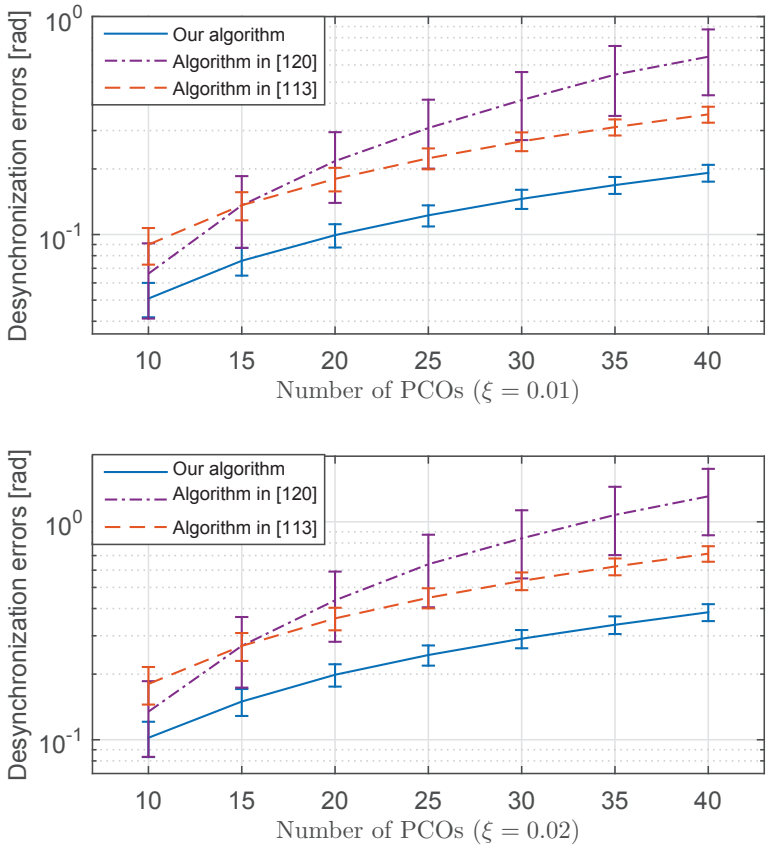

Figure 3.15: The desynchronization errors of the proposed algorithm, the DESYNC-STALE algorithm in [120], and the desynchronization algorithm in [113] in the constant frequency error case.

In the constant frequency error case, the natural frequencies of oscillators were assumed to be independently and uniformly distributed in $[2\pi - \xi,\ 2\pi + \xi]$ where ξ denotes the maximal error. The initial phases were randomly chosen from $[0, 2\pi)$. The coupling strengths (l_1, l_2) in (3.2) were set to $(0.6, 0.9)$. The jump size α in the DESYNC-STALE algorithm in [120] and the coupling parameter α in the desynchronization algorithm in [113] were set to 0.95 and 0.75, respectively, as given in their respective papers. It is worth noting that frequency errors lead to desynchronization errors in all three algorithms. We recorded the mean values of P over one round of firings after the transient period and plotted the results in Fig. 3.15 where ξ was set to 0.01 and 0.02, respectively. The error bars represent the standard variation of 1000 runs. The results show that our approach has less desynchronization error and thus better robustness than the results in [113, 120].

In the time-varying frequency error case, the natural frequencies were assumed to be of the form $\omega_k = 2\pi + \xi \sin(0.1t + \vartheta_k)$ for $k = 1, \ldots, N$, where ξ and ϑ_k denote the maximal error and initial frequency

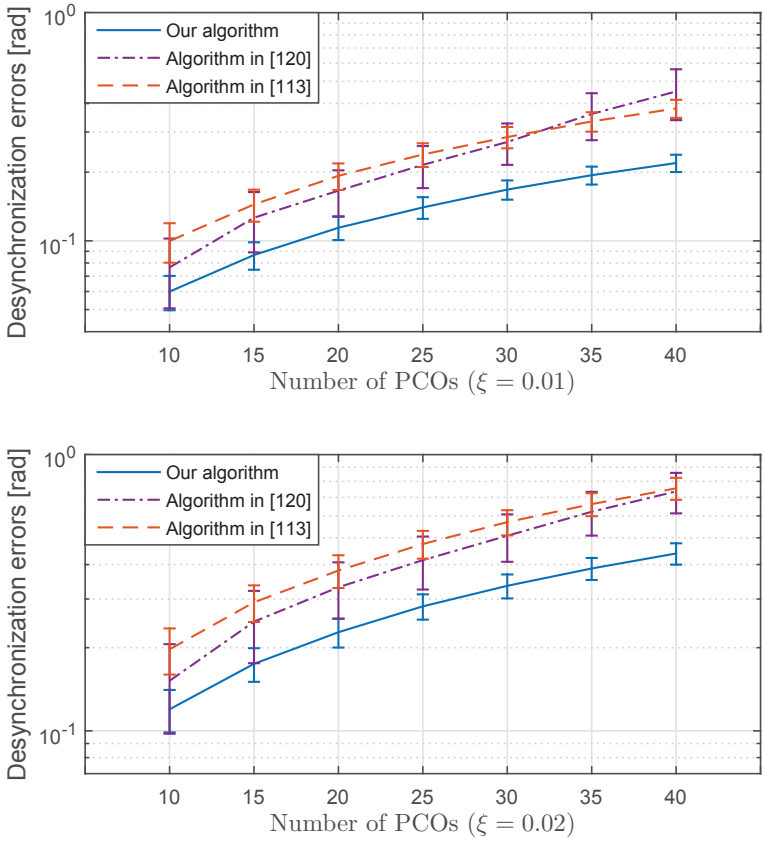

Figure 3.16: The desynchronization errors of the proposed algorithm, the DESYNC-STALE algorithm in [120], and the desynchronization algorithm in [113] in the time-varying frequency error case.

offset, respectively. ξ was set to 0.01 and 0.02, respectively, and ϑ_k was randomly chosen from $[0, 2\pi)$. Other parameters were the same as the constant frequency error case. The desynchronization errors of all three algorithms were illustrated in Fig. 3.16. It can be seen that our proposed algorithm has better robustness than the results in [113, 120].

3.5 Summaries

In this chapter, we proposed a general phase-desynchronizing phase response function, which includes existing results as special cases, and rigorously characterized the decentralized phase desynchronization process. Simulation results were given to show that the proposed phase response function can achieve better convergence speed and robustness to pulse losses, time delays, and frequency errors than existing results.

Chapter 4

Pulse-Based Collective Motion Coordination

4.1 Introduction

In this chapter, motivated by the pulse-based synchronization/desynchronization of PCOs and the close relationship between the phase dynamics of PCOs and the heading dynamics of vehicles, we will introduce a pulse-based approach for collective motion coordination. An increasing number of engineering applications rely on the collective motion of a group of autonomous systems. However, most existing results on collective motion do not address the kinematic dynamics of vehicles, which hampers their practical applications. In fact, incorporating vehicle dynamics significantly increases the difficulty in decentralized collective motion coordination. Therefore, even without considering the effects of communication (e.g., discretization, message losses, time delays), early results on collective motion coordination assumed special communication patterns such as cyclic [90, 116], circulant [117, 118], or all-to-all [140]. Restricting to synchronized collective motion (aligning headings to the same value), the authors in [25, 97] proved that collective motion can be achieved under general communication patterns. The authors in [29, 141] proved that if besides measurement information, relative estimation of global parameters can also be exchanged, then collective motion can be achieved for general communication patterns. The authors in [98] further considered the situation in which only vision clues can be continuously exchanged.

All above results are derived based on continuous exchange of information, which is key to guaran-

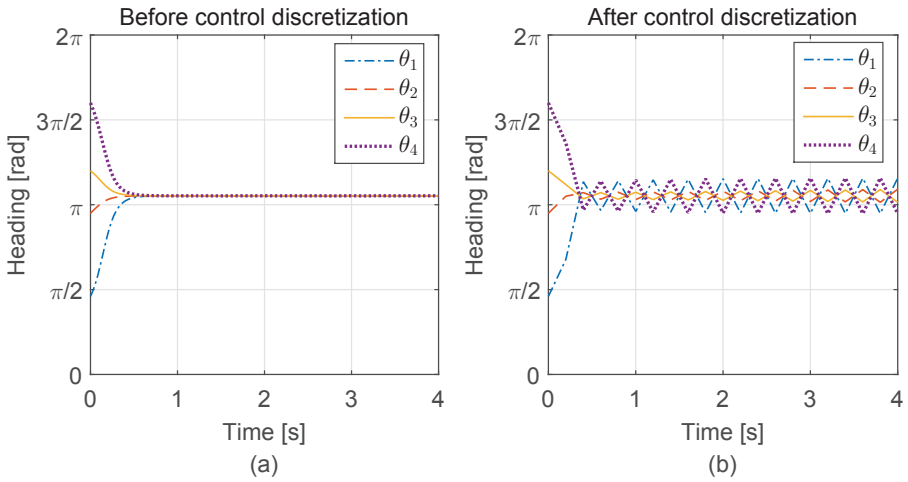

Figure 4.1: Discretization destabilizes controller in [140] designed in the continuous domain for heading alignment. The heading control in [140] works well in the continuous domain assuming continuous-time information exchange (cf. Fig. 4.1 (a)). However, it becomes unstable when practical communication can only occur at discrete-time instants with period 0.2s (cf. Fig. 4.1 (b), zero-order-hold is used between communication). The original vehicle model in [140] was used in the implementation.

tee overall continuous network dynamics and thus a simplified mathematical treatment. However, in practical implementation, information exchange between vehicles can only be conducted at discrete-time instants, making the overall dynamics much harder to address analytically. To reduce complexity, the controller design is usually performed in the continuous-time domain assuming continuous availability of neighbor's information, after which control discretization is used to conform to the actual discrete-time nature of communication. However, this approach is not appropriate in many situations, because to guarantee the design performance it usually requires a very small discretization period which leads to heavy communication burden [49]. To make things worse, discretization can *harm or even destabilize* the controller designed in the continuous-time domain [149] (cf. Fig. 4.1 for an example showing that discretization can destabilize the collective motion controller in [140] designed in the continuous domain).

Recently Morgansen and coauthors considered the required communication amount for cooperative control of a network of nonlinear vehicles [72, 126]. They showed that even without considering spacing control, incorporating communication effects significantly increases the complexity of heading coordination, as evidenced by the fact that analytical treatment of the splay state under all-to-all communication becomes seemingly intractable [72].

Motivated by pulse-based synchronization/desynchronization of pulse-coupled oscillators (PCOs) which can achieve synchronization/desynchronization with remarkable robustness and simplicity through ex-

changing simple identical pulses at discrete-time instants, we design a pulse-based integrated communication and control approach for motion coordination by exploiting the close relationship between phase dynamics of PCOs and the heading dynamics of connected vehicles/robots. The proposed unified approach offers a natural solution for communication pattern design, which only employs simple and identical pulses and hence significantly reduces processing latency and communication delay compared with conventional packet based communications. It also circumvents the problem of discretization and thus guarantees achieving original design performance in final implementation. Not only can heading control be achieved in the proposed approach to coordinate the headings (orientations) of motions in a network, but also spacing control for circular motion is achievable to design the spacing between neighboring nodes (e.g., vehicles or robots).

The remainder of this chapter is organized as follows. Problem formulation for collective motion is present in Section 4.2. A pulse-based integrated communication and control approach is proposed in Section 4.3. Heading control and spacing control for circular motion are studied in Sections 4.4 and 4.5, respectively. Finally, we conclude this chapter in Section 4.6.

4.2 Problem Formulation

4.2.1 Vehicle Model

Since the focus is not to control a single vehicle, but rather a vehicle network, we use a simplified vehicle model, i.e., a car-like vehicle [80,99], to guarantee that the network dynamics is amenable to analytical treatment. The model has been widely used to model nonholonomic vehicles such as cars, boats, planes, whose controllable degrees of freedom are less than the total degrees of freedom. As illustrated in Fig. 4.2, the dynamics of the car-like vehicle model is given by [99]:

$$\begin{cases} \dot{x} = v\cos\theta, \quad \dot{y} = v\sin\theta \\ \dot{\theta} = \dfrac{v}{L}\tan\psi \end{cases} \tag{4.1}$$

where (x, y) denotes the position of the midpoint of the rear axle in the two-dimensional Euclidean plane, $\theta \in \mathbb{S}^1$ denotes the heading of the vehicle relative to the x-axis in the Euclidean plane where $\mathbb{S}^1$ is the one-dimensional torus, v is the speed, L is the wheelbase, and ψ is the angle of the front wheels relative to the vehicle's X axle.

In this vehicle model, there are two control inputs v and ψ. It is worth noting that in many collective

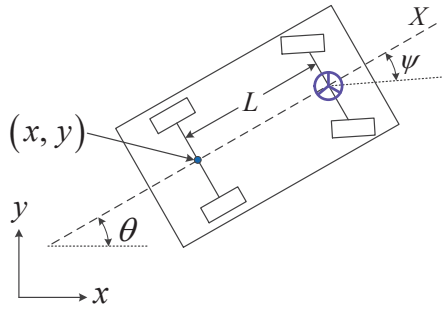

Figure 4.2: The car-like vehicle model.

motions, vehicles/robots are usually configured to have constant velocities. For example, two mostly widely studied vehicles in collective motion, i.e., unmanned aerial vehicles (UAVs) and autonomous underwater vehicles (AUVs), have constant velocities because the former must maintain a constant air speed to remain aloft [65] and the latter have a constant speed (relative to the flow field) due to effective operation requirements [81]. Therefore, in our work, vehicles are configured to have a constant velocity $v = 1$ and ψ is used to control collective motion. Using a complex variable $r = x + \mathrm{i}y \in \mathbb{C} \approx \mathbb{R}^2$ to represent the position of the midpoint of the rear axle (which will be abbreviated as the position of the vehicle in the rest of this chapter), the dynamics of a network of N vehicles is given by:

$$\begin{cases} \dot{r}_k = e^{\mathrm{i}\theta_k} \\ \dot{\theta}_k = \dfrac{1}{L}\tan\psi_k = u_k, \end{cases} \qquad k = 1, \ldots, N \tag{4.2}$$

where the subscript "k" represents vehicle k, $e^{\mathrm{i}\theta_k} = \cos\theta_k + \mathrm{i}\sin\theta_k$ represents the velocity of vehicle k, and u_k denotes the curvature control (normal to vehicle heading, a.k.a. steering control) of vehicle k. From (4.1) and (4.2), the relationship between u_k and ψ_k can be obtained as $\psi_k = \arctan(L \cdot u_k)$ for $k = 1, \ldots, N$. For ease of analysis, we focus on the design of u_k, from which ψ_k can be obtained.

4.2.2 Synchronized-State and Splay-State Collective Motions

In our work, the steering control u_k is designed in a decentralized manner so that desired relationships on both vehicle headings and spacing can be achieved. Thus, we first study two heading relationships, the synchronized-state and the splay-state collective motions [90,140], based on which we address the spacing control for circular motions.

Definition 4.1. *The synchronized-state collective motion is achieved when all vehicles/robots have the same*

heading, i.e., $\theta_1 = \theta_2 = \ldots = \theta_N$.

Definition 4.2. *The splay-state collective motion is achieved when the headings are uniformly spread apart (with equal distance between heading-adjacent vehicles/robots) in the phase space* $\mathbb{S}^1$. *In other words, when a network of* N *vehicles/robots achieve the splay-state collective motion, the heading difference between any two heading-adjacent vehicles/robots is* $\frac{2\pi}{N}$.

Remark 4.1. *In many results on collective motion or oscillator networks, the splay state is also called the "balanced state" and is defined as a state on which the headings (phases) satisfy* $\sum_{k=1}^{N} \sin\theta_k = \sum_{k=1}^{N} \cos\theta_k = 0$ *[140]. This definition cannot guarantee equal phase distance between two heading-adjacent nodes. Therefore, our Definition 4.2 is more stringent.*

Next we introduce two indices for the synchronized-state and the splay-state collective motions, respectively. We first introduce an index to measure the degree of achievement of the synchronized-state collective motion:

$$P_{\rm syn} \triangleq \frac{1}{N}\sum_{k=1}^{N} e^{{\rm i}\theta_k} \tag{4.3}$$

$P_{\rm syn}$ is also called order parameter in oscillator network study [145]. In the synchronized-state collective motion, when all headings are identical, the magnitude (absolute value) of $P_{\rm syn}$ reaches its maximum ($|P_{\rm syn}| = 1$).

Using the dynamics of r_k in (4.2), we have $P_{\rm syn} = \frac{1}{N}\sum_{k=1}^{N} \dot{r}_k$. Therefore, $P_{\rm syn}$ also measures the average linear momentum of a vehicle/robot network. In the synchronized-state collective motion, because the magnitude of $P_{\rm syn}$ reaches the maximal value, the average linear momentum of the vehicle/robot network also reaches the maximum.

Next, we introduce a new index to measure the degree of achievement of the splay-state collective motion. Without loss of generality, we suppose that the indices of vehicle/robot headings are arranged in a way such that $\theta_1 \geq \theta_2 \geq \ldots \geq \theta_N$ holds. Then the differences between neighboring headings are given by $\Delta_k = \theta_k - \theta_{k+1}$ for $k = 1, \ldots, N-1$ and $\Delta_N = \theta_N - \theta_1 + 2\pi$. Based on which we define the index measuring the degree of achievement of the splay-state collective motion

$$P_{\rm spl} \triangleq \sum_{k=1}^{N} |\Delta_k - \frac{2\pi}{N}| \tag{4.4}$$

When the splay-state collective motion is achieved, the phase differences between neighboring headings are $\frac{2\pi}{N}$ and $P_{\rm spl}$ in (4.4) will reach its minimum 0. It can also be easily verified that $P_{\rm spl}$ equals 0 only in the

splay-state collective motion.

4.2.3 Communication Graph

We use a graph $\mathcal{G} = (\mathcal{V}, \mathcal{E})$ to represent the communication structure among the vehicles. The node set $\mathcal{V} = \{1, 2, \ldots, N\}$ denotes all vehicles. $\mathcal{E} \subseteq \mathcal{V} \times \mathcal{V}$ is the edge set, whose elements are such that $(k, j) \in \mathcal{E}$ holds if and only if there is a communication link between vehicles k and j. The neighbor set $\mathcal{N}_k$ of vehicle k, which represents the set of vehicles that are connected with vehicle k, is denoted by $\mathcal{N}_k := \{j \in V : (k, j) \in E\}$.

The our work, we consider the following two undirected graphs for the vehicle network:

Definition 4.3. *An undirected graph $\mathcal{G}$ is connected when there is a path between every pair of nodes.*

Definition 4.4. *An undirected graph $\mathcal{G}$ is all-to-all when there is a communication link between every pair of nodes.*

It is obvious that all-to-all graph can be viewed as a special case of connected graph.

4.3 A Pulse-Based Integrated Communication and Control Framework for Collective Motion

Noticing that vehicle headings are similar to oscillator phases as they both evolve in the one-dimensional torus $\mathbb{S}^1$, we propose an integrated communication and control framework based on our study of pulse-coupled oscillators (PCOs) [109–111,157,158]. Pulse-coupled oscillators can synchronize/desynchronize oscillating phases via exchanging simple identical pulses. Inspired by the pulse-based interaction mechanism, we develop a pulse-based collective motion framework which achieves desired heading relationship via exchanging simple identical pulses. As the pulses are content-free, they can be implemented at the low layer of the protocol stack (even exclusively at the physical layer) with very short message lengths, which significantly reduces the high-layer processing latencies and channel communication delays. In this framework, the time instants for pulse exchanging are determined by vehicle dynamics, so communication and control are integrated. Compared with conventional approaches using continuous control design followed by discretization based implementation and communication, the proposed approach designs communication time instants explicitly and circumvents the problem of discretization, which in turn can guarantee that the original control design performance is attainable in final implementation.

Next we first review the interaction mechanism of pulse-coupled oscillators, based on which we propose a pulse-based integrated communication and control framework.

4.3.1 Pulse-Coupled Oscillators

In a network of N pulse-coupled oscillators interacting on a graph $\mathcal{G} = (\mathcal{V}, \mathcal{E})$, each oscillator has a phase variable ϕ_k ($k = 1, 2, \ldots, N$) evolving continuously from 0 to 2π with a constant speed determined by its natural frequency ω_o. The interaction mechanism of PCOs can be described as follows:

1. Each oscillator has a phase variable $\phi_k \in \mathbb{S}^1$ with initial value set to $\phi_k(0)$. ϕ_k evolves continuously from 0 to 2π with a constant speed determined by ω_o;

2. When the phase variable ϕ_k of oscillator k reaches 2π, this oscillator fires, i.e., emits a pulse, and simultaneously resets ϕ_k to 0. Then the same process repeats;

3. When oscillator k receives a pulse from others, it updates its phase according to the phase response function $P(\phi_k)$:

$$\phi_k^+ = \phi_k + P(\phi_k) \tag{4.5}$$

where ϕ_k^+ and ϕ_k denote the phases of oscillator k immediately after and before receiving the pulse. Therefore, the dynamics of oscillator k can be written as:

$$\dot{\phi}_k = \omega_o + \sum_{j \in \mathcal{N}_k} P(\phi_k)\delta(t - t_j) \tag{4.6}$$

where t_j denotes the time instants at which ϕ_j reaches 2π. The Dirac function $\delta(t)$ is 0 for all time t except $t = 0$ and satisfies $\int_{-\infty}^{\infty} \delta(t)dt = 1$ [157].

It is already known that if the phase response function (PRF) is chosen appropriately, pulse-coupled oscillators can exhibit desired collective behaviors. For example, results in [157] and [40] show that under phase response functions $P_1(\phi_k)$ and $P_2(\phi_k)$ in Fig. 4.3, oscillators interacting on all-to-all graph can achieve the synchronized state and splay state, respectively.

4.3.2 Pulse-Based Collective Motion Coordination Framework

Inspired by pulse-coupled oscillators, we propose a pulse-based motion coordination framework:

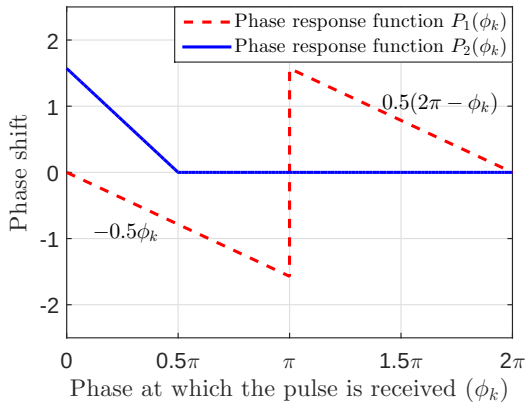

Figure 4.3: Examples of phase response function that can achieve the synchronized state (red dashed line) and the splay state (blue solid line).

1. Besides heading variable θ_k and position variable r_k in (4.2), each vehicle also has an auxiliary variable $\phi_k \in \mathbb{S}^1$ with initial value $\phi_k(0)$. ϕ_k evolves continuously from $\phi_k(0)$ to 2π with a constant speed ω_o, where $\phi_k(0)$ is determined by both the initial value of heading variable $\theta_k(0)$ and the desired heading relationship (synchronized state or splay state);

2. When the auxiliary variable ϕ_k of vehicle k reaches 2π, the vehicle sends a pulse, and simultaneously resets ϕ_k to 0. Then the same process repeats;

3. When a vehicle receives a pulse from its neighbor, it updates its auxiliary variable ϕ_k according to a control function $F(\phi_k, \mathbf{r})$. Note that $\mathbf{r} = [r_1, \ldots, r_N]^T$ contains the relative position information between vehicle k and its neighbors achieved by measuring the angle-of-arrival and power degradation of received pulses, and it needs to be taken into account in control design $F(\bullet)$ when spacing needs to be coordinated. Using Dirac function $\delta(t)$, the update can be mathematically formulated as follows:

$$\dot{\phi}_k = \omega_o + \sum_{j \in \mathcal{N}_k} F(\phi_k, \mathbf{r}) \delta(t - t_j) \tag{4.7}$$

   where t_j denotes the time instants at which ϕ_j reaches 2π;

4. The control input u_k for each vehicle is determined by its auxiliary variable ϕ_k by

$$u_k = \dot{\theta}_k = \omega_c + \dot{\phi}_k - \omega_o = \omega_c + \sum_{j \in \mathcal{N}_k} F(\phi_k, \mathbf{r}) \delta(t - t_j) \tag{4.8}$$

where ω_c should be set to 0 in a rectilinear motion and the desired angular velocity in a circular motion (angular velocity ω_c corresponds to radius $\frac{1}{\omega_c}$ in circular motions).

Remark 4.2. *The relationship between the dynamics of θ_k and the dynamics of ϕ_k can be written as*

$$\dot{\theta}_k = \omega_c + \dot{\phi}_k - \omega_o \tag{4.9}$$

where the oscillator's natural frequency ω_o is subtracted from the dynamics of ϕ_k because the dynamics of θ_k depends on the discrete-time update $F(\phi_k, \mathbf{r})$ of ϕ_k instead of its continuous evolution, and ω_c can be seen as a part of spacing control since it only affects the motion pattern (i.e., rectilinear or circular motion).

It is worth noting that in the above framework, the communicated messages are simple identical pulses and the communication time instants are determined by t_j, which are determined by the evolution of ϕ_k. As ϕ_k is in turn determined by $F(\phi_k, \mathbf{r})$, the control law, the above framework gives an integrated design of communication and control. The integrated design circumvents the effects of discretization and can guarantee that the design performance of control can be retained in final implementation. This is a great advantage over existing approaches using a continuous-domain control design followed by discretization based implementation which can harm or even destabilize the originally designed controller [149] (cf. Fig. 4.1). Furthermore, the design utilizes the analogy between phases in oscillator networks and headings in vehicle networks, which enables the treatment of nonlinear nonholonomic vehicle dynamics in (4.2). This is different from most event-triggered design for the collective motion of multi-agent systems which only addresses linear dynamics due to difficulties in designing a stabilizing event-triggered control. In addition, the pulse based communication embeds information in the timing rather than the content of exchanged messages, which falls within the pulse position modulation framework in communication.

Remark 4.3. *In the proposed integrated communication and control framework, ω_o is a design parameter controlling communication frequency. A larger ω_o leads to a higher communication frequency.*

Next, we give a solution to design $F(\phi_k, \mathbf{r})$. For any vehicle k, its control $F(\phi_k, \mathbf{r})$ is not only a function of its auxiliary variable ϕ_k, but also a function of the positions of all vehicles $\mathbf{r}$. This makes $F(\phi_k, \mathbf{r})$ very difficult to derive directly, if at all possible. Given this, similar to [139] we use the singularly perturbed theory [77] to enforce a time-scale separation between the heading dynamics θ_k and the spacing dynamics

r_k. We first decompose $F(\phi_k, \mathbf{r})$ into two parts:

$$F(\phi_k, \mathbf{r}) = \tilde{u}_k^{\text{orien}} + \tilde{u}_k^{\text{space}} \tag{4.10}$$

Similar to [139] we separate the control law u_k of vehicle k in (4.2) into two parts:

$$u_k = u_k^{\text{orien}} + u_k^{\text{space}} \tag{4.11}$$

where the first part u_k^{orien} controls the heading of vehicle k. To achieve a collective motion, it should depend on the heading value of vehicle k and the time instants when vehicle k receives pulses from its neighbors. The second part u_k^{space} controls the spacing (distance) among vehicles and depends on the relative position of vehicle k with respect to its neighbors which can be obtained by measuring the angle-of-arrival and power degradation of received pulses [65] or by using ranging and bearing sensors. Then according to (4.8), (4.10), and (4.11), u_k^{orien} and u_k^{space} are

$$\begin{cases} u_k^{\text{orien}} = \sum\limits_{j \in \mathcal{N}_k} \tilde{u}_k^{\text{orien}} \delta(t - t_j) \\ u_k^{\text{space}} = \omega_c + \sum\limits_{j \in \mathcal{N}_k} \tilde{u}_k^{\text{space}} \delta(t - t_j) \end{cases} \tag{4.12}$$

Based on the singularly perturbed theory, the separation between the heading dynamics and the spacing dynamics is achievable by designing the steering control u_k as follows:

$$\begin{aligned} u_k &= K u_k^{\text{orien}} + u_k^{\text{space}} \\ &= \omega_c + \sum_{j \in \mathcal{N}_k} (K \tilde{u}_k^{\text{orien}} + \tilde{u}_k^{\text{space}}) \delta(t - t_j) \end{aligned} \tag{4.13}$$

where K can be set to any large value to achieve time-scale separation (make overall dynamics singularly perturbed [77]).

Combining (4.2) and (4.13) gives

$$\begin{cases} \dot{r}_k = e^{\mathrm{i}\theta_k} \\ \epsilon \dot{\theta}_k = \epsilon \omega_c + \sum\limits_{j \in \mathcal{N}_k} (\tilde{u}_k^{\text{orien}} + \epsilon \tilde{u}_k^{\text{space}}) \delta(t - t_j) \end{cases} \tag{4.14}$$

for $1 \leq k \leq N$ where $\epsilon = \frac{1}{K}$ is very small so that a time-scale separation between fast dynamics in time-scale

$\tau = \frac{t-t_0}{\epsilon}$ and slow dynamics in time-scale t occurs.

The position variable r_k is almost invariant in the fast time-scale τ, consequently the kinematic model can be reduced to

$$\frac{d}{d\tau}\theta_k = \epsilon\omega_c + \sum_{j\in\mathcal{N}_k}(\tilde{u}_k^{\text{orien}} + \epsilon\tilde{u}_k^{\text{space}})\delta(t-t_j) \tag{4.15}$$

When K approaches infinity, ϵ approaches 0, leading to

$$\frac{d}{d\tau}\theta_k = \sum_{j\in\mathcal{N}_k}\tilde{u}_k^{\text{orien}}\delta(t-t_j) \tag{4.16}$$

It is clear that using the singularly-perturbed control strategy, the fast dynamics of heading θ_k is decoupled from the slow dynamics of position r_k. Therefore, we can first design $\tilde{u}_k^{\text{orien}}$ to achieve the desired heading relationship, then under the heading relationship we can design $\tilde{u}_k^{\text{space}}$ to achieve the desired spacing. Since spacing control is in the slow time-scale, it will not affect the achieved heading relationship.

4.4 Design of the Heading Dynamics

Note that the heading dynamics in (4.16) is similar to the dynamics of phases in pulse-coupled oscillators [157]. So taking inspiration from results on pulse-coupled synchronization [110, 157, 158], we propose the following heading control strategies for vehicle networks under connected graphs.

Theorem 4.1. *For a network of N vehicles with kinetic model given in (4.2) under a connected graph $\mathcal{G} = (\mathcal{V}, \mathcal{E})$, if the initial value of auxiliary variable $\phi_k(0)$ is set to $\theta_k(0)$ for $k = 1, 2, \ldots, N$ and all initial values of auxiliary variables are constrained in a half cycle of $\mathbb{S}^1$, then the network of vehicles will achieve the synchronized-state collective motion under the heading control $\tilde{u}_k^{\text{orien}}$ given by (4.17) in the singularly-perturbed control framework (4.13). Moreover, if the initial value of auxiliary variable $\phi_k(0)$ is set to $(\theta_k(0) - k\frac{2\pi}{N}) \bmod 2\pi$ for $k = 1, 2, \ldots, N$ and all initial values of auxiliary variables are constrained in a half cycle of $\mathbb{S}^1$, then the network of vehicles will achieve the splay-state collective motion under the heading control $\tilde{u}_k^{\text{orien}}$ given by (4.17) in the singularly-perturbed control framework (4.13).*

$$\tilde{u}_k^{\text{orien}} = \begin{cases} -l\phi_k & 0 \le \phi_k \le \pi \\ l(2\pi - \phi_k) & \pi < \phi_k \le 2\pi \end{cases} \quad \text{for } 0 < l < 1. \tag{4.17}$$

Proof. According to the fast dynamics of the heading variable θ_k in (4.16), we can obtain the fast time-scale

dynamics of the auxiliary variable ϕ_k from (4.7) as follows:

$$\dot{\phi}_k = \omega_o + \dot{\theta}_k = \omega_o + \sum_{j \in N_k} \tilde{u}_k^{\text{orien}} \delta(t - t_j) \tag{4.18}$$

Since ω_c is a part of u_k^{space} in (4.12), it will not show up in the fast dynamics of ϕ_k. Therefore, we have $\dot{\theta}_k = \dot{\phi}_k - \omega_o$.

Noting that $\tilde{u}_k^{\text{orien}}$ in (4.17) is the same as the phase response function $P(\phi_k)$ in Fig. 4.3, the dynamics of ϕ_k in (4.18) becomes the same as the oscillator dynamics in (4.6). According to Theorem 2 in [110], $\phi_1, \phi_2, \ldots, \phi_N$ with a connected graph will achieve the synchronized state under (4.17) if their initial values are constrained in a half cycle of $\mathbb{S}^1$.

Since $\phi_k(0) = \theta_k(0)$ and $\dot{\theta}_k = \dot{\phi}_k - \omega_o$ hold, we have $\theta_k = (\phi_k - \omega_o t) \bmod 2\pi$ for $1 \leq k \leq N$. As we discussed above, $\phi_1, \phi_2, \ldots, \phi_N$ will achieve the synchronized state under (4.17), thus the headings $\theta_1, \theta_2, \ldots, \theta_N$ will also achieve the synchronized state. Therefore, the network of vehicles will achieve the synchronized-state collective motion under the heading control $\tilde{u}_k^{\text{orien}}$ in (4.17).

Similarly, we can prove that the vehicles will achieve the splay-state collective motion. From $\phi_k(0) = (\theta_k(0) - k\frac{2\pi}{N}) \bmod 2\pi$ and $\dot{\theta}_k = \dot{\phi}_k - \omega_o$, we have $\theta_k = (\phi_k - \omega_o t + k\frac{2\pi}{N}) \bmod 2\pi$. Taking into account the fact that ϕ_1, ϕ_2,...,ϕ_N will achieve the synchronized state under (4.17), it can be inferred directly that the headings $\theta_1, \theta_2, \ldots, \theta_N$ will achieve the splay state since the differences between any two neighboring headings are $\frac{2\pi}{N}$. Therefore, the network of vehicles will achieve the splay-state collective motion under heading control $\tilde{u}_k^{\text{orien}}$ in (4.17). ■

As a special case of connected graph, vehicle network under all-to-all graph can achieve synchronized-state and splay-state collective motions following the above Theorem 4.1. Inspired by our results of PCO desynchronization on all-to-all graphs (cf. Corollary 3.2 in Section 3.3), we propose another heading control strategy for vehicle networks under all-to-all graphs to achieve splay-state collective motion.

Theorem 4.2. *For a network of N vehicles with kinetic model given in (4.2) under an all-to-all graph $\mathcal{G} = (\mathcal{V}, \mathcal{E})$, if the initial value of auxiliary variable $\phi_k(0)$ is set to $\theta_k(0)$ for $k = 1, 2, \ldots, N$ and no two vehicles have equal initial headings, then the network of vehicles will achieve the splay-state collective motion under the heading control $\tilde{u}_k^{\text{orien}}$ given by (4.19) in the singularly-perturbed control framework (4.13).*

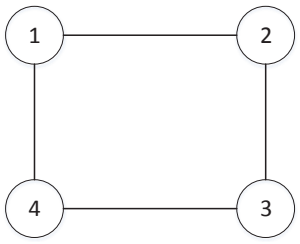

Figure 4.4: Connected graph of a vehicle network of 4 vehicles.

$$\tilde{u}_k^{\text{orien}} = \begin{cases} -l(\phi_k - \dfrac{2\pi}{N}) & 0 \le \phi_k < \dfrac{2\pi}{N} \\ 0 & \dfrac{2\pi}{N} \le \phi_k \le 2\pi \end{cases} \quad \textit{for } 0 < l < 1. \tag{4.19}$$

Proof. Following the same line of reasoning for Theorem 4.1, we have that the dynamics of ϕ_k in (4.18) is the same as the oscillator dynamics in (4.6). According to Corollary 3.2 in Section 3.3, $\phi_1, \phi_2, \ldots, \phi_N$ with an all-to-all graph will achieve the splay state under (4.19) if initial phases are distinct. Since $\phi_k(0) = \theta_k(0)$ and $\dot{\theta}_k = \dot{\phi}_k - \omega_o$ hold, we have $\theta_k = (\phi_k - \omega_o t) \bmod 2\pi$ for $1 \le k \le N$. As we discussed above, $\phi_1, \phi_2, \ldots, \phi_N$ will achieve the splay state under (4.19), thus the headings $\theta_1, \theta_2, \ldots, \theta_N$ will also achieve the splay state. Therefore, the network of vehicles interacting on all-to-all graph will achieve the splay-state collective motion under the heading control $\tilde{u}_k^{\text{orien}}$ in (4.19). ■

Next we use simulation results to demonstrate Theorem 4.1. We consider the fast time-scale dynamics (4.16) of a network of 4 vehicles under a connected graph given in Fig. 4.4. Communication occurs whenever ϕ_k reaches 2π (which happens repeatedly). The control is applied when a pulse is received. We considered both rectilinear motion ($\omega_c = 0$ rad/s) and circular motion ($\omega_c = 1$ rad/s) and simulated their behavior under the different heading controls (4.17) and (4.19), respectively. ω_o is set to 10π.

We first simulated the synchronized-state collective motion. The initial headings were randomly chosen from a half cycle of $\mathbb{S}^1$, and $\phi_k(0)$ was set to $\theta_k(0)$. The vehicle trajectories of the rectilinear motion case ($\omega_c = 0$ rad/s) and the circular motion case ($\omega_c = 1$ rad/s) are given in Fig. 4.5 (a) and (b), respectively. Note that the initial headings, starting points, and ending points of these vehicle trajectories are represented by dashed arrows, squares, and solid arrows, respectively. Also the evolutions of the magnitude of index P_{syn} in the two cases above are given in Fig. 4.5 (c). It can be seen that the synchronized-state collective motion can be achieved under heading control $\tilde{u}_k^{\text{orien}}$ in (4.17).

The splay-state collective motion was also evaluated. The initial headings were randomly chosen from $[0,\ 2\pi)$ such that $\phi_k(0) = (\theta_k(0) - k\frac{2\pi}{N}) \bmod 2\pi$ for $k = 1, 2, \ldots, N$ were constrained in a half cycle

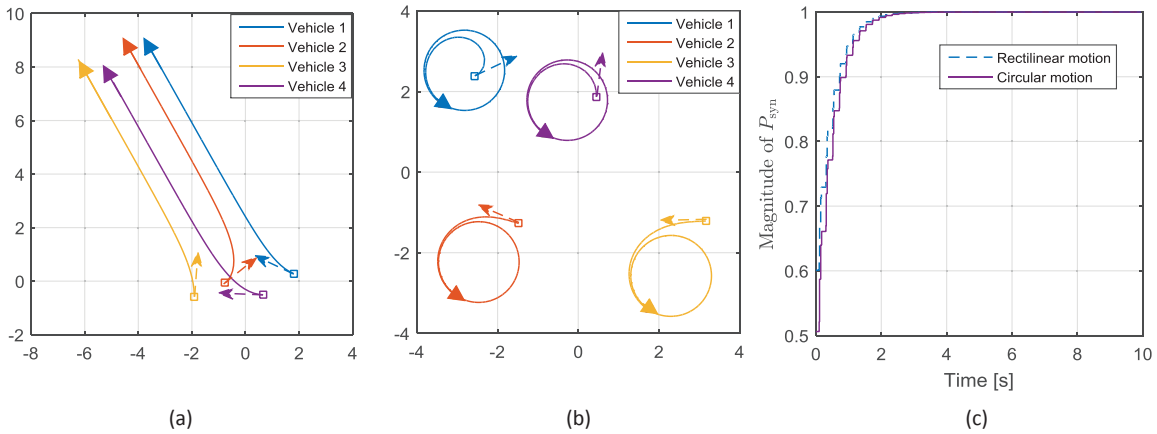

Figure 4.5: Synchronized-state collective motion under connected graph: (a) rectilinear motion trajectories ($\omega_c = 0$); (b) circular motion case trajectories ($\omega_c = 1$); (c) magnitude of P_{syn} of the rectilinear motion case and circular motion case.

of $\mathbb{S}^1$. The vehicle trajectories of the rectilinear motion case ($\omega_c = 0$ rad/s) and the circular motion case ($\omega_c = 1$ rad/s) are given in Fig. 4.6 (a) and (b), respectively. The evolutions of P_{spl} in the two cases above are given in Fig. 4.6 (c). It can be seen that the splay-state collective motion can be achieved under heading control $\tilde{u}_k^{\text{orien}}$ in (4.17).

Last we use simulation results to demonstrate Theorem 4.2. We consider a network of 4 vehicles under all-to-all graph. Effectiveness of the heading control (4.19) in achieving the splay state was evaluated. The initial headings are randomly chosen from $[0,\ 2\pi)$. The vehicle trajectories of the rectilinear motion case and the circular motion case are given in Fig. 4.7 (a) and (b), respectively. The evolutions of index P_{spl} in the two cases are given in Fig. 4.7 (c). It can be seen that the splay-state collective motion with all-to-all graph can be achieved under the heading control (4.19).

Remark 4.4. *The control in (4.17) requires instantaneous jumps in the heading angle, which may not be desirable in certain scenarios. Fortunately, according to results in [7] on pulse-coupled oscillators with guaranteed phase continuity, a continuous-heading-implementation mechanism can be used to spread the needed heading adjustment in a certain time interval without affecting the convergence stability: in implementation, instead of finishing all required heading adjustment $\Delta\theta_k$ at time instant t_j, i.e., $u(t) = \Delta\theta\delta(t - t_j)$, we can spread the adjustment in a half period $T/2$ with T given by $T = 2\pi/\omega_o$, i.e., $u(t) = 2\Delta\theta_k/T$ for $t \in (t_j,\ t_j + T/2)$. If vehicle k has not yet achieved its desired amount of heading adjustment before a new pulse arrives (i.e., rather than having adjusted the whole amount $\Delta\theta_k$, it has adjusted only a portion of $\Delta\theta_k$), then vehicle k will use the current value of ϕ_k at the time when the new pulse is received to redetermine the*

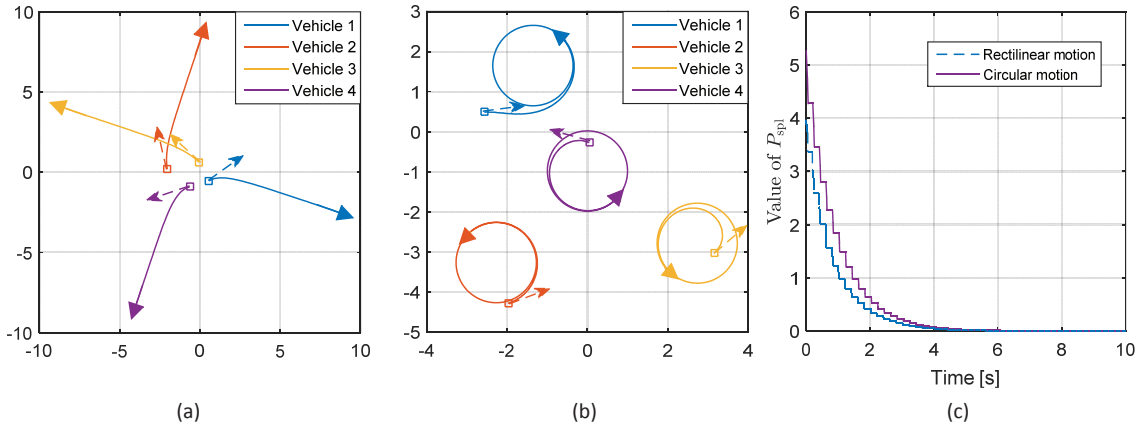

Figure 4.6: Splay-state collective motion under connected graph: (a) rectilinear motion trajectories ($\omega_c = 0$); (b) circular motion case trajectories ($\omega_c = 1$); (c) magnitude of P_{spl} of the rectilinear motion case and circular motion case.

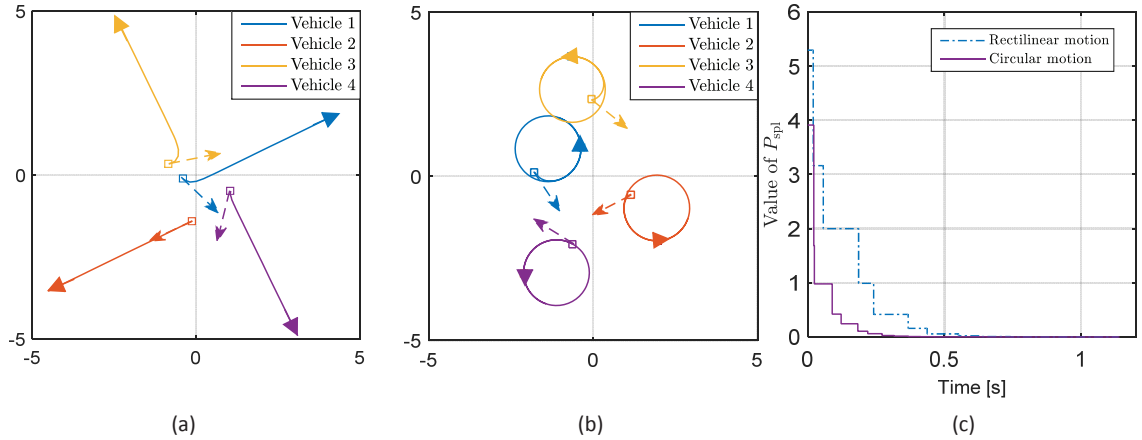

Figure 4.7: Splay-state collective motion under all-to-all graph: (a) rectilinear motion trajectories ($\omega_c = 0$); (b) circular motion case trajectories ($\omega_c = 1$); (c) magnitude of P_{spl} of the rectilinear motion case and circular motion case.

value for $\Delta\theta_k$ according to (4.17), and evenly spread the new adjustment in the following time interval $T/2$. Under the continuous-heading-implementation mechanism, the synchronized-state collective motion can still be achieved [7].

4.5 Stabilization of Circular Motion

Theorems 4.1 and 4.2 provide approaches to driving vehicle headings to the splay state by designing $\tilde{u}_k^{\rm orien}$ in (4.13) under connected graphs and all-to-all graphs, respectively. Splay-state collective motion is usually employed when vehicles perform circular motions in applications such as mobile sensor deployment [81]. In such applications, to maximize the information intake, it is usually also required that the vehicles (e.g., unmanned underwater vehicles) rotate around a same center [81]. Next we discuss how to design the spacing control $\tilde{u}_k^{\rm space}$ to stabilize the circular motion around an arbitrarily assigned center R^* for vehicle networks on connected graphs.

Theorem 4.3. *For a network of N vehicles with kinetic model given in (4.2) under a connected graph $\mathcal{G} = (\mathcal{V}, \mathcal{E})$, heading control $\tilde{u}_k^{\rm orien}$ in the singularly-perturbed control framework (4.13) is designed as (4.17). Then spacing control $\tilde{u}_k^{\rm space}$ in (4.20) will drive all vehicles to orbit around an arbitrarily assigned center R^* with a desired angular velocity ω_c if $\phi_k(0)$ is set to $(\theta_k(0) - k\frac{2\pi}{N}) \bmod 2\pi$ for $k = 1, 2, \ldots, N$ and all these values are constrained in a half cycle of $\mathbb{S}^1$.*

$$\tilde{u}_k^{\rm space} =< \omega_c(r_k - R^*), e^{{\rm i}\theta_k} > \tag{4.20}$$

where R^* is the arbitrarily assigned center.

Proof. Define the relative position between vehicle k and the arbitrarily assigned center R^* by $\tilde{r}_k^* = r_k - R^*$, thus the spacing control $\tilde{u}_k^{\rm space}$ can be rewritten as:

$$\tilde{u}_k^{\rm space} =< \omega_c \tilde{r}_k^*, e^{{\rm i}\theta_k} > \tag{4.21}$$

Since the center of vehicle k's circular motion is $c_k = r_k + {\rm i}\omega_c^{-1} e^{{\rm i}\theta_k}$, the relative position between c_k and the arbitrarily assigned center R^* is given by:

$$d_k = c_k - R^* = r_k + {\rm i}\omega_c^{-1} e^{{\rm i}\theta_k} - R^* = \tilde{r}_k^* + {\rm i}\omega_c^{-1} e^{{\rm i}\theta_k} \tag{4.22}$$

The Lyapunov function is defined by:

$$U = \frac{1}{2} \parallel \mathbf{d} \parallel^2 \tag{4.23}$$

where $\mathbf{d} = [d_1, \ldots, d_N]^T$. Note that U will reach its minimum 0 if every vehicle orbits around R^* due to $c_1 = \ldots = c_N = R^*$ and $d_1 = \ldots = d_N = 0$.

According to Theorem 4.1, $\theta_1, \theta_2, \ldots, \theta_N$ will achieve the splay state under the heading control (4.17) if $\phi_k(0)$ is set to $(\theta_k(0) - k\frac{2\pi}{N}) \bmod 2\pi$ for $k = 1, 2, \ldots, N$ and all these values are constrained in a half cycle of $\mathbb{S}^1$ under a connected graph. Since the heading control vanishes after achieving the splay state, the dynamics of d_k is given by:

$$\begin{aligned} \dot{d}_k = \dot{c}_k &= \dot{r}_k - \omega_c^{-1} e^{\mathrm{i}\theta_k} \dot{\theta}_k \\ &= -\omega_c^{-1} e^{\mathrm{i}\theta_k} \sum_{j \in N_k} \tilde{u}_k^{\text{space}} \delta(t - t_j) \end{aligned} \tag{4.24}$$

Therefore, the dynamics of U can be obtained as follows:

$$\begin{aligned} \dot{U} &= < \mathbf{d}, \dot{\mathbf{d}} > = \sum_{k=1}^{N} < d_k, \dot{d}_k > \\ &= -\sum_{k=1}^{N} \sum_{j \in N_k} < \tilde{r}_k^*, e^{\mathrm{i}\theta_k} >^2 \delta(t - t_j) \end{aligned} \tag{4.25}$$

Thus we have $\dot{U} \leq 0$. According to LaSalle Invariance principle, all solutions will converge to the largest invariant set Λ where

$$< \tilde{r}_k^*, e^{\mathrm{i}\theta_k} > \equiv 0 \tag{4.26}$$

holds for $k = 1, \ldots, N$. So $\tilde{u}_k^{\text{space}} = < \omega_c \tilde{r}_k^*, e^{\mathrm{i}\theta_k} > \equiv 0$ holds in the set Λ, meaning that d_k is constant in the set Λ due to $\dot{d}_k \equiv 0$. From (4.22), we have $\tilde{r}_k^* = d_k - \mathrm{i}\omega_c^{-1} e^{\mathrm{i}\theta_k}$. Thus the largest invariant set Λ can be rewritten as:

$$< \tilde{r}_k^*, e^{\mathrm{i}\theta_k} > = < d_k, e^{\mathrm{i}\theta_k} > \equiv 0 \tag{4.27}$$

for $k = 1, \ldots, N$. Because the spacing control $\tilde{u}_k^{\text{space}}$ is zero in the largest invariant set Λ and the heading control vanishes when the splay state is achieved, the steering control is reduced to $u_k = \dot{\theta}_k \equiv \omega_c$ in the set Λ. Since d_k is constant and θ_k is time varying because of $\dot{\theta}_k \equiv \omega_c$, (4.27) holds only if $d_k \equiv 0$ holds, meaning that each vehicle orbits around the arbitrarily assigned center R^*.

Therefore, under heading control (4.17), spacing control $\tilde{u}_k^{\text{space}}$ in (4.20) will drive all vehicles interacting on a connected graph to orbit around the arbitrarily assigned center R^* with the desired angular velocity ω_c if $\phi_k(0)$ is set to $(\theta_k(0) - k\frac{2\pi}{N}) \bmod 2\pi$ for $k = 1, 2, \ldots, N$ and all these initial values are constrained in a half cycle of $\mathbb{S}^1$. ■

From Theorem 4.2, we have the following theorem for vehicle networks on all-to-all graphs.

Theorem 4.4. *For a network of N vehicles with kinetic model given in (4.2) under an all-to-all graph $\mathcal{G} = (\mathcal{V}, \mathcal{E})$, heading control $\tilde{u}_k^{\text{orien}}$ in the singularly-perturbed control framework (4.13) is designed as (4.19). Then spacing control $\tilde{u}_k^{\text{space}}$ in (4.28) will drive all vehicles to orbit around the centroid $R = \frac{1}{N}\sum_{j=1}^{N} r_j$ with a desired angular velocity ω_c if $\phi_k(0)$ is set to $\theta_k(0)$ for $k = 1, 2, \ldots, N$ and no two vehicles have equal initial headings.*

$$\tilde{u}_k^{\text{space}} =< \omega_c(r_k - R), e^{\mathrm{i}\theta_k} >= \frac{1}{N}\sum_{j=1}^{N} < \omega_c(r_k - r_j), e^{\mathrm{i}\theta_k} > \tag{4.28}$$

Proof. Define the relative position between vehicle k and the centroid R by $\tilde{r}_k = r_k - R$, thus the spacing control $\tilde{u}_k^{\text{space}}$ can be rewritten as:

$$\tilde{u}_k^{\text{space}} =< \omega_c \tilde{r}_k, e^{\mathrm{i}\theta_k} > \tag{4.29}$$

The center of vehicle k's circular motion is

$$c_k = r_k + \mathrm{i}\omega_c^{-1} e^{\mathrm{i}\theta_k} \tag{4.30}$$

Following [140], define the Lyapunov function as $U = \frac{1}{2} \parallel \mathbf{Hc} \parallel^2$ where $\mathbf{H} = \mathbf{I}_N - \frac{1}{N}\mathbf{1}\mathbf{1}^T$, $\mathbf{1} = [1, 1, \ldots, 1]^T$, $\mathbf{c} = [c_1, c_2, \ldots, c_N]^T$, and $\mathbf{I}_N$ is the N-dimensional identity matrix.

When vehicles orbit around the same center, i.e., $c_1 = c_2 = \ldots = c_N$, we have $\mathbf{Hc} = \mathbf{0}$. Therefore, U reaches its minimum 0 when all vehicles orbit around the same center.

Since when the splay state is achieved, the heading control $\tilde{u}_k^{\text{orien}}$ vanishes, the dynamics of c_k is given by

$$\begin{aligned} \dot{c}_k &= \dot{r}_k - \omega_c^{-1} e^{\mathrm{i}\theta_k}\dot{\theta}_k = e^{\mathrm{i}\theta_k} - \omega_c^{-1} e^{\mathrm{i}\theta_k}\{\omega_c + \sum_{j\neq k} \tilde{u}_k^{\text{space}}\delta(t - t_j)\} \\ &= -\omega_c^{-1} e^{\mathrm{i}\theta_k} \sum_{j\neq k} \tilde{u}_k^{\text{space}}\delta(t - t_j) \end{aligned} \tag{4.31}$$

Then the dynamics of U can be obtained as

$$\begin{aligned}\dot{U} &=< \mathbf{Hc}, \mathbf{H}\dot{\mathbf{c}} >= \sum_{k=1}^{N} < \mathbf{H}_k\mathbf{c}, \dot{c}_k > \\ &= -\sum_{k=1}^{N} < \mathbf{H}_k\mathbf{c}, \omega_c^{-1} e^{\mathrm{i}\theta_k} > \{\sum_{j\neq k} \tilde{u}_k^{\text{space}} \delta(t-t_j)\}\end{aligned} \tag{4.32}$$

where we used $\mathbf{H}^H\mathbf{H} = \mathbf{HH} = \mathbf{H}$, and $\mathbf{H}_k$ denotes $\mathbf{H}$'s kth row. $\mathbf{H}_k\mathbf{c}$ can be rewritten as

$$\begin{aligned}\mathbf{H}_k\mathbf{c} &= c_k - \frac{1}{N}\mathbf{1}^T\mathbf{c} = r_k + \mathrm{i}\omega_c^{-1}e^{\mathrm{i}\theta_k} - R - \mathrm{i}\omega_c^{-1}\frac{1}{N}\sum_{j=1}^{N} e^{\mathrm{i}\theta_j} \\ &= \tilde{r}_k + \mathrm{i}\omega_c^{-1}e^{\mathrm{i}\theta_k}\end{aligned} \tag{4.33}$$

where we used $\frac{1}{N}\sum_{j=1}^{N} e^{\mathrm{i}\theta_j} = \dot{R} = 0$ (splay state is already achieved). So $< \mathbf{H}_k\mathbf{c}, \omega_c^{-1}e^{\mathrm{i}\theta_k} >$ in (4.32) can be rewritten as:

$$\begin{aligned}&< \mathbf{H}_k\mathbf{c}, \omega_c^{-1}e^{\mathrm{i}\theta_k} >=< \tilde{r}_k + \mathrm{i}\omega_c^{-1}e^{\mathrm{i}\theta_k}, \omega_c^{-1}e^{\mathrm{i}\theta_k} > \\ =& < \tilde{r}_k, \omega_c^{-1}e^{\mathrm{i}\theta_k} >= \omega_c^{-2} < \tilde{r}_k, \omega_c e^{\mathrm{i}\theta_k} >= \omega_c^{-2}\tilde{u}_k^{\text{space}}\end{aligned} \tag{4.34}$$

Therefore, (4.32) can be simplified as follows:

$$\begin{aligned}\dot{U} &= -\sum_{k=1}^{N} \omega_c^{-2}\tilde{u}_k^{\text{space}}\{\sum_{j\neq k}\tilde{u}_k^{\text{space}}\delta(t-t_j)\} \\ &= -\omega_c^{-2}\sum_{k=1}^{N}\sum_{j\neq k}(\tilde{u}_k^{\text{space}})^2\delta(t-t_j)\end{aligned} \tag{4.35}$$

Thus we have $\dot{U} \leq 0$ under the spacing control (4.28). According to LaSalle Invariance principle, all solutions will converge to the largest invariant set Λ where $\tilde{u}_k^{\text{space}} =< \omega_c\tilde{r}_k, e^{\mathrm{i}\theta_k} >\equiv 0$ holds for $k = 1, \ldots, N$. Accordingly from (4.34), we have $< \mathbf{H}_k\mathbf{c}, \omega_c^{-1}e^{\mathrm{i}\theta_k} >= \omega_c^{-2}\tilde{u}_k^{\text{space}} \equiv 0$ in the set Λ for $k = 1, \ldots, N$.

Since $\tilde{u}_k^{\text{space}} \equiv 0$ holds in set Λ, we have $\dot{c}_k = 0$ in (4.31) which implies that c_k is constant. Further taking into account the fact that $\tilde{u}_k^{\text{orien}}$ vanishes after achieving the splay state, we have $\dot{\theta}_k = u_k \equiv \omega_c$ for $k = 1, \ldots, N$. In the set Λ, $\mathbf{H}_k\mathbf{c}$ is constant since c_k is constant and θ_k is time varying because $\dot{\theta}_k \equiv \omega_c$ holds, so $< \mathbf{H}_k\mathbf{c}, \omega_c^{-1}e^{\mathrm{i}\theta_k} >\equiv 0$ holds only if $\mathbf{H}_k\mathbf{c} \equiv 0$ for $k = 1, \ldots, N$, which means $c_1 = c_2 = \ldots = c_N$. Since splay state has been achieved, according to (4.30), we know that all vehicles orbit around the centroid, i.e., $c_1 = c_2 = \ldots = c_N = R$.

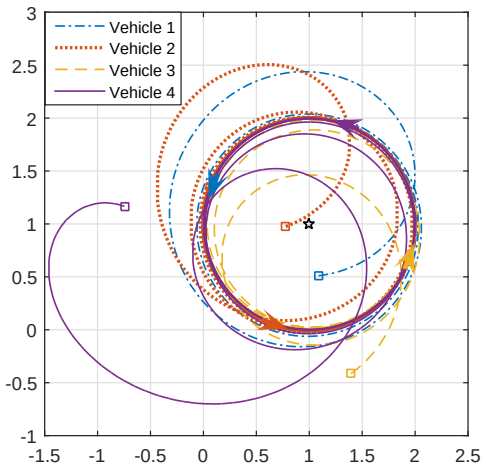

Figure 4.8: Vehicle trajectories of four vehicles in circular motion around the arbitrarily assigned center ($R^* = 1 + \mathrm{i}$ represented by the star) under a connected graph.

Therefore, under heading control (4.19), spacing control $\tilde{u}_k^{\text{space}}$ in (4.28) will drive all vehicles interacting on an all-to-all graph to orbit around the centroid $R = \frac{1}{N}\sum_{k=1}^{N} r_k$ with a desired angular velocity ω_c if $\phi_k(0)$ is set to $\theta_k(0)$ for $k = 1, 2, \ldots, N$ and no two vehicles have equal initial headings. ■

Now we use simulation results to demonstrate Theorems 4.3 and 4.4.

We first considered a network of $N = 4$ vehicles interacting on a connected graph given in Fig. 4.4. The vehicle network under $\tilde{u}_k^{\text{orien}}$ in (4.17) and $\tilde{u}_k^{\text{space}}$ in (4.20) was simulated. K in (4.13) was set to 5, ω_o was set to 10π, and ω_c in (4.20) was set to 1 rad/s. The center R^* was set to $1 + \mathrm{i}$. The initial positions of the vehicles were randomly chosen from the disk with radius 2 centering at the origin. The initial headings were randomly chosen from $[0,\ 2\pi)$ such that $\phi_k(0) = (\theta_k(0) - k\frac{2\pi}{N}) \bmod 2\pi$ for $k = 1, 2, \ldots, N$ were constrained in a half cycle of $\mathbb{S}^1$. The evolutions of the vehicle trajectories are given in Fig. 4.8, which confirmed Theorem 4.3. Note that the starting and ending points of vehicle trajectories are represented by squares and arrows, respectively.

Next we considered a network of $N = 4$ vehicles interacting on an all-to-all graph. The vehicle network under $\tilde{u}_k^{\text{orien}}$ in (4.19) and $\tilde{u}_k^{\text{space}}$ in (4.28) was simulated. K was set to 5, ω_o is set to 10π, and the desired angular velocity ω_c is set to 1 rad/s. The initial positions of the vehicles are randomly chosen from the disk with radius 2 centering at the origin. The initial headings are randomly chosen from $[0,\ 2\pi)$. The evolutions of the vehicle trajectories are given in Fig. 4.9, which confirmed Theorem 4.4.

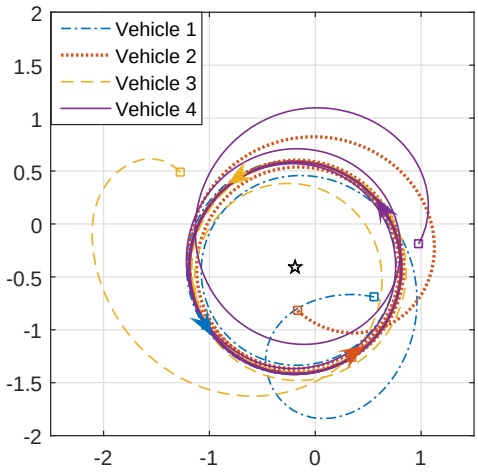

Figure 4.9: The trajectories of four vehicles in circular motion around the centroid R under an all-to-all graph.

4.6 Summaries

A pulse-based integrated communication and control approach was proposed for collective motion coordination. Different from existing results relying on a continuous control design followed by discretization based implementation, we designed communication and control in a unified framework, which can prevent the adverse effects of discretization and guarantee the design performance in implementation. The pulse-based message exchanging also significantly reduces processing latency and communication delay, and enhances robustness to channel interferences compared with conventional packet-based communication approaches.

Chapter 5

Privacy Preservation in Multi-Agent Systems

5.1 Introduction

In this chapter, we focus on the privacy-preserving average consensus in multi-agent systems. For a multi-agent system of N nodes (agents) interacting on a connected graph, average consensus can enable all nodes converge to the average of their initial values through iterations based on local interaction between neighboring nodes. Average consensus is key for multi-agent systems, with applications ranging from load balancing (with divisible tasks) in parallel computing [11, 21], network synchronization [85], distributed information fusion [136, 162], to decentralized control [112, 130].

To make all nodes converge to the average of their initial values, conventional average consensus algorithms require each node to exchange explicit state values with its neighbors. This leads to the disclosure of sensitive state information, which is undesirable in terms of privacy-preservation. In many collaborative applications such as smart grid, banking or health-care networks, privacy-preservation is crucial for encouraging participation in collaboration because individual nodes tend not to trade privacy for performance [58].

To enable privacy preservation in average consensus, some results have been reported. One commonly used approach is differential privacy from the database literature [45, 62, 63, 67, 107, 108, 163] (and its variants [68, 154]). In order to enable privacy preservation in average consensus, differential-privacy based approaches inject independent (and hence uncorrelated) noises directly to nodes' states, which leads to a

fundamental trade-off between enabled privacy and computational accuracy [108, 156]. To guarantee computational accuracy, [17, 50, 55–57, 89, 96, 125] proposed to inject additive correlated noise to exchanged messages, instead of uncorrelated noise used by differential-privacy. However, these prior works only consider average consensus under balanced and static network topologies. Different from injecting noises to nodes' states in the aforementioned approaches, [5] employed carefully designed mask maps to protect the actual states. Observability based approaches have also been discussed to protect the privacy of multi-agent systems [4, 121, 132]. The basic idea is to design the interaction topology so as to minimize the observability from a compromised agent, which amounts to minimizing its ability to infer the initial states of other network agents. However, observability based approaches cannot protect the privacy of the direct neighbors of the compromised agent. Recently, encryption based approaches have been proposed to enable privacy preservation by encrypting exchanged messages with the assistance of additive homomorphic encryption [33, 52, 71, 135], with the price of increasing computation and communication overhead. Another privacy-preserving approach was proposed in [155] where each node's privacy is protected by decomposing its state into two sub-states. However, [155] relies on undirected interactions and is inapplicable to time-varying directed graphs considered in our work.

In this chapter, we address privacy-preserving average consensus under time-varying directed graphs that are not necessarily balanced. Building on the conventional push-sum based consensus algorithm, we enable privacy preservation by judiciously adding randomness in interaction dynamics and leverage the inherent robustness of the push-sum algorithm to ensure consensus to the exact average value. More specifically, in the first several steps, each node sends completely independent random numbers to its out-neighbors and updates its own state under a sum-invariant (column-stochastic) constraint to completely obfuscate its initial value without affecting the final convergence result. This is in distinct difference from differential-privacy based average consensus approaches which enable privacy through sacrificing accuracy in obtained consensus value. The proposed approach is able to preserve privacy even when multiple honest-but-curious nodes collude with each other. Numerical simulations are provided to verify the effectiveness and efficiency of the proposed approach.

The remainder of this chapter is organized as follows. In Section 5.2, we introduce some preliminary concepts and problem formulation. A privacy-preserving average consensus algorithm is proposed and analyzed in Section 5.3. Numerical simulations are provided in Section 5.4. Finally, we conclude this chapter in Section 5.5.

5.2 Preliminaries and Problem Formulation

This section introduces some preliminaries of communication graph, the conventional push-sum algorithm, and the problem formulation.

5.2.1 Graph Representation

We represent a multi-agent system of N nodes as a sequence of time-varying directed graphs $\{\mathcal{G}(k) = (\mathcal{V}, \mathcal{E}(k))\}$ where $\mathcal{V} = \{1, 2, \ldots, N\}$ is the set of nodes and $k = 0, 1, \ldots$ is the time index. $\mathcal{E}(k) \subset \mathcal{V} \times \mathcal{V}$ is the edge set at time k, whose elements are such that $(i,\, j) \in \mathcal{E}(k)$ holds if and only if there exists a directed edge from node j to node i at time k, i.e., node j can send messages to node i at time k. For notational convenience, we assume that there are no self edges, i.e., $(i,\, i) \notin \mathcal{E}(k)$ for all k and $i \in \mathcal{V}$. At time k, each edge $(i,\, j) \in \mathcal{E}(k)$ has an associated weight, $p_{ij}(k) > 0$. The out-neighbor set of node i at time k, which represents the set of nodes that can receive messages from node i at time k, is denoted as $\mathcal{N}_i^{out}(k) = \{j \in \mathcal{V} \,|\, (j,\, i) \in \mathcal{E}(k)\}$. Similarly, at time k, the in-neighbor set of node i, which represents the set of nodes that can send messages to node i at time k, is denoted as $\mathcal{N}_i^{in}(k) = \{j \in \mathcal{V} \,|\, (i,\, j) \in \mathcal{E}(k)\}$. From the above definitions, it can be obtained that $i \in \mathcal{N}_j^{out}(k)$ and $j \in \mathcal{N}_i^{in}(k)$ are equivalent. Agent i's out-degree at time instant k is represented by $D_i^{out}(k) = |\mathcal{N}_i^{out}(k)|$ and its in-degree is represented by $D_i^{in}(k) = |\mathcal{N}_i^{in}(k)|$, where $|\mathcal{S}|$ is the cardinality of the set $\mathcal{S}$.

For a sequence of time-varying directed graphs $\{\mathcal{G}(k) = (\mathcal{V}, \mathcal{E}(k))\}$, we define $\mathcal{E}_\infty$ as the set of directed edges $(i,\, j)$ that exist for infinitely many time instants, i.e.,

$$\mathcal{E}_\infty = \big\{(i,\, j) \big| (i,\, j) \in \mathcal{E}(k) \text{ for infinitely many indices } k\big\} \tag{5.1}$$

We focus on time-varying directed graphs which satisfy the following assumptions:

Assumption 5.1. *For a sequence of time-varying directed graphs $\{\mathcal{G}(k) = (\mathcal{V}, \mathcal{E}(k))\}$, for any $i, j \in \mathcal{V}$ with $i \neq j$, there exists at least one directed path from i to j in $(\mathcal{V}, \mathcal{E}_\infty)$, i.e., $(\mathcal{V}, \mathcal{E}_\infty)$ is strongly connected.*

Assumption 5.2. *For a sequence of time-varying directed graphs $\{\mathcal{G}(k) = (\mathcal{V}, \mathcal{E}(k))\}$, there exists an integer $T \geq 1$ such that for every $(i,\, j) \in \mathcal{E}_\infty$, node j directly communicates with node i at least once every T consecutive time instants. T is called intercommunication interval bound.*

Assumption 5.3. *We assume that each node i has access to its out-degree $D_i^{out}(k)$ at each iteration k.*

Note that Assumption 5.3 is widely used in existing literature on time-varying directed graphs such as [102, 104, 166]. In fact, in many directed graphs, it is possible for a node to know its out-neighbors. For example, in many safety-critical systems such as industrial control systems, the exchange of data occurs in a directed way due to unidirectional gateways (aka data diode) whereas control messages (a special type of messages used to configure network connections) can be exchanged in a bidirectional manner to establish connections [137].

5.2.2 The Conventional Push-Sum Algorithm

The conventional push-sum considers N nodes interacting on a constant directed graph $\mathcal{G} = (\mathcal{V}, \mathcal{E})$, with each node having an initial state x_i^0 $(i = 1, 2, \ldots, N)$ [10, 51, 69]. Represent the average value of all initial states as $\alpha = \sum_{j=1}^{N} x_j^0/N$. The conventional push-sum algorithm conducts two iterative computations simultaneously, and allows each node to obtain the exact average of the initial values α in an asymptotic way. This mechanism of the conventional push-sum algorithm is summarized in Algorithm 5.1 below:

Algorithm 5.1 The conventional push-sum algorithm

1. N nodes interact on a constant directed graph $\mathcal{G} = (\mathcal{V}, \mathcal{E})$. Each node i is initialized with $s_i(0) = x_i^0$, $w_i(0) = 1$, and $\pi_i(0) = s_i(0)/w_i(0)$. The weight p_{ij} associated with the edge $(i, j) \in \mathcal{E}$ satisfies $p_{ij} \in (0, 1)$ if $j \in \mathcal{N}_i^{in} \cup \{i\}$ is true and $p_{ij} = 0$ otherwise. For any given $j = 1, 2, \ldots, N$, p_{ij} satisfies $\sum_{i=1}^{N} p_{ij} = 1$.
2. At iteration step k:
   (a) Agent i calculates $p_{ji}s_i(k)$ and $p_{ji}w_i(k)$, and sends both values to all of its out-neighbors $j \in \mathcal{N}_i^{out}$.
   (b) After receiving the values of $p_{ij}s_j(k)$ and $p_{ij}w_j(k)$ from all its in-neighbors $j \in \mathcal{N}_i^{in}$, node i updates s_i and w_i as follows:
   $$\begin{cases} s_i(k+1) = \displaystyle\sum_{j \in \mathcal{N}_i^{in} \cup \{i\}} p_{ij} s_j(k) \\ w_i(k+1) = \displaystyle\sum_{j \in \mathcal{N}_i^{in} \cup \{i\}} p_{ij} w_j(k) \end{cases} \tag{5.2}$$
   (c) Agent i uses the ratio $\pi_i(k+1) = s_i(k+1)/w_i(k+1)$ as an estimate of the average value $\alpha = \sum_{j=1}^{N} x_j^0/N$.

For the sake of notational simplicity, we rewrite (5.2) in the following more compact form:

$$\begin{cases} \mathbf{s}(k+1) = \mathbf{P}\mathbf{s}(k) \\ \mathbf{w}(k+1) = \mathbf{P}\mathbf{w}(k) \end{cases} \tag{5.3}$$

where $\mathbf{s}(k) = [s_1(k), s_2(k), \ldots, s_N(k)]^T$ and $\mathbf{w}(k) = [w_1(k), w_2(k), \ldots, w_N(k)]^T$, and $\mathbf{P} = [p_{ij}]$. From Algorithm 5.1, we have $\mathbf{s}(0) = [x_1^0, x_2^0, \ldots, x_N^0]^T$ and $\mathbf{w}(0) = \mathbf{1}$. We can also obtain that the matrix $\mathbf{P}$ is column-stochastic, i.e., $\sum_{i=1}^N p_{ij} = 1$ holds for $j = 1, 2, \ldots, N$.

At iteration step k, each node computes the ratio $\pi_i(k+1) = s_i(k+1)/w_i(k+1)$ to estimate the average value $\alpha = \sum_{j=1}^N x_j^0/N$. Since $\mathcal{G}$ is assumed to be a strongly connected directed graph, $\mathbf{P}^k$ will converge to a rank-1 matrix exponentially fast [37, 138]. Defining $\mathbf{P}^\infty$ as the limit of $\mathbf{P}^k$ as $k \to \infty$, we can obtain the form of $\mathbf{P}^\infty$ as $\mathbf{P}^\infty = \mathbf{v}\mathbf{1}^T$ where $\mathbf{v} = [v_1, v_2, \ldots, v_N]^T$. Using the facts $\mathbf{s}(k) = \mathbf{P}^k\mathbf{s}(0)$ and $\mathbf{w}(k) = \mathbf{P}^k\mathbf{w}(0)$, we can further have [51]:

$$\pi_i(\infty) = \frac{s_i(\infty)}{w_i(\infty)} = \frac{[\mathbf{P}^\infty\mathbf{s}(0)]_i}{[\mathbf{P}^\infty\mathbf{w}(0)]_i} = \frac{v_i\sum_{j=1}^N s_j(0)}{v_i\sum_{j=1}^N w_j(0)} = \alpha \tag{5.4}$$

where $[\mathbf{P}^\infty\mathbf{s}(0)]_i$ and $[\mathbf{P}^\infty\mathbf{w}(0)]_i$ represent the i-th element of vector $\mathbf{P}^\infty\mathbf{s}(0)$ and vector $\mathbf{P}^\infty\mathbf{w}(0)$, respectively. Hence, all estimates $\pi_1(k), \pi_2(k), \ldots, \pi_N(k)$ will asymptotically converge to the average $\alpha = \sum_{j=1}^N x_j^0/N$.

5.2.3 Problem Formulation

In our work, we will address average consensus under time-varying directed graphs while protecting the privacy of participating nodes against adversaries. To this end, we first present the attack model and our definition of privacy.

Definition 5.1. *We define an honest-but-curious adversary as an node who follows protocol steps correctly but collects received messages in an attempt to infer the initial value of other participating nodes.*

Definition 5.2. *We define that privacy of the initial value x_i^0 of node i is preserved if x_i^0 cannot be estimated by honest-but-curious adversaries with any accuracy. By "any accuracy," we mean that the honest-but-curious adversaries cannot distinguish whether the initial state of node i is x_i^0 or $x_i^0 + \delta$ where δ can be any value in $\mathbb{R}$.*

Our definition of privacy requires that honest-but-curious adversaries cannot even find a range of a sensitive value and therefore is more stringent than the privacy definition in [16, 27, 53, 83, 89] which defines privacy as the inability of an adversary to *uniquely* determine the sensitive value.

We consider two different scenarios: 1) a single adversarial node acting on its own (i.e., without colluding with other adversarial nodes) and 2) multiple adversarial nodes colluding with each other, as detailed below:

Assumption 5.4. *All N nodes are honest-but-curious and try to infer other nodes' initial states without sharing information with each other.*

Assumption 5.5. *A set of honest-but-curious nodes $\mathcal{A}$ share information with each other to infer the initial value x_i^0 of node $i \notin \mathcal{A}$.*

We next show that the conventional push-sum does not preserve privacy. From (5.2) and (5.3), an honest-but-curious node i can receive $p_{ij}s_j(0)$ and $p_{ij}w_j(0)$ from its in-neighbor node j after the first iteration step $k = 0$. Then node i is able to uniquely determine x_j^0 by $x_j^0 = s_j(0) = \frac{p_{ij}s_j(0)}{p_{ij}w_j(0)}$ using the fact $w_j(0) = 1$. Therefore, an honest-but-curious node can always infer the initial values of all its in-neighbors, and hence the conventional push-sum algorithm cannot provide protection against honest-but-curious adversaries. It is worth noting that using a similar argument, we can also obtain that the conventional push-sum is not privacy-preserving even when the weight is allowed to be time-varying (e.g., [10].)

5.3 The Privacy-Preserving Algorithm and Performance Analysis

In this section, we will propose our privacy-preserving average consensus algorithm for time-varying directed graphs, and then provide rigorous analysis of convergence rate and enabled strength of privacy, respectively.

5.3.1 Privacy-Preserving Average Consensus Algorithm

The analysis above reveals that using the same weight p_{ij} for both $p_{ij}s_j(0)$ and $p_{ij}w_j(0)$ leads to disclosing the initial state value. Motivated by this observation, we here introduce a novel privacy-preserving average consensus algorithm which injects randomness in the dynamics of interactions in iterations $k = 0, \ldots, K_i$ for each node i. Note that here K_i is a non-negative integer chosen by node i and is *only known* to node i. Its influence will be discussed in detail in Remark 5.7 and Remark 5.8.

Algorithm 5.2 Privacy-preserving average consensus algorithm

1. N nodes interact on a sequence of time-varying directed graphs $\{\mathcal{G}(k) = (\mathcal{V}, \mathcal{E}(k))\}$. Each node i is initialized with $s_i(0) = x_i^0$, $w_i(0) = 1$, and $\pi_i(0) = s_i(0)/w_i(0)$. Each node i chooses a non-negative integer K_i and keeps it private to itself.

2. At iteration step k:

   (a) Agent i generates a set of random weights $\left\{p_{ji}(k) \in (\varepsilon, 1) \,\middle|\, j \in \mathcal{N}_i^{out}(k) \cup \{i\}\right\}$ with the sum of this set equal to 1, and sets $\Delta w_{ji}(k) = p_{ji}(k) w_i(k)$ for $j \in \mathcal{N}_i^{out}(k) \cup \{i\}$.

   (b) If $k \leq K_i$, node i generates independently random numbers $\Delta s_{ji}(k)$ for $j \in \mathcal{N}_i^{out}(k)$ following some distributions *only known* to node i, and sets $\Delta s_{ii}(k) = s_i(k) - \sum_{j \in \mathcal{N}_i^{out}(k)} \Delta s_{ji}(k)$; otherwise, node i sets $\Delta s_{ji}(k) = p_{ji}(k) s_i(k)$ for $j \in \mathcal{N}_i^{out}(k) \cup \{i\}$.

   (c) Agent i sends $\Delta s_{ji}(k)$ and $\Delta w_{ji}(k)$ to node $j \in \mathcal{N}_i^{out}(k)$.

   (d) After receiving $\Delta s_{ij}(k)$ and $\Delta w_{ij}(k)$ from its in-neighbors $j \in \mathcal{N}_i^{in}(k)$, node i updates s_i and w_i as follows:

$$\begin{cases} s_i(k+1) = \displaystyle\sum_{j \in \mathcal{N}_i^{in}(k) \cup \{i\}} \Delta s_{ij}(k) \\ w_i(k+1) = \displaystyle\sum_{j \in \mathcal{N}_i^{in}(k) \cup \{i\}} \Delta w_{ij}(k) \end{cases} \tag{5.5}$$

   (e) Agent i uses the ratio $\pi_i(k+1) = s_i(k+1)/w_i(k+1)$ to estimate the average value $\alpha = \sum_{j=1}^N x_j^0/N$.

Remark 5.1. *Compared to the conventional privacy-violating push-sum algorithm which broadcasts messages, Algorithm 5.2 needs node i to send different random numbers to different out-neighbors in iterations $k \leq K_i$. This is a price of obtaining privacy without losing accuracy in the time-varying directed topology case.*

Remark 5.2. *Note that in Algorithm 5.2, node i can choose random numbers $\Delta s_{ji}(k)$ following any distribution, and its choice is unknown to any other node. Also note that for different out-neighbors $j \in \mathcal{N}_i^{out}(k)$ and different iteration steps $k \leq K_i$, node i can choose $\Delta s_{ji}(k)$ independently following different distributions. Therefore, the generation mechanism of random numbers used in Algorithm 5.2 does not cause loss of privacy.*

Remark 5.3. *The way of injecting randomness in $\Delta s_{ji}(k)$ is different in iterations $k \leq K_i$ from $k > K_i$. In fact, in iterations $k \leq K_i$, $\Delta s_{ji}(k)$ can be nonzero even when $s_i(k)$ is zero. This is crucial in enabling strong privacy as receiving $\Delta s_{ji}(k)$ of a value zero will not allow the recipient to infer information about $s_i(k)$.*

Setting $\Delta s_{ji}(k)$, $\Delta w_{ji}(k)$, and $p_{ji}(k)$ to 0 for $j \notin \mathcal{N}_i^{out}(k) \cup \{i\}$, we can rewrite the dynamics in

(5.5) as

$$s_i(k+1) = \sum_{j=1}^{N} \Delta s_{ij}(k) \tag{5.6}$$

and

$$w_i(k+1) = \sum_{j=1}^{N} \Delta w_{ij}(k) = \sum_{j=1}^{N} p_{ij}(k) w_j(k) \tag{5.7}$$

for $k \geq 0$. Denote $\bar{K}$ as $\bar{K} = \max_i\{K_i\}$. For $k \geq \bar{K}+1$, (5.6) can be rewritten as

$$s_i(k+1) = \sum_{j=1}^{N} \Delta s_{ij}(k) = \sum_{j=1}^{N} p_{ij}(k) s_j(k) \tag{5.8}$$

We can further rewrite (5.7) and (5.8) into a matrix form

$$\begin{cases} \mathbf{s}(k+1) = \mathbf{P}(k)\mathbf{s}(k) \ \text{ for } \ k \geq \bar{K}+1 \\ \mathbf{w}(k+1) = \mathbf{P}(k)\mathbf{w}(k) \ \text{ for } \ k \geq 0 \end{cases} \tag{5.9}$$

where $\mathbf{s}(k) = [s_1(k), s_2(k), \ldots, s_N(k)]^T$, $\mathbf{w}(k) = [w_1(k), w_2(k), \ldots, w_N(k)]^T$, and the ij-th entry of $\mathbf{P}(k)$ is the weight $p_{ij}(k)$. For iteration $k = 0$, we have $\mathbf{s}(0) = [x_1^0, x_2^0, \ldots, x_N^0]^T$ and $\mathbf{w}(0) = \mathbf{1}$. From Algorithm 5.2, we know that $\mathbf{P}(k) = \left[p_{ij}(k)\right]$ in (5.9) is time-varying and column-stochastic for $k \geq 0$.

Defining the transition matrix as follows

$$\mathbf{\Phi}(k:t) = \mathbf{P}(k) \cdots \mathbf{P}(t) \tag{5.10}$$

for all k and t with $k \geq t$, where $\mathbf{\Phi}(k:k) = \mathbf{P}(k)$, we can rewrite (5.9) as

$$\begin{cases} \mathbf{s}(k+1) = \mathbf{\Phi}(k:\bar{K}+1)\mathbf{s}(\bar{K}+1) \ \text{ for } \ k \geq \bar{K}+1 \\ \mathbf{w}(k+1) = \mathbf{\Phi}(k:0)\mathbf{w}(0) \ \text{ for } \ k \geq 0 \end{cases} \tag{5.11}$$

5.3.2 Convergence Analysis

Next we prove that Algorithm 5.2 can guarantee that the estimates of all nodes converge to the exact average value of initial values. We will also analyze the rate of convergence of Algorithm 5.2. Using the the convergence definition in [102] and [101], we define the rate of convergence to be at least $\gamma \in (0,\, 1)$ if there exists a positive constant value C such that $\left\|\boldsymbol{\pi}(k) - \alpha\mathbf{1}\right\| \leq C\gamma^k$ is true for all k, where $\boldsymbol{\pi}(k) = [\pi_1(k), \ldots, \pi_N(k)]^T$ and $\alpha = \sum_{j=1}^{N} x_j^0/N$ is the average value. Note that this definition means a smaller γ

corresponding to a faster convergence. To analyze the convergence rate of Algorithm 5.2, we first introduce Lemma 5.1 below:

Lemma 5.1. *For a network of N nodes represented by a sequence of time-varying directed graphs $\{\mathcal{G}(k) = (\mathcal{V}, \mathcal{E}(k))\}$ which satisfies Assumptions 5.1, 5.2, and 5.3, under Algorithm 5.2, each node i has $w_i(k) \geq \varepsilon^{T(N-1)}$ for $k \geq 1$ where T is defined in Assumption 5.2.*

Proof: For $k \geq 1$, from (5.11) we have

$$\mathbf{w}(k) = \mathbf{\Phi}(k-1:0)\mathbf{1} \tag{5.12}$$

Represent $\delta(k)$ as

$$\delta(k) \triangleq \min_{1\leq i\leq N} w_i(k) = \min_{1\leq i\leq N} [\mathbf{\Phi}(k-1:0)\,\mathbf{1}]_i \tag{5.13}$$

for $k \geq 1$. To prove $w_i(k) \geq \varepsilon^{T(N-1)}$ for $k \geq 1$, it is sufficient to prove $\delta(k) \geq \varepsilon^{T(N-1)}$ for $k \geq 1$. We divide our proof into two parts: $1 \leq k \leq T(N-1)$ and $k \geq T(N-1)+1$.

Part 1: $\delta(k) \geq \varepsilon^{T(N-1)}$ for $1 \leq k \leq T(N-1)$. One can verify that the following relationship holds

$$\begin{aligned}
\mathbf{\Phi}(k-1:0)t_{ii} &= [\mathbf{P}(k-1)\cdots\mathbf{P}(0)]_{ii} \\
&\geq [\mathbf{P}(k-1)]_{ii}\,[\mathbf{P}(k-2)\cdots\mathbf{P}(0)]_{ii} \\
&\geq \varepsilon\,[\mathbf{\Phi}(k-2:0)]_{ii}
\end{aligned}$$

Given $[\mathbf{\Phi}(0:0)]_{ii} = [\mathbf{P}(0)]_{ii} \geq \varepsilon$, one can obtain $[\mathbf{\Phi}(k-1:0)]_{ii} \geq \varepsilon^k$. Therefore, it follows that

$$[\mathbf{\Phi}(k-1:0)\,\mathbf{1}]_i \geq [\mathbf{\Phi}(k-1:0)]_{ii} \geq \varepsilon^k \geq \varepsilon^{T(N-1)}$$

is true for $i = 1, \ldots, N$ and $1 \leq k \leq T(N-1)$, implying that $\delta(k) \geq \varepsilon^{T(N-1)}$ holds for $1 \leq k \leq T(N-1)$.

Part 2: $\delta(k) \geq \varepsilon^{T(N-1)}$ for $k \geq T(N-1)+1$. Under Assumptions 5.1 and 5.2, and the requirements on weights $p_{ij}(k)$ in Algorithm 5.2, and following the arguments in Lemma 2 in [105], we can obtain

$$[\mathbf{\Phi}(k-1:k-T(N-1))]_{ij} \geq \varepsilon^{T(N-1)}$$

for $1 \leq i,\, j \leq N$. Since $k \geq T(N-1)+1$ holds and $\mathbf{P}(k)$ is a column-stochastic matrix,

$$\mathbf{\Phi}(k-T(N-1)-1:0) = \mathbf{P}(k-T(N-1)-1)\cdots\mathbf{P}(0)$$

should also be a column-stochastic matrix. Further using the fact $\mathbf{\Phi}(k-1:0) = \mathbf{\Phi}(k-1:k-T(N-1))\mathbf{\Phi}(k-T(N-1)-1:0)$ leads to $[\mathbf{\Phi}(k-1:0)]_{ij} \geq \varepsilon^{T(N-1)}$ for $1 \leq i,\, j \leq N$. Therefore, we have

$$[\mathbf{\Phi}(k-1:0)\,\mathbf{1}]_i \geq N\varepsilon^{T(N-1)} \geq \varepsilon^{T(N-1)}$$

for $i = 1, \ldots, N$, meaning $\delta(k) \geq \varepsilon^{T(N-1)}$ for $k \geq T(N-1)+1$.

Based on $\delta(k) \geq \varepsilon^{T(N-1)}$ for $k \geq 1$, we can obtain $w_i(k) \geq \varepsilon^{T(N-1)}$ for $k \geq 1$. In summary, we always have $w_i(k) \geq \varepsilon^{T(N-1)}$ when $k \geq 1$. ■

Theorem 5.1. *For a network of N nodes represented by a sequence of time-varying directed graphs $\{\mathcal{G}(k) = (\mathcal{V},\, \mathcal{E}(k))\}$ which satisfies Assumptions 5.1, 5.2, and 5.3, under Algorithm 5.2, the estimate $\pi_i(k) = s_i(k)/w_i(k)$ of each node i will converge to the average $\alpha = \sum_{j=1}^{N} x_j^0/N$. More specifically, the rate of convergence of Algorithm 5.2 is at least $\gamma = (1-\varepsilon^{T(N-1)})^{\frac{1}{T(N-1)}} \in (0,\, 1)$, meaning that there exists a positive constant value C satisfying $\left\|\boldsymbol{\pi}(k) - \alpha\mathbf{1}\right\| \leq C\gamma^k$ for all k.*

Proof: According to the requirements on $\Delta s_{ji}(k)$ in Algorithm 5.2, we have $\sum_{j=1}^{N} \Delta s_{ji}(k) = s_i(k)$ for $k \geq 0$. Therefore, from (5.6), we have the following mass conservation property for $\mathbf{s}(k)$:

$$\begin{aligned}\mathbf{1}^T\mathbf{s}(k+1) &= \sum_{i=1}^{N} s_i(k+1) = \sum_{i=1}^{N}\sum_{j=1}^{N} \Delta s_{ij}(k) = \sum_{j=1}^{N}\sum_{i=1}^{N} \Delta s_{ij}(k) \\ &= \sum_{j=1}^{N} s_j(k) = \sum_{i=1}^{N} s_i(k) = \mathbf{1}^T\mathbf{s}(k)\end{aligned} \tag{5.14}$$

for $k \geq 0$, which further implies

$$\mathbf{1}^T\mathbf{s}(k+1) = \mathbf{1}^T\mathbf{s}(k) = \cdots = \mathbf{1}^T\mathbf{s}(0) = \sum_{j=1}^{N} x_j^0 \tag{5.15}$$

and

$$\alpha = \frac{\sum_{j=1}^{N} x_j^0}{N} = \frac{\mathbf{1}^T\mathbf{s}(0)}{N} = \frac{\mathbf{1}^T\mathbf{s}(k+1)}{N} \tag{5.16}$$

for $k \geq 0$. Similarly, we have the following mass conservation property for $\mathbf{w}(k)$:

$$\mathbf{1}^T\mathbf{w}(k+1) = \mathbf{1}^T\mathbf{w}(k) = \cdots = \mathbf{1}^T\mathbf{w}(0) = N \tag{5.17}$$

for $k \geq 0$. Then we rewrite (5.11) as

$$\begin{cases} \mathbf{s}(\bar{K}+l+1) = \mathbf{\Phi}(\bar{K}+l:\bar{K}+1)\mathbf{s}(\bar{K}+1) \\ \mathbf{w}(\bar{K}+l+1) = \mathbf{\Phi}(\bar{K}+l:\bar{K}+1)\mathbf{w}(\bar{K}+1) \end{cases} \tag{5.18}$$

for $l \geq 1$. Under Assumptions 5.1 and 5.2, and the requirements on weights $p_{ij}(k)$ in Algorithm 5.2, following Proposition 1(b) in [103], we know that the transition matrix $\mathbf{\Phi}(\bar{K}+l:\bar{K}+1)$ will converge to a stochastic vector $\boldsymbol{\varphi}(\bar{K}+l)$ with a geometric rate with respect to i and j, i.e., for all $i,j = 1,\ldots,N$ and $l \geq 1$, we have

$$\left|[\mathbf{\Phi}(\bar{K}+l:\bar{K}+1)]_{ij} - \varphi_i(\bar{K}+l)\right| \leq C_0\gamma^{l-1} \tag{5.19}$$

with $C_0 = 2(1+\varepsilon^{-T(N-1)})/(1-\varepsilon^{T(N-1)})$ and $\gamma = (1-\varepsilon^{T(N-1)})^{\frac{1}{T(N-1)}}$. Defining $\mathbf{M}(\bar{K}+l:\bar{K}+1)$ as

$$\mathbf{M}(\bar{K}+l:\bar{K}+1) \triangleq \mathbf{\Phi}(\bar{K}+l:\bar{K}+1) - \boldsymbol{\varphi}(\bar{K}+l)\,\mathbf{1}^T \tag{5.20}$$

we can have

$$\left|\left[\mathbf{M}(\bar{K}+l:\bar{K}+1)\right]_{ij}\right| \leq C_0\gamma^{l-1} \tag{5.21}$$

for all $i,j = 1,\ldots,N$ and $l \geq 1$. Further combining (5.20) with (5.18) leads to

$$\begin{cases} \mathbf{s}(\bar{K}+l+1) = \mathbf{M}(\bar{K}+l:\bar{K}+1)\mathbf{s}(\bar{K}+1) + \boldsymbol{\varphi}(\bar{K}+l)\,\mathbf{1}^T\mathbf{s}(\bar{K}+1) \\ \mathbf{w}(\bar{K}+l+1) = \mathbf{M}(\bar{K}+l:\bar{K}+1)\mathbf{w}(\bar{K}+1) + N\boldsymbol{\varphi}(\bar{K}+l) \end{cases} \tag{5.22}$$

where we used $\mathbf{1}^T\mathbf{w}(\bar{K}+1) = N$ from (5.17) in the derivation.

Combining (5.16) and (5.22), we have

$$\begin{aligned}
&\pi_i(\bar{K}+l+1)-\alpha \\
=&\frac{s_i(\bar{K}+l+1)}{w_i(\bar{K}+l+1)}-\frac{\mathbf{1}^T\mathbf{s}(\bar{K}+1)}{N} \\
=&\frac{s_i(\bar{K}+l+1)}{w_i(\bar{K}+l+1)}-\frac{\mathbf{1}^T\mathbf{s}(\bar{K}+1)w_i(\bar{K}+l+1)}{Nw_i(\bar{K}+l+1)} \\
=&\frac{[\mathbf{M}(\bar{K}+l:\bar{K}+1)\mathbf{s}(\bar{K}+1)]_i+\varphi_i(\bar{K}+l)\mathbf{1}^T\mathbf{s}(\bar{K}+1)}{w_i(\bar{K}+l+1)} \\
&-\frac{\mathbf{1}^T\mathbf{s}(\bar{K}+1)[\mathbf{M}(\bar{K}+l:\bar{K}+1)\mathbf{w}(\bar{K}+1)]_i}{Nw_i(\bar{K}+l+1)}-\frac{\mathbf{1}^T\mathbf{s}(\bar{K}+1)N\varphi_i(\bar{K}+l)}{Nw_i(\bar{K}+l+1)} \\
=&\frac{[\mathbf{M}(\bar{K}+l:\bar{K}+1)\mathbf{s}(\bar{K}+1)]_i}{w_i(\bar{K}+l+1)}-\frac{\mathbf{1}^T\mathbf{s}(\bar{K}+1)[\mathbf{M}(\bar{K}+l:\bar{K}+1)\mathbf{w}(\bar{K}+1)]_i}{Nw_i(\bar{K}+l+1)}
\end{aligned} \tag{5.23}$$

Therefore, for $i=1,\ldots,N$ and $l\geq 1$, we can obtain

$$\begin{aligned}
&\big|\pi_i(\bar{K}+l+1)-\alpha\big| \\
\leq&\frac{\big|[\mathbf{M}(\bar{K}+l:\bar{K}+1)\mathbf{s}(\bar{K}+1)]_i\big|}{w_i(\bar{K}+l+1)}+\frac{\big|\mathbf{1}^T\mathbf{s}(\bar{K}+1)[\mathbf{M}(\bar{K}+l:\bar{K}+1)\mathbf{w}(\bar{K}+1)]_i\big|}{Nw_i(\bar{K}+l+1)} \\
\leq&\frac{1}{\varepsilon^{T(N-1)}}\big(\max_j\big|[\mathbf{M}(\bar{K}+l:\bar{K}+1)]_{ij}\big|\big)\big\|\mathbf{s}(\bar{K}+1)\big\|_1 \\
&+\frac{1}{\varepsilon^{T(N-1)}}\big|\mathbf{1}^T\mathbf{s}(\bar{K}+1)\big|\big(\max_j\big|[\mathbf{M}(\bar{K}+l:\bar{K}+1)]_{ij}\big|\big)
\end{aligned} \tag{5.24}$$

where we used $w_i(\bar{K}+l+1)\geq\varepsilon^{T(N-1)}$ from Lemma 5.1 and $\big\|\mathbf{w}(\bar{K}+1)\big\|_1=\sum_{i=1}^N|w_i(\bar{K}+1)|=\mathbf{1}^T\mathbf{w}(\bar{K}+1)=N$ from (5.17) in the derivation. Further using the relationship $\big|\mathbf{1}^T\mathbf{s}(\bar{K}+1)\big|\leq\big\|\mathbf{s}(\bar{K}+1)\big\|_1$ and (5.21), we have

$$\big|\pi_i(\bar{K}+l+1)-\alpha\big|\leq 2C_0\big\|\mathbf{s}(\bar{K}+1)\big\|_1\varepsilon^{-T(N-1)}\gamma^{l-1} \tag{5.25}$$

for $l\geq 1$.

From (5.25), we can obtain for $l\geq 1$

$$\begin{aligned}
\big\|\boldsymbol{\pi}(\bar{K}+l+1)-\alpha\mathbf{1}\big\|&\leq 2\sqrt{N}C_0\big\|\mathbf{s}(\bar{K}+1)\big\|_1\varepsilon^{-T(N-1)}\gamma^{l-1} \\
&=C_1\gamma^{\bar{K}+l+1}
\end{aligned} \tag{5.26}$$

with C_1 given by

$$C_1=2\sqrt{N}C_0\big\|\mathbf{s}(\bar{K}+1)\big\|_1\varepsilon^{-T(N-1)}\gamma^{-\bar{K}-2} \tag{5.27}$$

Therefore, we obtain $\big\|\boldsymbol{\pi}(k)-\alpha\mathbf{1}\big\| \le C_1\gamma^k$ for $k \ge \bar{K}+2$.

For $k \le \bar{K}+1$, from (5.16) we have

$$\pi_i(k)-\alpha = \frac{s_i(k)}{w_i(k)} - \frac{\mathbf{1}^T\mathbf{s}(k)}{N} \tag{5.28}$$

which further implies

$$\begin{aligned} |\pi_i(k)-\alpha| &\le |\frac{s_i(k)}{w_i(k)}| + |\frac{\mathbf{1}^T\mathbf{s}(k)}{N}| \le \frac{|s_i(k)|}{\varepsilon^{T(N-1)}} + \frac{|\mathbf{1}^T\mathbf{s}(k)|}{N} \\ &\le \frac{\big\|\mathbf{s}(k)\big\|_1}{\varepsilon^{T(N-1)}} + \frac{\big\|\mathbf{s}(k)\big\|_1}{N} = \frac{N+\varepsilon^{T(N-1)}}{N\varepsilon^{T(N-1)}}\big\|\mathbf{s}(k)\big\|_1 \end{aligned} \tag{5.29}$$

Thus, it follows for $k \le \bar{K}+1$

$$\big\|\boldsymbol{\pi}(k)-\alpha\mathbf{1}\big\| = \Big[\sum_{i=1}^{N}|\pi_i(k)-\alpha|^2\Big]^{\frac{1}{2}} \le \frac{N+\varepsilon^{T(N-1)}}{\sqrt{N}\varepsilon^{T(N-1)}}\big\|\mathbf{s}(k)\big\|_1 \tag{5.30}$$

Defining C as

$$C \triangleq \max\big\{C_1, \gamma^{-k}\frac{N+\varepsilon^{T(N-1)}}{\sqrt{N}\varepsilon^{T(N-1)}}\|\mathbf{s}(k)\|_1 \,\big|\, 0 \le k \le \bar{K}+1\big\} \tag{5.31}$$

we can have

$$\big\|\boldsymbol{\pi}(k)-\alpha\mathbf{1}\big\| \le C\gamma^k \tag{5.32}$$

for all k. Therefore, each node i will converge to the average value $\alpha = \sum_{j=1}^{N} x_j^0/N$ with the rate of convergence at least $\gamma = (1-\varepsilon^{T(N-1)})^{\frac{1}{T(N-1)}} \in (0,\,1)$. ■

From Theorem 5.1, we can see that a smaller γ means a faster convergence. Under the relationship $\gamma = (1-\varepsilon^{T(N-1)})^{\frac{1}{T(N-1)}}$, to expedite the convergence, i.e., a smaller γ, it is sufficient to increase ε, which amounts to reducing the width of the range $(\varepsilon,\,1)$ for the random selection of $p_{ji}(k)$. Note that although a reduced range $(\varepsilon,\,1)$ enables an honest-but-curious adversary to obtain a better estimation of the range of node i's intermediate states $s_i(k)$ and $w_i(k)$ for $k \ge K_i+1$ from received $p_{ji}(k)s_i(k)$ and $p_{ji}(k)w_i(k)$, it does not affect the privacy of node i's initial state x_i^0, as will be shown in the following subsection. It is also worth noting that to meet the requirement of randomly selecting weights in our algorithm, ε cannot be arbitrarily close to 1. In fact, ε must satisfy $\varepsilon < 1/\max_{i,k}(D_i^{out}(k)+1)$. An easy way to select ε is to set $0<\varepsilon<1/N$ since $D_i^{out}(k) \le N-1$ is true for all k and $i \in \mathcal{V}$.

Remark 5.4. *Theorem 5.1 provides a detailed analysis of the rate of convergence under time-varying directed graphs, the results on which are sparse in the literature on Push-Sum under time-varying random weights.*

5.3.3 Privacy-Preserving Performance Analysis

Next we rigorously prove that Algorithm 5.2 is able to achieve the privacy defined in Definition 5.2 under two different scenarios as follows.

5.3.3.1 Honest-but-curious nodes without colluding

In this scenario (cf. Assumption 5.4), we have the following theorems.

Theorem 5.2. *For a network of N nodes represented by a sequence of time-varying directed graphs $\{\mathcal{G}(k) = (\mathcal{V},\, \mathcal{E}(k))\}$ which satisfies Assumptions 5.1, 5.2, 5.3, and 5.4, Algorithm 5.2 can preserve the privacy of node i if there exists a time instant $0 \leq k^* \leq K_i$ such that $\left|\left\{l \in \mathcal{V} \,\middle|\, l \in \mathcal{N}_i^{out}(k^*) \cup \mathcal{N}_i^{in}(k^*),\ K_l \geq k^*\right\}\right| \geq 2$ is true.*

Proof: To show that the privacy of node i can be protected, we have to show that the initial value x_i^0 of node i cannot be inferred by any honest-but-curious node j with any accuracy. Our idea is to prove the indistinguishability of x_i^0's *arbitrary* variation to any node j, i.e., node j cannot distinguish whether the initial state of node i is x_i^0 or $x_i^0 + \delta$ where δ can be *any* value in $\mathbb{R}$. According to Algorithm 5.2 and Assumption 5.4, the parameter and state values known to node j, denoted as $\mathcal{I}_j$, can be summarized as follows:

$$\begin{aligned}\mathcal{I}_j =& \left\{\mathcal{I}_j^{\text{state}}(k) \cup \mathcal{I}_j^{\text{send}}(k) \cup \mathcal{I}_j^{\text{receive}}(k) \,\middle|\, k \geq 0\right\} \\ & \cup \left\{w_m(0) = 1 \,\middle|\, m \in \mathcal{V}\right\} \cup \left\{p_{mj}(k) \,\middle|\, m \in \mathcal{V},\ k \geq 0\right\}\end{aligned} \tag{5.33}$$

where

$$\begin{aligned}\mathcal{I}_j^{\text{state}}(k) &= \left\{s_j(k), w_j(k)\right\} \\ \mathcal{I}_j^{\text{send}}(k) &= \left\{\Delta s_{nj}(k), \Delta w_{nj}(k) \,\middle|\, n \in \mathcal{N}_j^{out}(k) \cup \{j\}\right\} \\ \mathcal{I}_j^{\text{receive}}(k) &= \left\{\Delta s_{jm}(k), \Delta w_{jm}(k) \,\middle|\, m \in \mathcal{N}_j^{in}(k)\right\}\end{aligned} \tag{5.34}$$

represent the states, sent messages, and received messages of node j at iteration k, respectively.

Agent j can only use the parameters and states known to him, i.e., $\mathcal{I}_j$, to infer x_i^0. Therefore, if we can prove that under *any* initial value $\tilde{x}_i^0 = x_i^0 + \delta$ (δ can be *any* value in $\mathbb{R}$), the parameter and state values known to node j, i.e., $\tilde{\mathcal{I}}_j$, could be exactly the same as $\mathcal{I}_j$ in (5.33) and (5.34), then node j has no way to

even estimate a range for x_i^0. Namely, we only need to prove that for any $\tilde{x}_i^0 = x_i^0 + \delta$, $\tilde{\mathcal{I}}_j = \mathcal{I}_j$ is true.

If there exists a time instant $0 \leq k^* \leq K_i$ such that $\left|\left\{l \in \mathcal{V} \;\middle|\; l \in \mathcal{N}_i^{out}(k^*) \cup \mathcal{N}_i^{in}(k^*),\ K_l \geq k^*\right\}\right| \geq 2$ is true, then there must exist an node $l \in \mathcal{N}_i^{out}(k^*) \cup \mathcal{N}_i^{in}(k^*)$ satisfying $l \neq j$ and $K_l \geq k^*$. Next we prove that there are initial values of x_l^0, exchanged messages, and weights satisfying the requirements in Algorithm 5.2 and making $\tilde{\mathcal{I}}_j = \mathcal{I}_j$ hold for any $\tilde{x}_i^0 = x_i^0 + \delta$. Specifically, under initial condition $\tilde{x}_l^0 = x_l^0 - \delta$, we consider two cases, $l \in \mathcal{N}_i^{out}(k^*)$ and $l \in \mathcal{N}_i^{in}(k^*)$, respectively (note that if $l \in \mathcal{N}_i^{out}(k^*) \cap \mathcal{N}_i^{in}(k^*)$ is true, either case can be used in the argument to reach a same conclusion):

Case I: If $l \in \mathcal{N}_i^{out}(k^*)$ holds, we can verify $\tilde{\mathcal{I}}_j = \mathcal{I}_j$ for any $\tilde{x}_i^0 = x_i^0 + \delta$ under the following exchanged messages and weights

$$\begin{cases} \Delta\tilde{s}_{mn}(k) = \Delta s_{mn}(k)\, \forall\, m \in \mathcal{V},\, n \in \mathcal{V} \setminus \{i,\, l\},\, 0 \leq k \leq k^* \\ \Delta\tilde{s}_{mi}(k) = \Delta s_{mi}(k) \quad \forall\, m \in \mathcal{V} \setminus \{i\}, 0 \leq k \leq k^* - 1 \\ \Delta\tilde{s}_{ii}(k) = \Delta s_{ii}(k) + \delta \quad \forall\, 0 \leq k \leq k^* - 1 \\ \Delta\tilde{s}_{ml}(k) = \Delta s_{ml}(k) \quad \forall\, m \in \mathcal{V} \setminus \{l\}, 0 \leq k \leq k^* - 1 \\ \Delta\tilde{s}_{ll}(k) = \Delta s_{ll}(k) - \delta \quad \forall\, 0 \leq k \leq k^* - 1 \\ \Delta\tilde{s}_{mi}(k^*) = \Delta s_{mi}(k^*) \quad \forall\, m \in \mathcal{V} \setminus \{l\} \\ \Delta\tilde{s}_{li}(k^*) = \Delta s_{li}(k^*) + \delta \\ \Delta\tilde{s}_{ml}(k^*) = \Delta s_{ml}(k^*) \quad \forall\, m \in \mathcal{V} \setminus \{l\} \\ \Delta\tilde{s}_{ll}(k^*) = \Delta s_{ll}(k^*) - \delta \\ \Delta\tilde{s}_{mn}(k) = \Delta s_{mn}(k) \quad \forall\, m, n \in \mathcal{V},\, k \geq k^* + 1 \\ \Delta\tilde{w}_{mn}(k) = \Delta w_{mn}(k) \quad \forall\, m, n \in \mathcal{V},\, k \geq 0 \\ \tilde{p}_{mn}(k) = p_{mn}(k) \quad \forall\, m, n \in \mathcal{V},\, k \geq 0 \end{cases} \tag{5.35}$$

where "\" represents set subtraction.

Case II: If $l \in \mathcal{N}_i^{in}(k^*)$ holds, we can verify $\tilde{\mathcal{I}}_j = \mathcal{I}_j$ for any $\tilde{x}_i^0 = x_i^0 + \delta$ under the following

exchanged messages and weights

$$\begin{cases} \Delta\tilde{s}_{mn}(k) = \Delta s_{mn}(k) \, \forall \, m \in \mathcal{V},\, n \in \mathcal{V} \setminus \{i,\, l\},\, 0 \leq k \leq k^* \\ \Delta\tilde{s}_{mi}(k) = \Delta s_{mi}(k) \quad \forall \, m \in \mathcal{V} \setminus \{i\}, 0 \leq k \leq k^* - 1 \\ \Delta\tilde{s}_{ii}(k) = \Delta s_{ii}(k) + \delta \quad \forall \, 0 \leq k \leq k^* - 1 \\ \Delta\tilde{s}_{ml}(k) = \Delta s_{ml}(k) \quad \forall \, m \in \mathcal{V} \setminus \{l\}, 0 \leq k \leq k^* - 1 \\ \Delta\tilde{s}_{ll}(k) = \Delta s_{ll}(k) - \delta \quad \forall \, 0 \leq k \leq k^* - 1 \\ \Delta\tilde{s}_{mi}(k^*) = \Delta s_{mi}(k^*) \quad \forall \, m \in \mathcal{V} \setminus \{i\} \\ \Delta\tilde{s}_{ii}(k^*) = \Delta s_{ii}(k^*) + \delta \\ \Delta\tilde{s}_{ml}(k^*) = \Delta s_{ml}(k^*) \quad \forall \, m \in \mathcal{V} \setminus \{i\} \\ \Delta\tilde{s}_{il}(k^*) = \Delta s_{il}(k^*) - \delta \\ \Delta\tilde{s}_{mn}(k) = \Delta s_{mn}(k) \quad \forall \, m, n \in \mathcal{V},\, k \geq k^* + 1 \\ \Delta\tilde{w}_{mn}(k) = \Delta w_{mn}(k) \quad \forall \, m, n \in \mathcal{V},\, k \geq 0 \\ \tilde{p}_{mn}(k) = p_{mn}(k) \quad \forall \, m, n \in \mathcal{V},\, k \geq 0 \end{cases} \tag{5.36}$$

Summarizing Case I and Case II, we have $\tilde{\mathcal{I}}_j = \mathcal{I}_j$ for $\tilde{x}_i^0 = x_i^0 + \delta$ under any δ in $\mathbb{R}$, meaning that node j cannot distinguish whether the initial state of node i is x_i^0 or $x_i^0 + \delta$ for any $\delta \in \mathbb{R}$. Therefore, under Assumptions 5.1, 5.2, 5.3, and 5.4, Algorithm 5.2 can protect the privacy of node i if there exists a time instant $0 \leq k^* \leq K_i$ such that $\left| \left\{ l \in \mathcal{V} \,\middle|\, l \in \mathcal{N}_i^{out}(k^*) \cup \mathcal{N}_i^{in}(k^*),\ K_l \geq k^* \right\} \right| \geq 2$ is true. ■

Next we proceed to show that if the conditions in Theorem 5.2 are not met, then the privacy of node i may be breached.

Theorem 5.3. *For a network of N nodes represented by a sequence of time-varying directed graphs $\{\mathcal{G}(k) = (\mathcal{V},\, \mathcal{E}(k))\}$ which satisfies Assumptions 5.1, 5.2, 5.3, and 5.4, the privacy of node i in Algorithm 5.2 cannot be preserved against node j if $\{\mathcal{N}_i^{out}(k) \cup \mathcal{N}_i^{in}(k) \,|\, k \geq 0\} = \{j\}$ is true. In fact, under $\{\mathcal{N}_i^{out}(k) \cup \mathcal{N}_i^{in}(k) \,|\, k \geq 0\} = \{j\}$, x_i^0 of node i can be uniquely determined by node j.*

Proof: Under $\{\mathcal{N}_i^{out}(k) \cup \mathcal{N}_i^{in}(k) \,|\, k \geq 0\} = \{j\}$, we can obtain that the only neighboring node that node i can communicate with is node j. But it is worth noting that node i may not communicate with node j at every iteration k since the graph is time-varying. Setting $\Delta s_{ij}(k)$ and $\Delta w_{ij}(k)$ to 0 when node j does not directly communicate with node i at iteration k, we can get the dynamics of s_i and w_i from (5.5) as

follows:

$$\begin{cases} s_i(k+1) = \Delta s_{ii}(k) + \Delta s_{ij}(k) \\ w_i(k+1) = \Delta w_{ii}(k) + \Delta w_{ij}(k) \end{cases} \tag{5.37}$$

Under requirements in Algorithm 5.2, we have

$$\begin{cases} s_i(k) = \Delta s_{ii}(k) + \Delta s_{ji}(k) \\ w_i(k) = \Delta w_{ii}(k) + \Delta w_{ji}(k) \end{cases} \tag{5.38}$$

for all k where $\Delta s_{ji}(k)$ and $\Delta w_{ji}(k)$ are set to 0 if node i does not directly communicate with node j at iteration k. Combining (5.37) and (5.38) leads to

$$\begin{cases} s_i(k+1) - s_i(k) = \Delta s_{ij}(k) - \Delta s_{ji}(k) \\ w_i(k+1) - w_i(k) = \Delta w_{ij}(k) - \Delta w_{ji}(k) \end{cases} \tag{5.39}$$

and further

$$\begin{cases} s_i(k) - s_i(0) = \sum_{l=0}^{k-1} [\Delta s_{ij}(l) - \Delta s_{ji}(l)] \\ w_i(k) - w_i(0) = \sum_{l=0}^{k-1} [\Delta w_{ij}(l) - \Delta w_{ji}(l)] \end{cases} \tag{5.40}$$

Note that the right-hand side of (5.40) is accessible to the honest-but-curious node j because $\Delta s_{ij}(l)$ and $\Delta w_{ij}(l)$ are computed and sent by node j, and $\Delta s_{ji}(l)$ and $\Delta w_{ji}(l)$ are received by node j. Further using the fact $w_i(0) = 1$, node j can uniquely determine $w_i(k)$ for all k.

Under Assumption 5.1 and $\{\mathcal{N}_i^{out}(k) \cup \mathcal{N}_i^{in}(k) \,\big|\, k \geq 0\} = \{j\}$, one can obtain $(j, i) \in \mathcal{E}_\infty$. According to Assumption 5.2, node i directly communicates with node j at least once every T consecutive time instants. So there must exist $k' \geq K_i + 1$ such that node i directly communicates with node j at iteration k', i.e., node i sends $\Delta s_{ji}(k')$ and $\Delta w_{ji}(k')$ to node j at iteration k'. Then node j can easily infer $s_i(k')$ as below

$$s_i(k') = \frac{\Delta s_{ji}(k')}{\Delta w_{ji}(k')} w_i(k') = \frac{p_{ji}(k') s_i(k')}{p_{ji}(k') w_i(k')} w_i(k') \tag{5.41}$$

Therefore, node j can uniquely determine $x_i^0 = s_i(0)$ based on (5.40). ■

5.3.3.2 Honest-but-curious nodes colluding with each other

In this scenario (cf. Assumption 5.5), we have the following theorems.

Theorem 5.4. *For a network of N nodes represented by a sequence of time-varying directed graphs $\{\mathcal{G}(k) = (\mathcal{V}, \mathcal{E}(k))\}$ which satisfies Assumptions 5.1, 5.2, 5.3, and 5.5, Algorithm 5.2 can preserve the privacy of node i against the set of honest-but-curious nodes $\mathcal{A}$ if there exists a time instant $0 \leq k^* \leq K_i$ such that $\left|\left\{l \in \mathcal{V} \,\middle|\, l \in \mathcal{N}_i^{out}(k^*) \cup \mathcal{N}_i^{in}(k^*),\ l \notin \mathcal{A},\ K_l \geq k^*\right\}\right| \geq 1$ is true, i.e., there exits at least one node l belonging to $\mathcal{N}_i^{out}(k^*) \cup \mathcal{N}_i^{in}(k^*)$ but not $\mathcal{A}$ with $K_l \geq k^*$.*

Proof: To prove that the privacy of node i can be preserved, we have to prove that no honest-but-curious node $j \in \mathcal{A}$ can estimate x_i^0 with any accuracy. Under Assumption 5.5, each node in $\mathcal{A}$ has access to the parameter and state values known to any node in $\mathcal{A}$. So we represent the accessible parameter and state values as

$$\mathcal{I}_{\mathcal{A}} = \left\{\mathcal{I}_j \,\middle|\, j \in \mathcal{A}\right\} \tag{5.42}$$

where $\mathcal{I}_j$ is given by (5.33). Following the same line of reasoning in Theorem 5.2, to prove that node $j \in \mathcal{A}$ cannot estimate x_i^0 with any accuracy, it is sufficient to prove that for any initial value $\tilde{x}_i^0 = x_i^0 + \delta$ (δ can be any value in $\mathbb{R}$), the parameter and state values known to node j, i.e., $\tilde{\mathcal{I}}_{\mathcal{A}}$, could be exactly the same as $\mathcal{I}_{\mathcal{A}}$.

If there exists a time instant $0 \leq k^* \leq K_i$ such that $\left|\left\{l \in \mathcal{V} \,\middle|\, l \in \mathcal{N}_i^{out}(k^*) \cup \mathcal{N}_i^{in}(k^*),\ l \notin \mathcal{A},\ K_l \geq k^*\right\}\right| \geq 1$ is true, then there must exist an node $l \in \mathcal{N}_i^{out}(k^*) \cup \mathcal{N}_i^{in}(k^*)$ such that $l \notin \mathcal{A}$ and $K_l \geq k^*$ hold. It can be easily verified that under the initial condition $\tilde{x}_l^0 = x_l^0 - \delta$, there exist respective exchanged messages and weights in (5.35) and (5.36) for $l \in \mathcal{N}_i^{out}(k^*)$ and $l \in \mathcal{N}_i^{in}(k^*)$ that satisfy requirements in Algorithm 5.2 and make $\tilde{\mathcal{I}}_{\mathcal{A}} = \mathcal{I}_{\mathcal{A}}$ hold under any $\tilde{x}_i^0 = x_i^0 + \delta$.

Therefore, we can have $\tilde{\mathcal{I}}_{\mathcal{A}} = \mathcal{I}_{\mathcal{A}}$ for $\tilde{x}_i^0 = x_i^0 + \delta$ under any δ in $\mathbb{R}$, meaning that node $j \in \mathcal{A}$ cannot estimate x_i^0 with any accuracy even based on the parameter and state values known to the entire set $\mathcal{A}$. ■

Next we prove that if the conditions in Theorem 5.4 are not met, the privacy of node i could be breached.

Theorem 5.5. *For a network of N nodes represented by a sequence of time-varying directed graphs $\{\mathcal{G}(k) = (\mathcal{V}, \mathcal{E}(k))\}$ which satisfies Assumptions 5.1, 5.2, 5.3, and 5.5, the privacy of node i in Algorithm 5.2 cannot be preserved when all in-neighbors and out-neighbors belong to $\mathcal{A}$, i.e., $\{\mathcal{N}_i^{out}(k) \cup \mathcal{N}_i^{in}(k) \,|\, k \geq 0\} \subset \mathcal{A}$. In fact, when $\{\mathcal{N}_i^{out}(k) \cup \mathcal{N}_i^{in}(k) \,|\, k \geq 0\} \subset \mathcal{A}$ is true, the initial value x_i^0 of node i can be uniquely determined by honest-but-curious nodes $j \in \mathcal{A}$.*

Proof: From (5.5), we can have the dynamics of s_i and w_i as follows:

$$\begin{cases} s_i(k+1) = \sum\limits_{n\in\mathcal{N}_i^{in}(k)} \Delta s_{in}(k) + \Delta s_{ii}(k) \\ w_i(k+1) = \sum\limits_{n\in\mathcal{N}_i^{in}(k)} \Delta w_{in}(k) + \Delta w_{ii}(k) \end{cases} \tag{5.43}$$

The requirements in Algorithm 5.2 guarantee $\Delta s_{ii}(k) + \sum_{m\in\mathcal{N}_i^{out}(k)} \Delta s_{mi}(k) = s_i(k)$ and $\Delta w_{ii}(k) + \sum_{m\in\mathcal{N}_i^{out}(k)} \Delta w_{mi}(k) = w_i(k)$. Plugging these relationships into (5.43), we can obtain

$$\begin{cases} s_i(k+1) - s_i(k) = \sum\limits_{n\in\mathcal{N}_i^{in}(k)} \Delta s_{in}(k) - \sum\limits_{m\in\mathcal{N}_i^{out}(k)} \Delta s_{mi}(k) \\ w_i(k+1) - w_i(k) = \sum\limits_{n\in\mathcal{N}_i^{in}(k)} \Delta w_{in}(k) - \sum\limits_{m\in\mathcal{N}_i^{out}(k)} \Delta w_{mi}(k) \end{cases} \tag{5.44}$$

and further

$$\begin{cases} s_i(k) - s_i(0) = \sum\limits_{l=0}^{k-1} \Big[\sum\limits_{n\in\mathcal{N}_i^{in}(k)} \Delta s_{in}(l) - \sum\limits_{m\in\mathcal{N}_i^{out}(k)} \Delta s_{mi}(l) \Big] \\ w_i(k) - w_i(0) = \sum\limits_{l=0}^{k-1} \Big[\sum\limits_{n\in\mathcal{N}_i^{in}(k)} \Delta w_{in}(l) - \sum\limits_{m\in\mathcal{N}_i^{out}(k)} \Delta w_{mi}(l) \Big] \end{cases} \tag{5.45}$$

Note that under Assumption 5.5, every honest-but-curious node $j \in \mathcal{A}$ has access to $\mathcal{I}_{\mathcal{A}}$ in (5.42). If $\{\mathcal{N}_i^{out}(k) \cup \mathcal{N}_i^{in}(k) \,\big|\, k \geq 0\} \subset \mathcal{A}$ is true, all terms on the right-hand side of (5.45) belong to $\mathcal{I}_{\mathcal{A}}$, and hence are known to any node $j \in \mathcal{A}$. Further taking into account $w_i(0) = 1$, we have that every node $j \in \mathcal{A}$ can uniquely determine $w_i(k)$ for all k.

Under Assumption 5.1 and $\{\mathcal{N}_i^{out}(k) \cup \mathcal{N}_i^{in}(k) \,\big|\, k \geq 0\} \subset \mathcal{A}$, there must exist at least one node $q \in \mathcal{A}$ such that $(q,\, i) \in \mathcal{E}_\infty$ is true. This is because otherwise graph $(\mathcal{V},\, \mathcal{E}_\infty)$ is not strongly connected, which does not satisfy Assumption 5.1. According to Assumption 5.2, node i directly communicates with node q at least once in every T consecutive time instants. So there must exist $k' \geq K_i + 1$ at which node i directly communicates with node q, i.e., node i sends $\Delta s_{qi}(k')$ and $\Delta w_{qi}(k')$ to node q at iteration k'. As $q \in \mathcal{A}$, each honest-but-curious node $j \in \mathcal{A}$ has access to $\Delta s_{qi}(k')$ and $\Delta w_{qi}(k')$. So each node $j \in \mathcal{A}$ can easily infer $s_i(k')$ by using the following relationship

$$s_i(k') = \frac{\Delta s_{qi}(k')}{\Delta w_{qi}(k')} w_i(k') = \frac{p_{qi}(k') s_i(k')}{p_{qi}(k') w_i(k')} w_i(k') \tag{5.46}$$

Further making use of (5.45), each honest-but-curious node $j \in \mathcal{A}$ can uniquely determine the value of $x_i^0 = s_i(0)$. ■

Remark 5.5. *It is worth noting that in privacy-preserving average consensus, topology requirements such as the ones in Theorem 5.2 and Theorem 5.4 are widely used. In fact, to guarantee both accuracy and privacy, [5, 17, 33, 50, 57, 89, 96, 121, 125, 132, 135, 155] all rely on similar topology requirements.*

Remark 5.6. *Our algorithm can protect the privacy of an node even when all its neighbors interact (at least one does not collude) with adversaries, which is not allowed in [96] and [89].*

Remark 5.7. *From the above analysis, we know that introducing randomness into interaction dynamics by each node i for $k \leq K_i$ is key to protect privacy against honest-but-curious nodes. It is worth noting that compared with the conventional push-sum approach which does not take privacy into consideration, the introduced randomness in our approach has no influence on the convergence rate ρ. However, the randomness does delay the convergence process and hence leads to a trade-off between privacy preservation and convergence time. This is confirmed in our numerical simulations in Fig. 5.2 which shows that convergence only initiates after $k = \bar{K} + 1$.*

Remark 5.8. *If an adversary can obtain side information, then a larger K_i protects the privacy of more intermediate states $s_i(k)$ for $1 \leq k \leq K_i$. This is because for $k \geq K_i + 1$, $\pi_i(k)$ can be easily obtained by its out-neighbor j due to the relationship $\pi_i(k) = \Delta s_{ji}(k)/\Delta w_{ji}(k)$ for $k \geq K_i + 1$, which makes states $s_i(k)$ for $k \geq K_i + 1$ easier to infer through $s_i(k) = \pi_i(k)w_i(k)$ if side information about K_i and $w_i(k)$ is available to the adversary. Therefore, although a larger K_i leads to more delay in the convergence process, as discussed in Remark 5.7, it can protect more intermediate states ($s_i(k)$ for $1 \leq k \leq K_i$) when an adversary can obtain side information. Of course, if side information is not of concern, a smaller K_i is preferable to minimize the delay in the convergence process.*

Remark 5.9. *In Algorithm 5.2, K_i and the distribution of random number $\Delta s_{ji}(k)$ being only known to node i is not an assumption but a natural consequence of implementing our algorithm. Although bring additional protection against side-information attacks, they are not necessary to guarantee the defined privacy in Definition 5.2. In fact, even if K_i and the distribution of $\Delta s_{ji}(k)$ were shared with every node, following the arguments in the proofs of Theorem 5.2 and Theorem 5.4, we can still prove that our algorithm provides the privacy defined in Definition 5.2.*

Remark 5.10. *It is worth noting that our approach can provide information-theoretic privacy under a special selection of private parameters and an additional constraint on the update of $s_i(0)$. More specifically, if we normalize the initial states between 0 and $\frac{1}{N}$, set $K_i = 0$, and choose $\Delta s_{ji}(0)$ independently and uniformly in $[0, 1)$ for all $j \in \mathcal{N}_i^{out}(0)$, then following the reasoning in [50], we can prove that our approach can enable information-theoretic privacy against a set of honest-but-curious adversaries that cannot form a vertex cut of the graph, even in the time-varying directed graph case. This is because under the above setting, the distribution of information set gathered by the set of honest-but-curious nodes keeps unchanged under different initial states of nodes other than the set of honest-but-curious nodes, as long as the sum of initial states keeps unchanged.*

Remark 5.11. *Our algorithm can be extended to preserve privacy against external eavesdroppers wiretapping all communication links without compromising algorithmic accuracy by patching partially homomorphic encryption. More specifically, using public-key cryptosystems (e.g., Paillier [115], RSA [133], and ElGamal [30]), each node generates and floods its public key before the consensus iteration starts. Then in decentralized implementation, an node encrypts its messages to be sent, which can be decrypted by a legitimate recipient without the help of any third party. Note that since public-key cryptosystems can only deal with integers, the final consensus result would be subject to a quantization error. However, as indicated in our previous work [135], the quantization error can be made arbitrarily small in implementation.*

5.4 Numerical Experiments

We conducted numerical simulations to verify the correctness and the effectiveness of our proposed approach.

We first evaluated our proposed Algorithm 5.2 under a network of $N = 5$ nodes interacting on a time-varying directed graph. More specifically, we used the interaction graph in Fig. 5.1(a) when k is even and Fig. 5.1(b) when k is odd. It can be verified that this time-varying directed graph satisfies Assumptions 5.1 and 5.2. Parameter ε was set to 0.05. For iterations $k \leq K_i$, node i chose independently random numbers $\Delta s_{ji}(k)$ for $j \in \mathcal{N}_i^{out}(k)$ following normal distribution $\mathcal{N}(\mu_{ji}(k), \sigma_{ji}^2(k))$ where $\mu_{ji}(k)$ and $\sigma_{ji}(k)$ were randomly chosen from $(-500,\ 500)$. The initial values x_i^0 for $i = 1, \ldots, N$ were randomly chosen from $(0,\ 50)$. We used $e(k)$ to measure the estimation error between the estimate $\pi_i(k) = s_i(k)/w_i(k)$ and the

true average value $\alpha = \sum_{j=1}^{N} x_j^0/N$ at iteration k, i.e.,

$$e(k) = \left\|\boldsymbol{\pi}(k) - \alpha\mathbf{1}\right\| = \Big(\sum_{i=1}^{N}(\pi_i(k) - \alpha)^2\Big)^{1/2} \tag{5.47}$$

Three experiments were conducted with $\bar{K} = \max_i K_i$ being 10, 20, and 30, respectively. The evolution of $e(k)$ is shown in Fig. 5.2. It can be seen that $e(k)$ approached to 0, meaning that every node converged to the average value $\alpha = \sum_{j=1}^{N} x_j^0/N$. It is also worth noting that we can see from Fig. 5.2 that Algorithm 5.2 did not start to converge until iteration step $k \geq \bar{K} + 1$, which confirms our analysis in Remark 5.7.

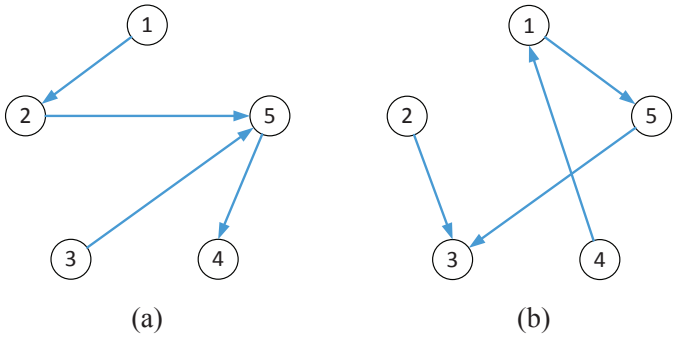

Figure 5.1: A time-varying directed graph with 5 nodes.

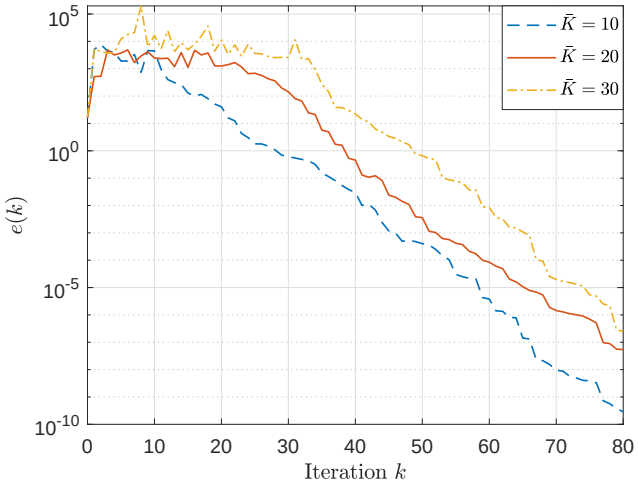

Figure 5.2: The evolution of error $e(k)$ under different $\bar{K}$.

We also evaluated the influence of parameter ε on the convergence rate ρ. The interaction graph was

the same as above. $\bar{K} = \max_i\{K_i\}$ was set to 10. The simulation results are given in Fig. 5.3 where the mean and variance of ρ from $1,000$ runs of the algorithm are shown under different values of ε. Fig. 5.3 shows that as ε increases, the convergence rate ρ decreases (i.e., the convergence speed increases), which confirms our analysis in Section 5.3.

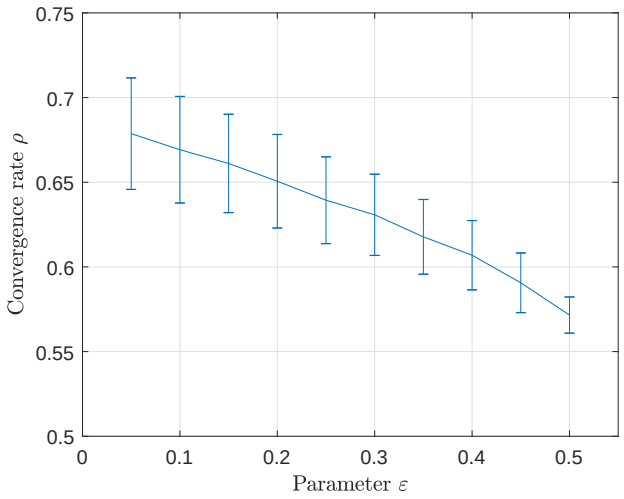

Figure 5.3: The influence of ε on the convergence rate ρ.

We then evaluated the privacy-preserving performance of Algorithm 5.2. Because letting attackers receive more information makes privacy more difficult to protect, we consider the extreme case where the graph is the union of Fig. 5.1(a) and Fig. 5.1(b) at every time instant. We assumed that nodes 2, 3, and 4 colluded to infer the initial value x_1^0 of node 1. Note that in this case, we have that $\mathcal{N}_1^{out}(k) \cup \mathcal{N}_1^{in}(k) = \{2,\, 4,\, 5\} \not\subset \mathcal{A}$ holds for node 1 at every time instant. Two experiments were conducted with x_1^0 set to 40 and -40, respectively. $x_2^0, \ldots, x_5^0$ were randomly chosen from $(0,\, 50)$. K_i was set to 10 for each node i. The other parameters were the same as the first simulation, and the maximal iteration step was $M = 100$. To infer the value of x_1^0, the nodes in set $\mathcal{A}$ could construct the following equations based on the accessible parameter and state values $\mathcal{I}_{\mathcal{A}}$

$$\begin{cases} s_1(k+1) - s_1(k) + \Delta s_{51}(k) = \Delta s_{14}(k) - \Delta s_{21}(k) \\ w_1(k+1) - w_1(k) + \Delta w_{51}(k) = \Delta w_{14}(k) - \Delta w_{21}(k) \end{cases} \tag{5.48}$$

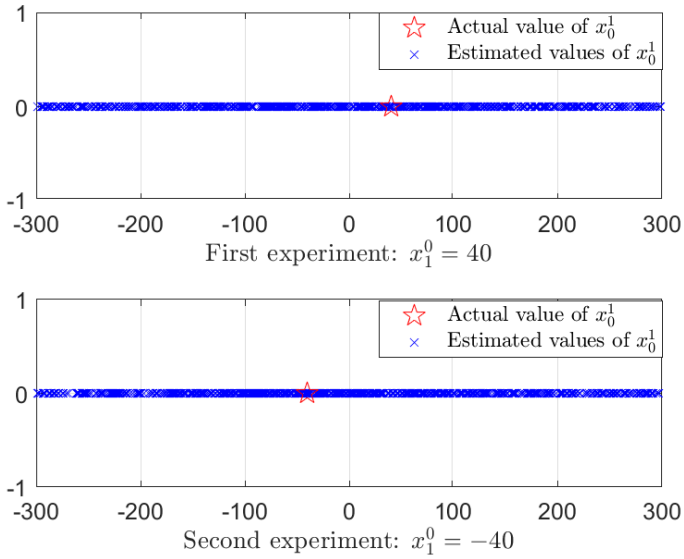

Figure 5.4: Estimation results of x_1^0 by the set of honest-but-curious nodes 2, 3, and 4. In each experiment, the actual value of x_1^0 is represented by star, and the estimated values of x_1^0 are represented by x-marks.

for $k = 0, 1, \ldots, M$. Furthermore, nodes in set $\mathcal{A}$ also have

$$s_1(k) - \pi_1(k) w_1(k) = 0 \tag{5.49}$$

for $k = K_1 + 1, K_1 + 2, \ldots, M$ where $\pi_1(k)$ can be inferred by nodes in set $\mathcal{A}$ using

$$\pi_1(k) = \frac{\Delta s_{21}(k)}{\Delta w_{21}(k)} = \frac{p_{21}(k) s_1(k)}{p_{21}(k) w_1(k)} \tag{5.50}$$

since both $\Delta s_{21}(k)$ and $\Delta w_{21}(k)$ belong to $\mathcal{I}_{\mathcal{A}}$.

The number of linear equations (5.48) and (5.49) is $3M - K_1 + 2$, and within these equations there exist $4M+5$ variables unknown to nodes in set $\mathcal{A}$, i.e., $s_1(0), \ldots, s_1(M+1), \Delta s_{51}(0), \ldots, \Delta s_{51}(M), w_1(1), \ldots, w_1(M+1), \Delta w_{51}(0), \ldots, \Delta w_{51}(M)$. Therefore, there are infinitely many solutions because the number of unknown variables is more than the number of equations. To uniquely determine the value of x_1^0, we used the least-squares solution to estimate x_1^0. In each experiment, the nodes in set $\mathcal{A}$ estimated x_1^0 for $1,000$ times, with recorded estimation results given in Fig. 5.4. It is clear that set $\mathcal{A}$ cannot have a good estimate of x_1^0.

We also compared the proposed Algorithm 5.2 with existing data-obfuscation based approaches,

more specifically, the differential-privacy based approach in [62], the decaying-noise approach in [96], and the finite-noise-sequence approach in [89]. Under the same setup as in the previous simulation, we chose the initial values as $\{10, 15, 20, 25, 30\}$, which led to an average value 20. We adopted the weight matrix $\mathbf{W}$ from [62], i.e., the ij-th entry was $w_{ij} = 1/(|\mathcal{N}_j^{out}| + 1)$ for $i \in \mathcal{N}_j^{out} \cup \{j\}$ and $w_{ij} = 0$ for $i \notin \mathcal{N}_j^{out} \cup \{j\}$. As the graph is directed and imbalanced, and does not meet the undirected or balanced assumption in [62,89,96], all three approaches failed to achieve average consensus, as shown in the numerical simulation results in Fig. 5.5, Fig. 5.7, and Fig. 5.6, respectively.

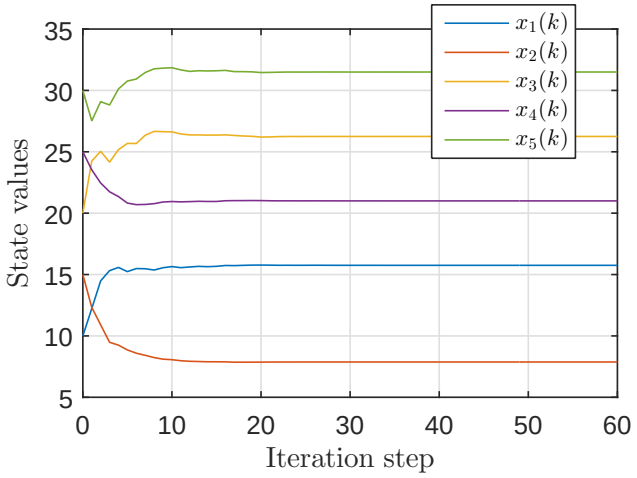

Figure 5.5: The evolution of $x_i(k)$ under the approach in [62].

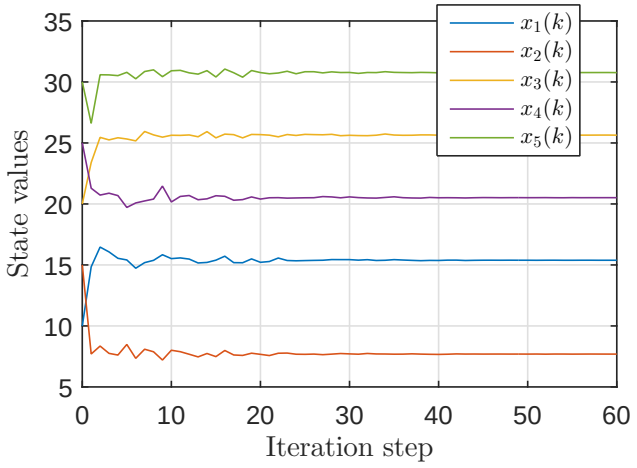

Figure 5.6: The evolution of $x_i(k)$ under the approach in [96].

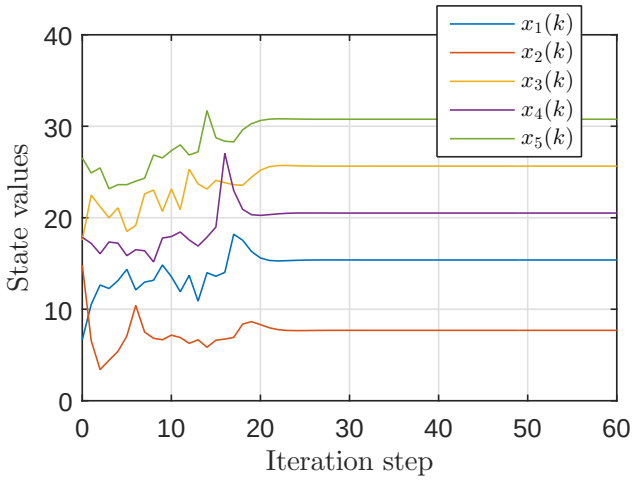

Figure 5.7: The evolution of $x_i(k)$ under the approach in [89].

5.5 Summaries

In this chapter, we proposed a privacy-preserving average consensus algorithm for time-varying directed graphs. In distinct difference from existing differential-privacy based approaches which add independent (and hence uncorrelated) noises to nodes' states and thus compromise the accuracy of average consensus, we leveraged the inherent robustness of average consensus to embed randomness in interaction dynamics, which guarantees privacy of participating nodes without sacrificing the accuracy of average consensus. Finally, we provided numerical simulation results to confirm the effectiveness and efficiency of our proposed approach.

Chapter 6

Conclusions

In this dissertation, we considered coordination (including synchronization and desynchronization) and privacy preservation in multi-agent systems.

In the first part, we first addressed global synchronization of PCOs interacting on chain and directed tree graphs. It was proven that PCOs can be synchronized from an arbitrary initial phase distribution under heterogeneous phase response functions (PRFs) and coupling strengths. The results are also applicable when oscillators are heterogeneous and subject to time-varying perturbations on their natural frequencies. Different from existing global synchronization results, the coupling strengths in our results can be freely chosen between zero and one, which is desirable since a very strong coupling strength, although can bring fast convergence, has been shown to be detrimental to the robustness of synchronization to disturbances. Given that a very weak coupling may not be desirable either due to low convergence speed which may allow disturbances to accumulate, the results give flexibility in meeting versatile requirements in practical PCO applications.

Next we focused on desynchronization of PCOs. We proposed a general phase-desynchronizing phase response function, which includes existing results as special cases, and rigorously characterized the decentralized phase desynchronization process. Simulation results show that our proposed phase response function can achieve better convergence speed and robustness to pulse losses, time delays, and frequency errors than existing results.

Then we considered the applications of PCOs in collective motion coordination. Inspired by the close relationship between phase synchronization/desynchronization of PCOs and the heading dynamics of connected vehicles/robots, we proposed a pulse-based integrated communication and control approach for decentralized collective motion coordination. Different from existing results relying on a continuous control

design followed by discretization based implementation, we design communication and control in a unified framework, which can prevent the adverse effects of discretization and guarantee the design performance in implementation. The pulse-based message exchanging also significantly reduces processing latency and communication delay, and enhances robustness to channel interferences compared with conventional packet-based communication approaches.

In the second part, we focused on privacy-preserving average consensus as it is key for multi-agent systems. We proposed a privacy-preserving average consensus approach for time-varying directed graphs. Different from existing differential-privacy based approaches which inject independent noise to exchanged states and thus compromise accuracy, we enable privacy preservation by judiciously adding randomness in interaction dynamics and leverage the inherent robustness of the push-sum algorithm to ensure consensus to the exact average value. Our proposed approach is able to preserve privacy even when multiple honest-but-curious nodes collude with each other. Numerical simulations are provided to verify the effectiveness and efficiency of the proposed approach.

Appendices

Appendix A Lemmas and Their Proofs in Chapter 2

A.1 Lemma A.1

Lemma A.1. *For N PCOs interacting on an undirected chain, if the PRF $F_j(x_j)$ satisfies Assumption 2.3 and $l_j \in (0,\, 1)$ holds for all $j \in \mathcal{V}$, then L in (2.10) cannot be retained at any nonzero value along a complete solution ϕ.*

Proof. We use proof of contradiction. Since $L \in [0, N\pi]$ holds, we suppose that for some $r \in (0,\, N\pi]$, L is retained at r along a complete solution ϕ. From Lemma 2.5, to keep L at r, we must have

$$\Delta_{i-1}^{+} = \Delta_{i-1} - \delta_{i-1}, \quad \Delta_{i-2}^{+} = \Delta_{i-2} + \delta_{i-1} \tag{A.1}$$

or

$$\Delta_{i}^{+} = \Delta_{i} - \delta_{i+1}, \quad \Delta_{i+1}^{+} = \Delta_{i+1} + \delta_{i+1} \tag{A.2}$$

if the left-neighbor oscillator $i-1$ or right-neighbor oscillator $i+1$ exists when oscillator i fires, respectively. Next we show that Δ_N will exceed π, which contradicts the constraint $0 \le \Delta_i \le \pi$ for $i \in \mathcal{V}$.

Given $1 \notin \mathcal{N}_i^{out}$ and $N \notin \mathcal{N}_i^{out}$ for $i = 3, 4, \ldots, N-2$, both $x_1^{+} = x_1$ and $x_N^{+} = x_N$ hold when oscillators $3, 4, \ldots, N-2$ fire, which leads to $\Delta_N^{+} = \Delta_N$. Similarly, $N \notin \mathcal{N}_1^{out}$ (resp. $1 \notin \mathcal{N}_N^{out}$) implies $x_N^{+} = x_N$ (resp. $x_1^{+} = x_1$) when oscillator 1 (resp. N) fires, which leads to $\Delta_N^{+} = \Delta_N$ when oscillator 1 or N fires.

So we focus on the evolution of Δ_N when oscillators 2 and $N-1$ fire. According to Lemma A.2 in Appendix A.2, neither oscillator 2 nor oscillator $N-1$ will stop firing. Without loss of generality, we assume that oscillator 2 fires at time $(t_2^*,\, k_2^*)$. From (A.1) we have $\Delta_N^{+} = \Delta_N + \delta_1$. Similarly, from (A.2) we have $\Delta_N^{+} = \Delta_N + \delta_N$ when oscillator $N-1$ fires. Since δ_1 and δ_N are nonnegative, we have $\Delta_N^{+} \ge \Delta_N$. To prove that Δ_N will surpass π, we need to show that at least one of the following statements is true:

1. $\delta_1 = 0$ cannot always hold when oscillator 2 fires;
2. $\delta_N = 0$ cannot always hold when oscillator $N-1$ fires.

Proof of statement 1: Given $l_1 \in (0,\, 1)$, according to (2.7) and (2.12), $\delta_1 = 0$ holds if and only if $x_1 = 0$ or $x_1 = 2\pi$ holds, which means that oscillators 1 and 2 are synchronized when oscillator 2 fires. So we need to show that oscillators 1 and 2 cannot always be synchronized when oscillator 2 fires. More

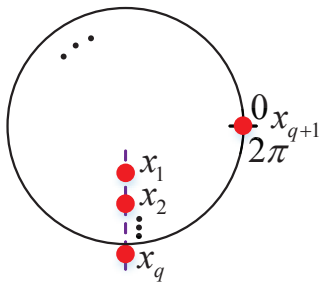

Figure A.1: Illustration of a set of $q \geq 2$ neighboring oscillators being synchronized.

generally, we assume that there is a set of $q \geq 2$ oscillators $1, 2, \ldots, q$ being synchronized and having phases different from oscillator $q+1$. According to Lemma A.2 in Appendix A.2, oscillator $q+1$ will not stop firing in this situation. We assume that oscillator $q+1$ fires at time (t^*_{q+1}, k^*_{q+1}), and $x_1 = \ldots = x_q \in [\pi, 2\pi)$ holds when oscillator $q+1$ fires, as illustrated in Fig. A.1. Note that the case of $x_1 = \ldots = x_q \in (0, \pi]$ can be proved by following the same line of reasoning. Given $0 < l_q < 1$, from (2.7) and (2.12) we have $0 < \delta_q < 2\pi - x_q$. Since oscillator q is the left-neighbor of oscillator $q+1$, according to (A.1), when oscillator $q+1$ fires we have $\Delta^+_q = \Delta_q - \delta_q = 2\pi - x_q - \delta_q > 0$ and $\Delta^+_{q-1} = \Delta_{q-1} + \delta_q = 0 + \delta_q > 0$. So oscillator q escapes from the set of synchronized oscillators due to $\Delta^+_{q-1} > 0$ and will fire next. Similarly, when oscillator q fires, the left-neighbor oscillator $q-1$ will escape from the set of synchronized oscillators and fire next. Iterating this argument, when oscillator 3 fires, the left-neighbor oscillator 2 will escape from the set of synchronized oscillators and fire next. So we have $x_2 \neq x_1$, i.e., oscillators 1 and 2 are not synchronized when oscillator 2 fires. Therefore, $\delta_1 = 0$ cannot always hold when oscillator 2 fires.

Similarly, we can prove statement 2, i.e., δ_N cannot always be 0 when oscillator $N-1$ fires, and thus Δ_N will keep increasing. Since δ_1 and δ_N will not converge to 0 unless synchronization is achieved, Δ_N will surpass π, which contradicts the constraint $0 \leq \Delta_i \leq \pi$ for $i \in \mathcal{V}$. Therefore, L cannot be retained at any nonzero value along a complete solution ϕ. ■

A.2 Lemma A.2

Lemma A.2. *For N PCOs interacting on an undirected chain, if the PRF $F_j(x_j)$ satisfies Assumption 2.3 and $l_j \in (0, 1)$ holds for all $j \in \mathcal{V}$, we have the following results:*

1. *Neither oscillator 2 nor oscillator $N-1$ will stop firing;*

2. *Oscillator $q+1$ will not stop firing if oscillators $1, \ldots, q$ ($2 \leq q \leq N-1$) have been synchronized and*

oscillator $q+1$ is not synchronized with these q oscillators. Similarly, oscillator $N-q$ will not stop firing if oscillators $N-q+1,\ldots,N$ have been synchronized and oscillator $N-q$ is not synchronized with these q oscillators.

Proof. We first use proof of contradiction to prove statement 1. Suppose that oscillator 2 stops firing after time instant $(t_2',\, k_2')$, then x_2 will stay in $[0,\pi]$. This is because if $x_2 \in (\pi, 2\pi)$ holds, it will evolve continuously to 2π and fire, and receiving pulses from other oscillators can only expedite this process under the PRFs in Assumption 2.3. Since oscillator 2 only receives pulses from oscillators 1 and 3, without loss of generality, we suppose at time $(t_1',\, k_1')$ that oscillator 1 fires and resets its phase to 0. Note that oscillator 1 will fire at a period of $T_1 = 2\pi/\omega$ since its only neighbor oscillator 2 stops firing. After receiving the pulse, oscillator 2 updates its phase to $x_2^+ = x_2 + l_2 F_2^{(1)}(x_2) \in [0,\pi)$. If oscillator 2 does not receive any other pulse before its phase surpasses π, it will fire, which contradicts the assumption. So we suppose that oscillator 3 fires at time $(t_3',\, k_3')$ before x_2 surpasses π, which implies $t_3' - t_1' \le \pi/\omega$. Since the time it takes for phase evolving from 0 to π is at least π/ω and after reaching π oscillator 3 will not fire immediately even if it receives a pulse under given PRFs and coupling strengths, the length of oscillator 3's firing period T_3 satisfies $T_3 > \pi/\omega$. There are two cases in this situation, $t_1' = t_3'$ and $t_1' < t_3'$, respectively:

Case 1: If $t_1' = t_3'$ holds, then the length of time interval for oscillator 2 receiving the next pulse after $(t_3',\, k_3'+1)$ is greater than π/ω. Since $x_2(t_3',\, k_3'+1) \ge 0$ holds, x_2 will be greater than π when receiving the next pulse. So oscillator 2 will fire again, which contradicts the assumption.

Case 2: If $t_1' < t_3'$ holds, then we have $x_2(t_3',\, k_3'+1) > 0$ due to $x_2(t_3',\, k_3') = x_2(t_1',\, k_1'+1) + \omega(t_3' - t_1') > 0$ under given PRFs and coupling strengths. Since $t_3' - t_1' \le \pi/\omega$ holds, after time interval $[\pi - x_2(t_3',\, k_3'+1)]/\omega$ which is less than π/ω, we have $x_1 < 2\pi$, $x_3 < \pi$, and $x_2 = \pi$. So x_2 will be greater than π when receiving the next pulse, and thus oscillator 2 will fire again, which contradicts the assumption.

Therefore, oscillator 2 will not stop firing. Similarly, we can prove that oscillator $N-1$ will not stop firing either.

Next we prove statement 2. Suppose that oscillator $q+1$ stops firing after time $(t_{q+1}',\, k_{q+1}')$. Since oscillators $1,\ldots,q$ will not receive any pulses from other oscillators, they will remain synchronized and oscillator q will fire with a period of $T_q = 2\pi/\omega$. The same as statement 1, the length of oscillator $q+2$'s firing period T_{q+2} satisfies $T_{q+2} > \pi/\omega$ and oscillator $q+1$ will not stop firing if oscillator $q+1$ has a phase different from synchronized oscillators $1,\ldots,q$. Similarly, we can prove that oscillator $N-q$ will not stop firing either if oscillator $N-q$ has a phase different from synchronized oscillators $N-q+1,\ldots,N$. ■

Appendix B Lemmas and Their Proofs in Chapter 3

B.1 Lemma B.1

Lemma B.1. ***Case 3'*** *and* ***Case 3"*** *cannot always exist before phase desynchronization is achieved.*

Proof. It can be easily inferred that before achieving phase desynchronization there always exists one phase difference smaller than $\frac{2\pi}{N}$ and one phase difference larger than $\frac{2\pi}{N}$, and in between the two phase differences there may be some phase differences (represent the number as Q, $0 \leq Q \leq N-2$) that are equal to $\frac{2\pi}{N}$, which is defined as **State A**. Denote the phase difference smaller than $\frac{2\pi}{N}$ and the phase difference larger than $\frac{2\pi}{N}$ as Δ_j and $\Delta_{\widehat{j+Q+1}}$, respectively. There are Q phase differences between Δ_j and $\Delta_{\widehat{j+Q+1}}$ which are equal to $\frac{2\pi}{N}$ and denoted as $\Delta_{\widehat{j+1}}, \ldots, \Delta_{\widehat{j+Q}}$ (cf. Fig. B.1).

As illustrated in Fig. B.1, if $\phi_{\widehat{j+Q+2}} < \frac{2\pi}{N}$, we have $\Delta_{\widehat{j+Q+2}} < \frac{2\pi}{N}$. Then we can infer that **Case 3'** does not exist when oscillator j fires because $\phi_{\widehat{j+Q+2}}$ resides in $(0,\ \frac{2\pi}{N})$ and $\Delta_{\widehat{j+Q+1}} > \frac{2\pi}{N}$ is true.

Thus we only need to consider the situation when $\phi_{\widehat{j+Q+2}} \geq \frac{2\pi}{N}$ holds. It can be proven that under this situation **State A** must evolve to **State B** (cf. Fig. B.2) after Q pulses. In **State B**, the Q phase differences which were equal to $\frac{2\pi}{N}$ in **State A** become smaller than $\frac{2\pi}{N}$, meaning that the condition in **Case 3"** is not satisfied when oscillator $\widehat{j+Q}$ fires because phase $\phi_{\widehat{j+Q+1}}$ resides in $(2\pi - \frac{2\pi}{N},\ 2\pi)$ and $\Delta_{\widehat{j+Q+1}} > \frac{2\pi}{N}$ is true.

Now we illustrate how those phase differences equal to $\frac{2\pi}{N}$ become smaller than $\frac{2\pi}{N}$ after Q pulses. Suppose that at $t = t_j$, an "active pulse" is emitted by oscillator j. This pulse only affects $\phi_{\widehat{j+1}}$ since only $\phi_{\widehat{j+1}}$ resides in $(2\pi - \frac{2\pi}{N},\ 2\pi)$ and it decreases the value of $\phi_{\widehat{j+1}}$ since $\phi^+_{\widehat{j+1}} - \phi_{\widehat{j+1}} = l_2(2\pi - \frac{2\pi}{N} - \phi_{\widehat{j+1}}) < 0$ holds, which in turn makes $\Delta_{\widehat{j+1}}$ smaller than $\frac{2\pi}{N}$ after this pulse. Because $\phi_{\widehat{j+2}}, \ldots, \phi_{\widehat{j+Q+2}}$ reside in $[\frac{2\pi}{N},\ 2\pi - \frac{2\pi}{N}]$, they will keep unchanged, meaning that $\Delta_{\widehat{j+Q+1}}$ is still larger than $\frac{2\pi}{N}$, and $\Delta_{\widehat{j+2}}, \ldots, \Delta_{\widehat{j+Q}}$ are equal to $\frac{2\pi}{N}$. Therefore, after one firing, the number of phase differences equal to $\frac{2\pi}{N}$ is reduced by one to $Q-1$, as illustrated in Fig. B.3. Following the same line of reasoning, we can obtain that after Q firings, the phase differences equal to $\frac{2\pi}{N}$ in **State A** become smaller than $\frac{2\pi}{N}$, which means that **State B** is achieved.

So **State A** must evolve to **State B**, and thus the condition in **Case 3"** cannot always exist before achieving phase desynchronization because under **State B** $\Delta_{\widehat{j+Q+1}} > \frac{2\pi}{N}$ will be true when PCO $\widehat{j+Q}$ fires.

Therefore, **Case 3'** and **Case 3"** cannot always exist before phase desynchronization is achieved. ■

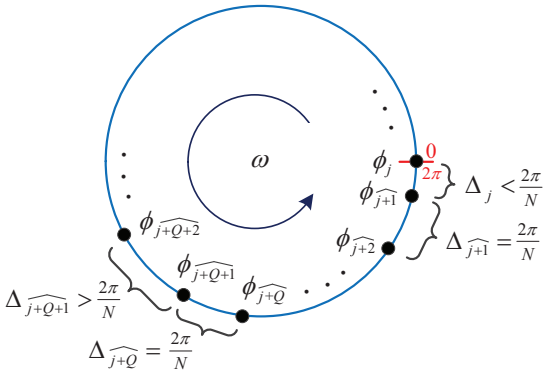

Figure B.1: **State A** on which Q ($0 \leq Q \leq N-2$) phase differences between the smaller phase difference and the larger phase difference are equal to $\frac{2\pi}{N}$.

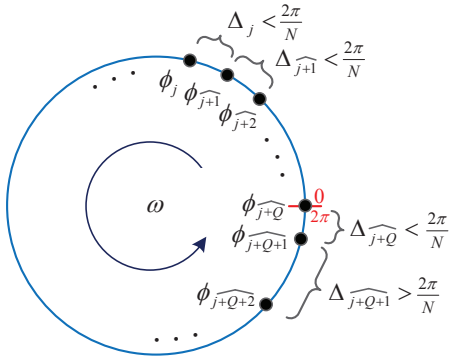

Figure B.2: **State B** on which Q ($0 \leq Q \leq N-2$) phase differences between the smaller phase difference and the larger phase difference become smaller than $\frac{2\pi}{N}$.

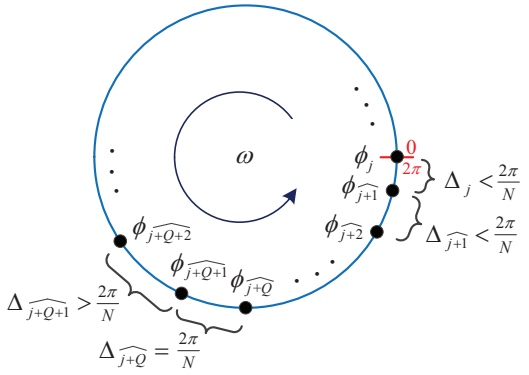

Figure B.3: $Q-1$ ($0 \leq Q \leq N-2$) phase differences between the smaller phase difference and the larger phase difference are equal to $\frac{2\pi}{N}$ after one firing.

B.2 Proof of Corollary 3.1

Proof. Since $l_1 = 0$ and $0 < l_2 < 1$ hold, the PRF $F(\phi_k)$ in (3.2) and the phase update rule in (3.3) can be rewritten as:

$$F(\phi_k) = \begin{cases} 0 & 0 < \phi_k \leq 2\pi - \frac{2\pi}{N} \\ -l_2(\phi_k - (2\pi - \frac{2\pi}{N})) & 2\pi - \frac{2\pi}{N} < \phi_k < 2\pi \end{cases} \tag{B.1}$$

and

$$\phi_k^+ = \begin{cases} \phi_k & 0 < \phi_k \leq 2\pi - \frac{2\pi}{N} \\ (1-l_2)\phi_k + l_2(2\pi - \frac{2\pi}{N}) & 2\pi - \frac{2\pi}{N} < \phi_k < 2\pi \end{cases} \tag{B.2}$$

It is worth noting that the phase update rule in (B.2) is the same as the phase update rule in [113]. So the rule in [113] is a special case of our phase update rule in (3.3) for $l_1 = 0$. As pointed out in [82], there is still a lack of rigorous mathematical proof for the convergence of the desynchronization algorithm in [113] since the proof of Corollary 1 in [113] did not provide clear condition where the cardinality must decrease. Now we give a rigorous proof for the convergence of phase desynchronization under this situation.

Following the same line of reasoning as the proof of Theorem 3.1, the value of P will keep unchanged between two consecutive pulses, so we only need to concentrate on how P evolves at discrete-time instants when pulses are emitted. If there are no phase variables within $(2\pi - \frac{2\pi}{N}, 2\pi)$, then all the phase differences will not change, neither will P. Thus we only need to consider the situation in which there are some phase variables within $(2\pi - \frac{2\pi}{N}, 2\pi)$. If $N-1$ phase variables are within $(2\pi - \frac{2\pi}{N}, 2\pi)$, then this situation becomes the same as **Situation 5** in Remark 3.3. According to (3.29), we have $P^+ - P < 0$, which means P will decrease under this situation. If there are S phase variables within $(2\pi - \frac{2\pi}{N}, 2\pi)$ (cf. Fig. B.4), where S satisfies $1 \leq S \leq N-2$, then according to (B.2), the phase differences after the update can be rewritten as:

$$\begin{cases} \Delta_k^+ = 2\pi - (1-l_2)\phi_{\widehat{k+1}} - l_2(2\pi - \frac{2\pi}{N}) \\ \Delta_{\widehat{k+j}}^+ = (1-l_2)(\phi_{\widehat{k+j}} - \phi_{\widehat{k+j+1}}),\ j = 1, \ldots, S-1 \\ \Delta_{\widehat{k+S}}^+ = (1-l_2)\phi_{\widehat{k+S}} + l_2(2\pi - \frac{2\pi}{N}) - \phi_{\widehat{k+S+1}} \\ \Delta_{\widehat{k+q}}^+ = \phi_{\widehat{k+q}} - \phi_{\widehat{k+q+1}},\ q = S+1, \ldots, N-2 \\ \Delta_{\widehat{k+N-1}}^+ = \phi_{\widehat{k+N-1}} \end{cases} \tag{B.3}$$

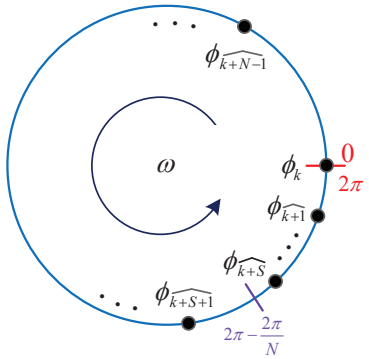

Figure B.4: The phase variables $\phi_{\widehat{k+1}}, \ldots, \phi_{\widehat{k+S}}$ reside in $(2\pi - \frac{2\pi}{N}, 2\pi)$ when oscillator k sends the first "active pulse" at $t = t_k$.

Combining (3.4), (3.5), (3.8), and (B.3) leads to:

$$P^+ - P = |\Delta^+_{\widehat{k+S}} - \frac{2\pi}{N}| - |\Delta_{\widehat{k+S}} - \frac{2\pi}{N}| + l_2(2\pi - \frac{2\pi}{N} - \phi_{\widehat{k+S}}) \tag{B.4}$$

which is the same as **Part B** in (3.16). According to the proof of Theorem 3.1, P will decrease under **Case 1"** and **Case 2"** and keep unchanged under **Case 3"**.

Now we show that **Case 3"** cannot always exist before the achievement of phase desynchronization. As illustrated in Fig. B.1, **State A** always exists unless phase desynchronization is achieved. Note that different from the proof of Lemma B.1, we do not need to consider the relationship between $\phi_{\widehat{j+Q+2}}$ and $\frac{2\pi}{N}$ since $l_1 = 0$ holds. When oscillator j fires, it emits an "active pulse." This pulse only affects $\phi_{\widehat{j+1}}$ since only $\phi_{\widehat{j+1}}$ resides in $(2\pi - \frac{2\pi}{N}, 2\pi)$, and it decreases the value of $\phi_{\widehat{j+1}}$ according to (B.2). Thus $\Delta_{\widehat{j+1}}$ becomes smaller than $\frac{2\pi}{N}$, $\Delta_{\widehat{j+2}}, \ldots, \Delta_{\widehat{j+Q}}$ are still equal to $\frac{2\pi}{N}$, and $\Delta_{\widehat{j+Q+1}}$ is still larger than $\frac{2\pi}{N}$. Therefore, after one firing, the number of phase differences equal to $\frac{2\pi}{N}$ is reduced by one to $Q - 1$, as illustrated in Fig. B.3. Following the same line of reasoning, we can obtain that after Q firings, the phase differences equal to $\frac{2\pi}{N}$ in the **State A** become smaller than $\frac{2\pi}{N}$, which means that **State B** in Fig. B.2 is achieved. Thus the condition in **Case 3"** cannot always exist before achieving phase desynchronization because under **State B** $\Delta_{\widehat{j+Q+1}} > \frac{2\pi}{N}$ will be true when PCO $\widehat{j+Q}$ fires.

Consequently, P will keep decreasing until it reaches 0, i.e., until phase desynchronization is achieved. Therefore, the PCOs will achieve phase desynchronization under the PRF (3.2) for $l_1 = 0$ and $0 < l_2 < 1$. ■

Bibliography

[1] S. Achuthan and C. C. Canavier. Phase-resetting curves determine synchronization, phase locking, and clustering in networks of neural oscillators. *J. Neurosci.*, 29(16):5218–5233, 2009.

[2] C. D. Acker, N. Kopell, and J. A. White. Synchronization of strongly coupled excitatory neurons: relating network behavior to biophysics. *J. Comput. Neurosci.*, 15(1):71–90, 2003.

[3] A. P. Aguiar, J. Hespanha, and A. M. Pascoal. Switched seesaw control for the stabilization of underactuated vehicles. *Automatica*, 43(12):1997–2008, 2007.

[4] A. Alaeddini, K. Morgansen, and M. Mesbahi. Adaptive communication networks with privacy guarantees. In *Proceedings of 2017 American Control Conference*, pages 4460–4465, 2017.

[5] Claudio Altafini. A dynamical approach to privacy preserving average consensus. In *2019 IEEE 58th Conference on Decision and Control (CDC)*, pages 4501–4506. IEEE, 2019.

[6] Z. An, H. Zhu, X. Li, C. Xu, Y. Xu, and X. Li. Nonidentical linear pulse-coupled oscillators model with application to time synchronization in wireless sensor networks. *IEEE Trans. Ind. Electron.*, 58(6):2205–2215, 2011.

[7] T. Anglea and Y. Q. Wang. Pulse-coupled synchronization with guaranteed clock continuity. *IEEE Transactions on Signal Processing*, 67(6):1596–1609, 2019.

[8] S. Ashkiani and A. Scaglione. Pulse coupled discrete oscillators dynamics for network scheduling. In *the 50th Annual Allerton Conference on Communication, Control, and Computing*, pages 1551–1558, UIUC, USA, 2012.

[9] J. Benda, A. Longtin, and L. Maler. A synchronization-desynchronization code for natural communication signals. *Neuron*, 52(2):347–358, 2006.

[10] F. Bénézit, V. Blondel, P. Thiran, J. Tsitsiklis, and M. Vetterli. Weighted gossip: Distributed averaging using non-doubly stochastic matrices. In *Proceedings of 2010 IEEE International Symposium on Information Theory*, pages 1753–1757, 2010.

[11] J. E. Boillat. Load balancing and poisson equation in a graph. *Concurrency and Computation: Practice and Experience*, 2(4):289–313, 1990.

[12] D. Buranapanichkit, N. Deligiannis, and Y. Andreopoulos. On the stochastic modeling of desynchronization convergence in wireless sensor networks. In *IEEE International Conference on Acoustics, Speech and Signal Processing (ICASSP)*, pages 5045–5049, 2014.

[13] D. Buranapanichkit, N. Deligiannis, and Y. Andreopoulos. Convergence of desynchronization primitives in wireless sensor networks: A stochastic modeling approach. *IEEE Trans. Signal Process.*, 63(1):221–233, 2015.

[14] C. C. Canavier and S. Achuthan. Pulse coupled oscillators and the phase resetting curve. *Math. Biosci.*, 226(2):77–96, 2010.

[15] C. C. Canavier and R. A. Tikidji-Hamburyan. Globally attracting synchrony in a network of oscillators with all-to-all inhibitory pulse coupling. *Phys. Rev. E*, 95(3):032215, 2017.

[16] N. Cao, C. Wang, M. Li, K. Ren, and W. Lou. Privacy-preserving multi-keyword ranked search over encrypted cloud data. *IEEE Trans. Parallel Distrib. Syst.*, 25(1):222–233, 2014.

[17] Themistoklis Charalambous, Nikolas E Manitara, and Christoforos N Hadjicostis. Privacy-preserving average consensus over digraphs in the presence of time delays. In *2019 57th Annual Allerton Conference on Communication, Control, and Computing (Allerton)*, pages 238–245. IEEE, 2019.

[18] C. C. Chen. Threshold effects on synchronization of pulse-coupled oscillators. *Phys. Rev. E*, 49:2668–2672, 1994.

[19] S. Chung and J. E. Slotine. Cooperative robot control and concurrent synchronization of lagrangian systems. *IEEE Trans. Robot.*, 25(3):686–700, 2009.

[20] J. Cortes, S. Martinez, T. Karatas, and F. Bullo. Coverage control for mobile sensing networks. *IEEE Trans. Robot. Autom.*, 20(2):243–255, 2004.

[21] G. Cybenko. Dynamic load balancing for distributed memory multiprocessors. *J. Parallel Distrib. Comput.*, 7(2):279–301, 1989.

[22] J. Degesys, I. Rose, A. Patel, and R. Nagpal. Desync: self-organizing desynchronization and TDMA on wireless sensor networks. In *Proceedings of the 6th International Conference on Information Processing in Sensor Networks*, pages 11–20. ACM, 2007.

[23] N. Deligiannis, J. F. C. Mota, G. Smart, and Y. Andreopoulos. Decentralized multichannel medium access control: Viewing desynchronization as a convex optimization method. In *Proceedings of the 14th International Conference on Information Processing in Sensor Networks*, pages 13–24. ACM, 2015.

[24] N. Deligiannis, J. F. C. Mota, G. Smart, and Y. Andreopoulos. Fast desynchronization for decentralized multichannel medium access control. *IEEE Trans. Commun.*, 63(9):3336–3349, 2015.

[25] D. V. Dimarogonas and K. J. Kyriakopoulos. On the rendezvous problem for multiple nonholonomic agents. *IEEE Trans. Autom. Control*, 52(5):916–922, 2007.

[26] R. Dror, C. C. Canavier, R. J. Butera, J. W. Clark, and J. H. Byrne. A mathematical criterion based on phase response curves for stability in a ring of coupled oscillators. *Biol. Cybern.*, 80(1):11–23, 1999.

[27] X. Duan, J. He, P. Cheng, Y. Mo, and J. Chen. Privacy preserving maximum consensus. In *2015 IEEE 54th Annual Conference on Decision and Control (CDC)*, pages 4517–4522, 2015.

[28] M. Egerstedt and X. Hu. Formation constrained multi-agent control. *IEEE Trans. Robot. Autom.*, 17(4):947–951, 2001.

[29] M. El-Hawwary and M. Maggiore. Distributed circular formation stabilization for dynamic unicycles. *IEEE Trans. Autom. Control*, 58(1):149–162, 2013.

[30] Taher ElGamal. A public key cryptosystem and a signature scheme based on discrete logarithms. *IEEE transactions on information theory*, 31(4):469–472, 1985.

[31] B. Ermentrout. Type I membrances, phase resetting curves, and synchrony. *Neural Comput.*, 8(5):979–1001, 1996.

[32] U. Ernst, K. Pawelzik, and T. Geisel. Synchronization induced by temporal delays in pulse-coupled oscillators. *Phys. Rev. Lett.*, 74:1570–1573, 1995.

[33] Wentuo Fang, Mohsen Zamani, and Zhiyong Chen. Secure and privacy preserving consensus for second-order systems based on paillier encryption. *arXiv preprint arXiv:1805.01065*, 2018.

[34] J. Fax and R. Murray. Information flow and cooperative control of vehicle formations. *IEEE Trans. Autom. Control*, 49(9):1465–1476, 2004.

[35] F. Ferrante and Y. Q. Wang. A hybrid systems approach to splay state stabilization of pulse coupled oscillators. In *Proc. IEEE 55th Conf. Decision Control*, pages 1763–1768. IEEE, 2016.

[36] F. Ferrante and Y. Q. Wang. Robust almost global splay state stabilization of pulse coupled oscillators. *IEEE Trans. Autom. Control*, 62(6):3083–3090, 2017.

[37] J. A. Fill. Eigenvalue bounds on convergence to stationarity for nonreversible markov chains, with an application to the exclusion process. *The annals of applied probability*, pages 62–87, 1991.

[38] T. Furukawa, H. F. Durrant-Whyte, G. Dissanayake, and S. Sukkarieh. The coordination of multiple uavs for engaging multiple targets in a time-optimal manner. In *2003 IEEE/RSJ International Conference on Intelligent Robots and Systems*, volume 1, pages 36–41. IEEE, 2003.

[39] H. Gao and Y. Q. Wang. Integrated communication and control for collective motion with limited communication. In *Proc. 20th IFAC World Congress, Toulouse, France*, volume 50, pages 8826–8831. Elsevier, 2017.

[40] H. Gao and Y. Q. Wang. On phase response function based decentralized phase desynchronization. *IEEE Trans. Signal Process.*, 65(21):5564–5577, 2017.

[41] H. Gao and Y. Q. Wang. Dynamics based privacy protection for average consensus on directed graphs. *arXiv preprint arXiv:1812.02255*, 2018.

[42] H. Gao and Y. Q. Wang. A pulse based integrated communication and control design for decentralized collective motion coordination. *IEEE Trans. Autom. Control*, 63(6):1858–1864, 2018.

[43] H. Gao and Y. Q. Wang. On the global synchronization of pulse-coupled oscillators interacting on chain and directed tree graphs. *Automatica*, 104:196–206, 2019.

[44] H. Gao, C. Zhang, M. Ahmad, and Y. Q. Wang. Privacy-preserving average consensus on directed graphs using push-sum. In *2018 IEEE Conference on Communications and Network Security (CNS)*. IEEE, 2018.

[45] Lan Gao, Shaojiang Deng, Wei Ren, and Chunqiang Hu. Differentially private consensus with quantized communication. *IEEE Trans. Cybern.*, 2019.

[46] R. Goebel, R. G. Sanfelice, and A. R. Teel. *Hybrid Dynamical Systems: Modeling, Stability, and Robustness*. Princeton University Press, Princeton, 2012.

[47] P. Goel and B. Ermentrout. Synchrony, stability, and firing patterns in pulse-coupled oscillators. *Physica D*, 163(3):191–216, 2002.

[48] M. Golubitsky and I. Stewart. *The symmetry perspective: from equilibrium to chaos in phase space and physical space*, volume 200. Springer Science & Business Media, 2003.

[49] L. Grüne, K. Worthmann, and D. Nešic. Continuous-time controller redesign for digital implementation: A trajectory based approach. *Automatica*, 44(1):225–232, 2008.

[50] Nirupam Gupta, Jonathan Kat, and Nikhil Chopra. Statistical privacy in distributed average consensus on bounded real inputs. In *2019 American Control Conference (ACC)*, pages 1836–1841. IEEE, 2019.

[51] C. N. Hadjicostis, A. D. Domínguez-García, and T. Charalambous. Distributed averaging and balancing in network systems: with applications to coordination and control. *Foundations and Trends® in Systems and Control*, 5(2-3):99–292, 2018.

[52] Christoforos N Hadjicostis and Alejandro D Dominguez-Garcia. Privacy-preserving distributed averaging via homomorphically encrypted ratio consensus. *IEEE Trans. Autom. Control*, 2020.

[53] S. Han, W. K. Ng, L. Wan, and V. C. S. Lee. Privacy-preserving gradient-descent methods. *IEEE Trans. Knowl. Data Eng.*, 22(6):884–899, 2010.

[54] D. Hansel, G. Mato, and C. Meunier. Synchrony in excitatory neural networks. *Neural Comput.*, 7(2):307–337, 1995.

[55] Jianping He, Lin Cai, Peng Cheng, Jianping Pan, and Ling Shi. Distributed privacy-preserving data aggregation against dishonest nodes in network systems. *IEEE Internet of Things Journal*, 6(2):1462–1470, 2018.

[56] Jianping He, Lin Cai, Peng Cheng, Jianping Pan, and Ling Shi. Consensus-based data-privacy preserving data aggregation. *IEEE Transactions on Automatic Control*, 64(12):5222–5229, 2019.

[57] Jianping He, Lin Cai, Chengcheng Zhao, Peng Cheng, and Xinping Guan. Privacy-preserving average consensus: privacy analysis and algorithm design. *IEEE Transactions on Signal and Information Processing over Networks*, 5(1):127–138, 2018.

[58] R. Hoenkamp, G. B. Huitema, and A. J. C. de Moor-van Vugt. The neglected consumer: the case of the smart meter rollout in the netherlands. *Renew. Energy Law Policy Rev.*, pages 269–282, 2011.

[59] G. M. Hoffmann and C. J. Tomlin. Mobile sensor network control using mutual information methodls and particle filters. *IEEE Trans. Autom. Control*, 55(1):32–47, 2010.

[60] Y. W. Hong and A. Scaglione. A scalable synchronization protocol for large scale sensor networks and its applications. *IEEE J. Sel. Areas Commun.*, 23:1085–1099, 2005.

[61] A. Hu and S. D. Servetto. On the scalability of cooperative time synchronization in pulse-connected networks. *IEEE Trans. Inform. Theory*, 52:2725–2748, 2006.

[62] Z. Huang, S. Mitra, and G. Dullerud. Differentially private iterative synchronous consensus. In *Proceedings of the 2012 ACM workshop on Privacy in the electronic society*, pages 81–90, 2012.

[63] Z. Huang, S. Mitra, and N. Vaidya. Differentially private distributed optimization. In *Proceedings of the 2015 International Conference on Distributed Computing and Networking*, pages 4:1–4:10, 2015.

[64] E. Izhikevich. *Dynamical systems in neuroscience: the geometry of excitability and bursting*. MIT Press, London, 2007. Pages 438–448.

[65] E. W. Justh and P. S. Krishnaprasad. Equilibria and steering laws for planar formations. *Syst. Control Lett.*, 52:25–38, 2004.

[66] D. Kannapan and F. Bullo. Synchronization in pulse-coupled oscillators with delayed excitatory/inhibitory coupling. *SIAM J. Control Optim.*, 54(4):1872–1894, 2016.

[67] V. Katewa, F. Pasqualetti, and V. Gupta. On privacy vs cooperation in multi-agent systems. *Int. J. Control*, (accepted):1–20, 2017.

[68] M. Kefayati, M. S. Talebi, B. H. Khalaj, and H. R. Rabiee. Secure consensus averaging in sensor networks using random offsets. In *IEEE International Conference on Telecommunications and Malaysia International Conference on Communications*, pages 556–560, 2007.

[69] D. Kempe, A. Dobra, and J. Gehrke. Gossip-based computation of aggregate information. In *Proceedings of 44th Annual IEEE Symposium on Foundations of Computer Science*, pages 482–491, 2003.

[70] V. Kirk and E. Stone. Effect of a refractory period on the entrainment of pulse-coupled integrate-and-fire oscillators. *Phys. Lett. A*, 21:70–76, 1997.

[71] Masako Kishida. Encrypted average consensus with quantized control law. In *2018 IEEE Conference on Decision and Control (CDC)*, pages 5850–5856. IEEE, 2018.

[72] D. J. Klein, P. Lee, K. A. Morgansen, and T. Javidi. Integration of communication and control using discrete time kuramoto models for multivehicle coordination over broadcast networks. *IEEE J. Sel. Areas Commun.*, 26(4):695–705, 2008.

[73] J. Klinglmayr and C. Bettstetter. Synchronization of inhibitory pulse-coupled oscillators in delayed random and line networks. In *Proc. 3rd IEEE Int. Symp. Appl. Sci. Biomed. Commun. Technol.*, pages 1–5, Rome, Italy, 2010.

[74] J. Klinglmayr and C. Bettstetter. Self-organizing synchronization with inhibitory-coupled oscillators: Convergence and robustness. *ACM Trans. Auton. Adapt. Syst.*, 7(3):30, 2012.

[75] J. Klinglmayr, C. Bettstetter, M. Timme, and C. Kirst. Convergence of self-organizing pulse-coupled oscillator synchronization in dynamic networks. *IEEE Trans. Autom. Control*, 62(4):1606–1619, 2017.

[76] J. Klinglmayr, C. Kirst, C. Bettstetter, and M. Timme. Guaranteeing global synchronization in networks with stochastic interactions. *New J. Phys.*, 14(7):073031, 2012.

[77] P. Kokotovic, H. Khalil, and J. OReilly. *Singular perturbation methods in control: Analysis and design*. SIAM, PA, 1999.

[78] K. Konishi and H. Kokame. Synchronization of pulse-coupled oscillators with a refractory period and frequency distribution for a wireless sensor network. *Chaos*, 18:033132, 2008.

[79] M. D. LaMar and G. D. Smith. Effect of node-degree correlation on synchronization of identical pulse-coupled oscillators. *Phys. Rev. E*, 81(4):046206, 2010.

[80] F. Lamiraux and J. P. Lammond. Smooth motion planning for car-like vehicles. *IEEE Trans. Robot. Autom.*, 17(4):498–501, 2001.

[81] N. E. Leonard, D. Paley, F. Lekien, R. Sepulchre, D. M. Fratantoni, and R. Davis. Collective motion, sensor networks, and ocean sampling. *Proc. IEEE*, 95(1):48–74, 2007.

[82] C.-M. Lien, S.-H. Chang, C.-S. Chang, and D.-S. Lee. Anchored desynchronization. In *IEEE INFOCOM*, pages 2966–2970, 2012.

[83] K. Liu, H. Kargupta, and J. Ryan. Random projection-based multiplicative data perturbation for privacy preserving distributed data mining. *IEEE Trans. Knowl. Data Eng.*, 18(1):92–106, 2006.

[84] Youcheng Lou, Lean Yu, Shouyang Wang, and Peng Yi. Privacy preservation in distributed subgradient optimization algorithms. *IEEE Trans. Cybern.*, 48(7):2154–2165, 2017.

[85] N. A. Lynch. *Distributed algorithms*. Morgan Kaufmann Publishers, San Francisco, CA, 1996.

[86] Hanbaek Lyu. Synchronization of finite-state pulse-coupled oscillators. *Physica D: Nonlinear Phenomena*, 303:28–38, 2015.

[87] Hanbaek Lyu. Global synchronization of pulse-coupled oscillators on trees. *SIAM J. Appl. Dyn. Syst.*, 17(2):1521–1559, 2018.

[88] Olvi L Mangasarian. Privacy-preserving linear programming. *Optimization Letters*, 5(1):165–172, 2011.

[89] N. E. Manitara and C. N. Hadjicostis. Privacy-preserving asymptotic average consensus. In *2013 European Control Conference (ECC)*, pages 760–765, 2013.

[90] J. Marshall, M. Broucke, and B. Francis. Formations of vehicles in cyclic pursuit. *IEEE Trans. Autom. Control*, 49(11):1963–1974, 2004.

[91] R. Mathar and J. Mattfeldt. Pulse-coupled decentral synchronization. *SIAM J. Applied Mathematics*, 56:1094–1106, 1996.

[92] A. Mauroy. *On the dichotomic collective behaviors of large populations of pulse-coupled firing oscillators*. PhD thesis, Université de Liège, Liège, Belgium, 2011.

[93] R. M. Memmesheimer and M. Timme. Stable and unstable periodic orbits in complex networks of spiking neurons with delays. *Dynam. Syst.*, 28(4):1555–1588, 2010.

[94] N. Michael and V. Kumar. Control of ensembles of aerial robots. *Proc. IEEE*, 99(9):1587–1602, 2011.

[95] R. Mirollo and S. Strogatz. Synchronization of pulse-coupled biological oscillators. *SIAM J. Appl. Math.*, 50:1645–1662, 1990.

[96] Y. Mo and R. M. Murray. Privacy preserving average consensus. *IEEE Trans. Autom. Control*, 62(2):753–765, 2017.

[97] N. Moshtagh and A. Jadbabaie. Distributed geodesic control laws for flocking of nonholonomic agents. *IEEE Trans. Autom. Control*, 52(4):681–686, 2007.

[98] N. Moshtagh, N. Michael, A. Jadbabaie, and K. Daniilidis. Vision-based, distributed control laws for motion coordination of nonholonomic robots. *IEEE Trans. Robot.*, 25(4):851–860, 2009.

[99] R. M. Murray and S. S. Sastry. Nonholonomic motion planning: Steering using sinusoids. *IEEE Trans. Autom. Control*, 38(5):700–716, 1993.

[100] A. Nabi and J. Moehlis. Nonlinear hybrid control of phase models for coupled oscillators. In *American Control Conference*, pages 922–923, Baltimore, USA, 2010.

[101] A. Nedić, A. Olshevsky, and W. Shi. A geometrically convergent method for distributed optimization over time-varying graphs. In *Decision and Control (CDC), 2016 IEEE 55th Conference on*, pages 1023–1029. IEEE, 2016.

[102] A. Nedić, A. Olshevsky, and W. Shi. Achieving geometric convergence for distributed optimization over time-varying graphs. *SIAM Journal on Optimization*, 27(4):2597–2633, 2017.

[103] A. Nedić, A. Ozdaglar, and P. A. Parrilo. Constrained consensus and optimization in multi-agent networks. *IEEE Transactions on Automatic Control*, 55(4):922–938, 2010.

[104] Angelia Nedić and Alex Olshevsky. Distributed optimization over time-varying directed graphs. *IEEE Transactions on Automatic Control*, 60(3):601–615, 2014.

[105] Angelia Nedic and Asuman Ozdaglar. Distributed subgradient methods for multi-agent optimization. *IEEE Transactions on Automatic Control*, 54(1):48–61, 2009.

[106] J. Nishimura and E. J. Friedman. Robust convergence in pulse-coupled oscillators with delays. *Phys. Rev. Lett.*, 106(19):194101, 2011.

[107] E. Nozari, P. Tallapragada, and J. Cortés. Differentially private average consensus with optimal noise selection. *IFAC-PapersOnLine*, 48(22):203–208, 2015.

[108] E. Nozari, P. Tallapragada, and J. Cortés. Differentially private average consensus: obstructions, trade-offs, and optimal algorithm design. *Automatica*, 81:221–231, 2017.

[109] F. Núñez, Y. Q. Wang, and F. J. Doyle III. Global synchronization of pulse-coupled oscillators interacting on cycle graphs. *Automatica*, 52:202–209, 2015.

[110] F. Núñez, Y. Q. Wang, and F. J. Doyle III. Synchronization of pulse-coupled oscillators on (strongly) connected graphs. *IEEE Trans. Autom. Control*, 60(6):1710–1715, 2015.

[111] F. Núñez, Y. Q. Wang, A. R. Teel, and F. J. Doyle III. Synchronization of pulse-coupled oscillators to a global pacemaker. *Syst. Control Lett.*, 88:75–80, 2016.

[112] R. Olfati-Saber and R. M. Murray. Consensus problems in networks of agents with switching topology and time-delays. *IEEE Trans. Autom. Control*, 49(9):1520–1533, 2004.

[113] R. Pagliari, Y.-W. Hong, and A. Scaglione. Bio-inspired algorithms for decentralized round-robin and proportional fair scheduling. *IEEE J. Sel. Areas Commun.*, 28(4):564–575, 2010.

[114] R. Pagliari and A. Scaglione. Scalable network synchronization with pulse-coupled oscillators. *IEEE. Trans. Mob. Comput.*, 10:392–405, 2011.

[115] P. Paillier. Public-key cryptosystems based on composite degree residuosity classes. In *Eurocrypt*, volume 99, pages 223–238. Springer Berlin Heidelberg, 1999.

[116] D. Paley and N. Leonard. Collective motion of ring-coupled planar particles. In *Proc. Joint 44th IEEE Conf. Decision Control Eur. Control Conf.*, pages 3929–3934, Spain, 2005.

[117] D. Paley, N. Leonard, and R. Sepulchre. Collective motion of self-propelled particles: Stabilizing symmetric formations on closed curves. In *Proc. IEEE 45th Conf. Decision Control*, pages 5067–5072, CA, 2006.

[118] D. A. Paley, N. E. Leonard, and R. Sepulchre. Stabilization of symmetric formations to motion around convex loops. *Syst. Control Lett.*, 57(3):209–215, 2008.

[119] D. A. Paley, N. E. Leonard, R. Sepulchre, D. Grunbaum, and J. K. Parrish. Oscillator models and collective motion. *IEEE Control Systems*, 27(4):89–105, 2007.

[120] A. Patel, J. Degesys, and R. Nagpal. Desynchronization: The theory of self-organizing algorithms for round-robin scheduling. In *the 1st International Conference on Self-Adaptive and Self-Organizing Systems*, pages 87–96, 2007.

[121] S. Pequito, S. Kar, S. Sundaram, and A. P. Aguiar. Design of communication networks for distributed computation with privacy guarantees. In *2014 IEEE 53rd Annual Conference on Decision and Control (CDC)*, pages 1370–1376, 2014.

[122] C. S. Peskin. *Mathematical aspects of heart physiology*. Courant Institute of Mathematical Science, New York University, 1975.

[123] S. Phillips and R. G. Sanfelice. Results on the asymptotic stability properties of desynchronization in impulse-coupled oscillators. In *American Control Conference*, pages 3272–3277, Washington DC, USA, 2013.

[124] S. Phillips and R. G. Sanfelice. Robust asymptotic stability of desynchronization in impulse-coupled oscillators. *IEEE Trans. Control Netw. Syst.*, 3(2):127–136, 2016.

[125] Amaury Bouchra Pilet, Davide Frey, and Francois Taiani. Robust privacy-preserving gossip averaging. In *International Symposium on Stabilizing, Safety, and Security of Distributed Systems*, pages 38–52. Springer, 2019.

[126] N. D. Powel and K. A. Morgansen. Communication-based performance bounds in nonlinear coordinated control. *Int. J. Robust. Nonlinear Control*, 21(12):1410–1420, 2011.

[127] A. V. Proskurnikov and M. Cao. Event-based synchronization in biology: Dynamics of pulse coupled oscillators. In *Proceedings of the First Intern. Conf. on Event-Based Control, Communication and Signal Processing*, 2015.

[128] A. V. Proskurnikov and M. Cao. Synchronization of pulse-coupled oscillators and clocks under minimal connectivity assumptions. *IEEE Trans. Autom. Control*, 62(11):5873–5879, 2017.

[129] W. Ren and R. Beard. Formation feedback control for multiple spacecraft via virtual structures. *IEE Proc. Control Theory Appl.*, 151(3):357–368, 2004.

[130] W. Ren and R. W. Beard. Consensus seeking in multiagent systems under dynamically changing interaction topologies. *IEEE Trans. Autom. Control*, 50(5):655–661, 2005.

[131] M. B. H. Rhouma and H. Frigui. Self-organization of pulse-coupled oscillators with application to clustering. *IEEE Trans. Pattern Anal. Mach. Intell.*, 23(2):180–195, 2001.

[132] Israel Donato Ridgley, Randy A Freeman, and Kevin M Lynch. Simple, private, and accurate distributed averaging. In *2019 57th Annual Allerton Conference on Communication, Control, and Computing (Allerton)*, pages 446–452. IEEE, 2019.

[133] Ronald L Rivest, Adi Shamir, and Leonard Adleman. A method for obtaining digital signatures and public-key cryptosystems. *Communications of the ACM*, 21(2):120–126, 1978.

[134] R. T. Rockafellar and R. J.-B. Wets. *Variational Analysis*, volume 317. Springer Science & Business Media, Princeton, 2009.

[135] M. Ruan, H. Gao, and Y. Wang. Secure and privacy-preserving consensus. *IEEE Transactions on Automatic Control*, in press, 2019.

[136] D. S. Scherber and H. C. Papadopoulos. Locally constructed algorithms for distributed computations in ad-hoc networks. In *Proceedings of the 3rd international symposium on Information processing in sensor networks*, pages 11–19. ACM, 2004.

[137] Austin Scott. Tactical data diodes in industrial automation and control systems. *SANS Institute InfoSec Reading Room*, 2015.

[138] E. Seneta. *Non-negative Matrices and Markov Chains*. Springer, 1973.

[139] R. Sepulchre, D. Paley, and N. Leonard. Collective motion and oscillator synchronization. In *Cooperative Control: 2003 Block Island Workshop on Cooperative Control*, pages 189–228, New York: Springer-Verlag, V. Kumar, N. Leonard, and A. S. Morse, Eds., 2005.

[140] R. Sepulchre, D. A. Paley, and N. E. Leonard. Stabilization of planar collective motion: All-to-all communication. *IEEE Trans. Autom. Control*, 52(5):811–824, 2007.

[141] R. Sepulchre, D. A. Paley, and N. E. Leonard. Stabilization of planar collective motion with limited communication. *IEEE Trans. Autom. Control*, 53(3):706–718, 2008.

[142] T. Settawatcharawanit, S. Choochaisri, C. Intanagonwiwat, and K. Rojviboonchai. V-desync: Desynchronization for beacon broadcasting on vehicular networks. In *IEEE 75th Vehicular Technology Conference*, pages 1–5, 2012.

[143] O. Simeone, U. Spagnolini, Y. Bar-Ness, and S Strogatz. Distributed synchronization in wireless networks. *IEEE Signal Process. Mag.*, 25:81–97, 2008.

[144] M. Stopfer, S. Bhagavan, B. H. Smith, and G. Laurent. Impaired odour discrimination on desynchronization of odour-encoding neural assemblies. *Nature*, 390(6655):70–74, 1997.

[145] S. Strogatz. From kuramoto to crawford: Exploring the onset of synchronization in populations of coupled oscillators. *Phys. D*, 143(1–4):1–20, 2000.

[146] Y. Taniguchi, G. Hasegawa, and H. Nakano. Self-organizing transmission scheduling considering collision avoidance for data gathering in wireless sensor networks. *J. Commun.*, 8(6):389–397, 2013.

[147] M. Timme and F. Wolf. The simplest problem in the collective dynamics of neural networks: is synchrony stable? *Nonlinearity*, 21(7):1579, 2008.

[148] M. Timme, F. Wolf, and T. Geisel. Coexistence of regular and irregular dynamics in complex networks of pulse-coupled oscillators. *Phys. Rev. Lett.*, 89(25):258701, 2002.

[149] R. Tóth, M. Lovera, P. S. C. Heuberger, M. Corno, and P. M. J. Van den Hof. On the discretization of linear fractional representations of lpv systems. *IEEE Trans. Control Syst. Technol.*, 20(6):1473–1489, 2012.

[150] J. N. Tsitsiklis. *Problems in decentralized decision making and computation*. PhD thesis, 1984.

[151] A. Tyrrell, G. Auer, and C. Bettstetter. Emergent slot synchronization in wireless networks. *IEEE. Trans. Mob. Comput.*, 9:719–732, 2010.

[152] L. Valbuena, P. Cruz, R. Figueroa, F. Sorrentino, and R. Fierro. Stable formation of groups of robots via synchronization. In *2014 IEEE/RSJ International Conference on Intelligent Robots and Systems*, pages 376–381. IEEE, 2014.

[153] C. V. Vreeswijk, L. F. Abbott, and G. B. Ermentrout. When inhibition not excitation synchronizes neural firing. *J. Comput. Neurosci.*, 1:313–321, 1994.

[154] Xin Wang, Jianping He, Peng Cheng, and Jiming Chen. Privacy preserving average consensus with different privacy guarantee. In *2018 Annual American Control Conference (ACC)*, pages 5189–5194. IEEE, 2018.

[155] Y. Wang. Privacy-preserving average consensus via state decomposition. *IEEE Transactions on Automatic Control*, in press, 2019.

[156] Y. Wang, Z. Huang, S. Mitra, and G. E. Dullerud. Differential privacy in linear distributed control systems: Entropy minimizing mechanisms and performance tradeoffs. *IEEE Trans. Control Netw. Syst.*, 4(1):118–130, 2017.

[157] Y. Q. Wang and F. J. Doyle III. Optimal phase response functions for fast pulse-coupled synchronization in wireless sensor networks. *IEEE Trans. Signal Process.*, 60(10):5583–5588, 2012.

[158] Y. Q. Wang, F. Núñez, and F. J. Doyle III. Energy-efficient pulse-coupled synchronization strategy design for wireless sensor networks through reduced idle listening. *IEEE Trans. Signal Process.*, 60:5293–5306, 2012.

[159] Y. Q. Wang, F. Núñez, and F. J. Doyle III. Increasing sync rate of pulse-coupled oscillators via phase response function design: theory and application to wireless networks. *IEEE Trans. Control Syst. Technol.*, 21:1455–1462, 2013.

[160] Y. Q. Wang, F. Núñez, and F. J. Doyle III. Statistical analysis of the pulse-coupled synchronization strategy for wireless sensor networks. *IEEE Trans. Signal Process.*, 61:5193–5204, 2013.

[161] G. Werner-Allen, G. Tewari, A. Patel, M. Welsh, and R. Nagpal. Firefly inspired sensor network synchronicity with realistic radio effects. In *Proc. SenSys 05*, pages 142 –153, USA, 2005.

[162] L. Xiao, S. Boyd, and S. Lall. A scheme for robust distributed sensor fusion based on average consensus. In *Proceedings of the 4th international symposium on Information processing in sensor networks*, page 9. IEEE Press, 2005.

[163] Dayong Ye, Tianqing Zhu, Wanlei Zhou, and S Yu Philip. Differentially private malicious agent avoidance in multiagent advising learning. *IEEE Trans. Cybern.*, 2019.

[164] S. Yun, J. Ha, and B. J. Kwak. Robustness of biologically inspired pulse-coupled synchronization against static attacks. In *Proc. IEEE Global Commun. Conf*, pages 1–6. IEEE, 2015.

[165] Z. Zhang and M. Y. Chow. Incremental cost consensus algorithm in a smart grid environment. In *2011 IEEE Power and Energy Society General Meeting*, pages 1–6, 2011.

[166] Junlong Zhu, Changqiao Xu, Jianfeng Guan, and Dapeng Oliver Wu. Differentially private distributed online algorithms over time-varying directed networks. *IEEE Transactions on Signal and Information Processing over Networks*, 4(1):4–17, 2018.